CONSTANT DISPLACEMENT RATE EXPERIMENTS AND CONSTITUTIVE MODELING OF ASPHALT MIXTURES

A Dissertation

by

PRADEEP HARIHARAKUMAR

Submitted to the Office of Graduate Studies of
Texas A&M University
in partial fulfillment of the requirements for the degree of

DOCTOR OF PHILOSOPHY

December 2004

Major Subject: Mechanical Engineering

CONSTANT DISPLACEMENT RATE EXPERIMENTS AND CONSTITUTIVE MODELING OF ASPHALT MIXTURES

A Dissertation

by

PRADEEP HARIHARAKUMAR

Submitted to Texas A&M University
in partial fulfillment of the requirements
for the degree of

DOCTOR OF PHILOSOPHY

Approved as to style and content by:

K. R. Rajagopal (Co-Chair of Committee)	D. N. Little (Co-Chair of Committee)
J. D. Humphrey (Member)	Jay R. Walton (Member)
Darbha Swaroop (Member)	Dennis O'Neal (Head of Department)

December 2004

Major Subject: Mechanical Engineering

ABSTRACT

Constant Displacement Rate Experiments and Constitutive

Modeling of Asphalt Mixtures. (December 2004)

Pradeep Hariharakumar, B. Tech, Indian Institute of Technology, Madras;

M.S, Texas A&M University

Co–Chairs of Advisory Committee: Dr. K. R. Rajagopal
Dr. D. N. Little

The focus of this dissertation is on constant displacment rate experiments on asphalt concrete and on developing continuum models in a general thermo-mechanical setting which will corroborate with the experimental results. Modeling asphalt concrete and predicting its response is of great importance to the pavement industry. More than 90 percent of the US Highways uses asphalt concrete as a pavement material.

Asphalt concrete exhibits nonlinear response even at small strains and the response of asphalt concrete to different types of loading is quite different. The properties of asphalt concrete are highly influenced by the type and amount of the aggregates and the asphalt used. The internal structure of asphalt concrete keeps on evolving during the loading process. This is due to the influence of different kinds of activities at the microlevel and also due to the interaction with the environment. The properties of asphalt concrete depend on its internal structure. Hence we need to take the evolution of the internal structure in modeling the response of asphalt concrete.

Experiments were carried out at different confinement pressures and displacement rates on cylindrical samples of asphalt concrete. Two different aggregates were used to make the sample - limestone and granite. The samples were tested at a constant displacement rate at a given confinement pressure. The force required to maintain

this constant displacement rate is measured and recorded.

The frame-work has been developed using the idea of multiple natural configurations that was introduced recently to study a variety of non-linear dissipative response of materials. By specifying the forms of the stored energy and rate of dissipation function of the material, specific models were developed using this frame work. In this work both a compressible and an incompressible model were developed by choosing appropriate forms of stored energy and rate of dissipation function. Finally the veracity of the models were tested by corroborating with the experimental results.

It is anticipated that the present work will aid in the development of better constitutive equations which in turn will accurately model asphalt concrete in laboratory and in field.

To my Mother, Father and Kiran

ACKNOWLEDGMENTS

I would like to thank Prof. Rajagopal for his constant support and encouragement throughout the course of this work. Although, at times it was painful and difficult, his constant guidance and support helped me to keep my focus at difficult times. Dr. Little helped me to look at my work from a practical view point. It is through Prof. Walton's classes that I started looking at mathematics from a wholly different view point. His course on "Analysis" was one of the best classes that I have ever taken. I would also like to thank Prof. Humphrey for his help and support in this project. I would like to thank Dr. Swaroop for his constant support and encouragement. I am grateful to Dr. Luoyi Tao and Dr. J. Murali Krishnan for helping me out at difficult times throughout this work. Last, but not the least, I would like to thank all my lab mates for all their help and for the many fruitful discussions that I had with them.

TABLE OF CONTENTS

CHAPTER Page

I INTRODUCTION 1

A. Kinematics 1
1. Homogeneous deformation 5
B. Kinetics 6
1. Stress tensor 6
2. Balance of mass, linear momentum and angular momentum 8
3. Conservation of energy 9
C. Constitutive Equations 10
1. Elastic body 10
2. Material frame indifference 11
3. Isotropy 12
4. Neo-Hookean material 13

II CONSTANT AXIAL DISPLACEMENT RATE EXPERIMENTS OF ASPHALT CONCRETE SPECIMENS 15

A. Introduction 15
B. Sample Preparation 15
1. Aggregate separation 16
2. Mix design 17
3. Preparation of batch mixes 21
4. Preheat batch mixes and asphalt to mixing temperature 23
5. Mixing 23
6. Oven aging 23
7. Compaction 24
8. Determination of air voids 26
C. Constant Displacement Rate Experiments 29

III AN INCOMPRESSIBLE CONSTITUTIVE MODEL FOR ASPHALT MIXTURES 33

A. Introduction 33
B. Preliminaries 38
C. Modeling of Asphalt Concrete 41

CHAPTER Page

D. Experiment - Constant axial displacement rate testing of asphalt mixtures 48
E. Corroboration of the model with the experimental data . . 52
F. Conclusions 60
G. Acknowledgment 65

IV A COMPRESSIBLE MODEL FOR ASPHALT MIXTURES . . 66

A. Introduction 66
B. Preliminaries 68
C. Modeling of Asphalt Concrete 70
D. Corroboration of the Model with the Experimental Data . 76

V CONCLUDING REMARKS AND DISCUSSION 81

A. Summary 81
B. Recommendations for Future Work 83

REFERENCES 86

APPENDIX A 96

VITA 108

LIST OF TABLES

TABLE		Page
I	ASTM D 3515 Gradation specification for dense mixtures	20
II	Gradation of the mixes	21
III	Materials, confinement pressures and displacement rates used in the experiment	29
IV	Mix design factors for the mixes	49
V	Gradation of limestone and granite mixes	50
VI	Table showing the different materials, confinement pressures and displacement rates used	51
VII	Material constants used in modeling	59

LIST OF FIGURES

FIGURE		Page
1	Gradation used for the aggregates	22
2	Mechanical mixer for mixing asphalt and the aggregates	24
3	Mould used in the preparation of the samples	25
4	Superpave gyratory compactor	26
5	Compacted specimen	27
6	Cross section of a granite sample	28
7	Schematic of the experiment	30
8	MTS machine with the temperature chamber	31
9	MTS machine with temperature chamber removed	32
10	Typical experimental result	32
11	Natural configuration associated with the current configuration	42
12	Experiment	51
13	Typical experimental result	52
14	Limestone, Disp rate = 2.5 mm/min (Incompressible)	61
15	Limestone, Disp rate = 0.5 mm/min (Incompressible)	61
16	Limestone, Disp rate = 12.5 mm/min (Incompressible)	62
17	Limestone, Disp rate = 0.1 mm/min (Incompressible)	62
18	Granite, Disp rate = 0.1 mm/min (Incompressible)	63
19	Granite, Disp rate = 0.5 mm/min (Incompressible)	63

FIGURE Page

20 Granite, Disp rate = 2.5 mm/min (Incompressible) 64

21 Granite, Disp rate = 12.5 mm/min (Incompressible) 64

22 Limestone, Disp rate = -0.1 mm/min (Compressible) 78

23 Limestone, Disp rate = -0.5 mm/min (Compressible) 79

24 Limestone, Disp rate = -2.5 mm/min (Compressible) 79

25 Limestone, Disp rate = -12.5 mm/min (Compressible) 80

26 Limestone, Confinement Pressure = 0 psi, Displacement Rate = 0.1 mm/min 96

27 Limestone, Confinement Pressure = 0 psi, Displacement Rate = 0.5 mm/min 96

28 Limestone, Confinement Pressure = 0 psi, Displacement Rate = 2.5 mm/min 97

29 Limestone, Confinement Pressure = 0 psi, Displacement Rate = 12.5 mm/min 97

30 Limestone, Confinement Pressure = 15 psi, Displacement Rate = 0.1 mm/min 98

31 Limestone, Confinement Pressure = 15 psi, Displacement Rate = 0.5 mm/min 98

32 Limestone, Confinement Pressure = 15 psi, Displacement Rate = 2.5 mm/min 99

33 Limestone, Confinement Pressure = 15 psi, Displacement Rate = 12.5 mm/min 99

34 Limestone, Confinement Pressure = 30 psi, Displacement Rate = 0.1 mm/min 100

35 Limestone, Confinement Pressure = 30 psi, Displacement Rate = 0.5 mm/min 100

FIGURE Page

36 Limestone, Confinement Pressure = 30 psi, Displacement Rate = 2.5 mm/min 101

37 Limestone, Confinement Pressure = 30 psi, Displacement Rate = 12.5 mm/min 101

38 Granite, Confinement Pressure = 0 psi, Displacement Rate = 0.1 mm/min 102

39 Granite, Confinement Pressure = 0 psi, Displacement Rate = 0.5 mm/min 102

40 Granite, Confinement Pressure = 0 psi, Displacement Rate = 2.5 mm/min 103

41 Granite, Confinement Pressure = 0 psi, Displacement Rate = 12.5 mm/min 103

42 Granite, Confinement Pressure = 15 psi, Displacement Rate = 0.1 mm/min 104

43 Granite, Confinement Pressure = 15 psi, Displacement Rate = 0.5 mm/min 104

44 Granite, Confinement Pressure = 15 psi, Displacement Rate = 2.5 mm/min 105

45 Granite, Confinement Pressure = 15 psi, Displacement Rate = 12.5 mm/min 105

46 Granite, Confinement Pressure = 30 psi, Displacement Rate = 0.1 mm/min 106

47 Granite, Confinement Pressure = 30 psi, Displacement Rate = 0.5 mm/min 106

48 Granite, Confinement Pressure = 30 psi, Displacement Rate = 2.5 mm/min 107

49 Granite, Confinement Pressure = 30 psi, Displacement Rate = 12.5 mm/min 107

CHAPTER I

INTRODUCTION

In this chapter we will quickly review some of the basics of continuum mechanics. We will introduce all the basic notions including stress and strain measures. A more detailed description can be found in standard text books [1], [2], [3].

A. Kinematics

A body $\mathcal{B}$ is a set whose elements can be put into bijective correspondence with the points of a region of a Euclidean point space $\mathcal{E}$. The elements of the body are called particles. Mappings of this body $\mathcal{B}$ to a three dimensional Euclidean point space are called *embodiers*. The image of $\mathcal{B}$ through the embodier, $\mathcal{K}(\mathcal{B})$, is called the configuration of the body. The body may occupy different configurations ($\mathcal{K}_t(\mathcal{B})$) at different instances of time. A motion $\mathcal{X}$ of $\mathcal{B}$ is a mapping of the elements of $\mathcal{B}$ onto points in $\mathcal{E}$ at time t:

$$\mathbf{x} = \mathcal{X}(P, t) \qquad \forall P \in \mathcal{B},\ \forall t \in \mathcal{I} \tag{1.1}$$

where $\mathcal{I}$ is an interval of the reals $\mathcal{R}$. At any time t, $\mathbf{x} \in \mathcal{K}_t(\mathcal{B}))$, the configuration occupied by the body at time t.

It is convenient to refer everything concerning $\mathcal{B}$ and its motion to a particular configuration, called the reference configuration, which is need not necessarily be the configuration occupied by the body. Since the $\mathcal{K}$'s are one to one, we can always find a one to one mapping $\mathcal{X}_{\mathcal{K}_R}$ which maps the reference configuration to the configuration

---

This dissertation follows the style of *IEEE Transactions on Automatic Control*.

occupied by the body at any time t:

$$\mathbf{x} = \mathcal{X}_{\mathcal{K}_R}(\mathbf{X}, t) \qquad \forall \mathbf{X} \in \mathcal{K}_{\mathbf{R}}(\mathcal{B}),\ \forall t \in \mathcal{I} \tag{1.2}$$

where $\mathcal{K}_{\mathbf{R}}(\mathcal{B})$ denotes the reference configuration of the body $\mathcal{B}$). Henceforth we will drop the subscript $\mathcal{K}_{\mathbf{R}}$ for simplicity of notation and denote $\mathbf{x} = \mathcal{X}(\mathbf{X}, t)$.

Any physical quantity can be defined on the body, either on $\mathcal{K}_{\mathbf{R}}(\mathcal{B}) \times \mathcal{R}$ or on $\mathcal{K}_t(\mathcal{B}) \times \mathcal{R}$. i.e. for any function ϕ,

$$\phi = \tilde{\phi}(\mathbf{X}, t) = \hat{\phi}(\mathbf{x}, t) \tag{1.3}$$

If you define a quantity (ϕ) in terms of the position of a particle in the reference configuration ($\phi(\mathbf{X}, t)$) it is called Lagrangean description or material description, while if you define it in terms of the position of a particle in the current configuration ($\phi(\mathbf{x}, t)$) it is called Eulerian description or spatial description. The velocity of a particle is defined by

$$\mathbf{v}(\mathbf{X}, t) := \frac{\partial \mathcal{X}(\mathbf{X}, t)}{\partial t} \tag{1.4}$$

The acceleration of a particle is given by

$$\mathbf{a}(\mathbf{X}, t) := \frac{\partial^2 \mathcal{X}(\mathbf{X}, t)}{\partial t^2} \tag{1.5}$$

The spatial description of acceleration field can be expressed as:

$$\mathbf{a}(\mathbf{x}, t) = \frac{\partial \mathbf{v}(\mathbf{x}, t)}{\partial t} + \mathrm{grad}\mathbf{v}(\mathbf{x}, t)\mathbf{v}(\mathbf{x}, t) \tag{1.6}$$

where

$$\mathrm{grad}\mathbf{v}(\mathbf{x}, t) = \frac{\partial \mathbf{v}(\mathbf{x}, t)}{\partial \mathbf{x}}$$

For convenience of notation we define the following:

$$\frac{\partial p}{\partial t} := \frac{\partial p(\mathbf{x},t)}{\partial t} \tag{1.7}$$

$$\frac{Dp}{Dt} := \frac{\partial p(\mathbf{X},t)}{\partial t} \tag{1.8}$$

$$\dot{p} := \frac{\partial p(\mathbf{X},t)}{\partial t} \tag{1.9}$$

$$\text{grad}p := \frac{\partial p(\mathbf{x},t)}{\partial \mathbf{x}} \tag{1.10}$$

$$\nabla p := \frac{\partial p(\mathbf{X},t)}{\partial \mathbf{X}} \tag{1.11}$$

$$\text{Div}(\mathbf{u}) := trace(\nabla \mathbf{u}) \tag{1.12}$$

$$\text{div}(\mathbf{u}) := trace(\text{grad}\mathbf{u}) \tag{1.13}$$

Here p can be a scalar, vector or a tensor and $\mathbf{u}$ is a vector.

The spatial gradient of the velocity is denoted by $\mathbf{L}$:

$$\mathbf{L}(\mathbf{x},t) := \frac{\partial \mathbf{v}(\mathbf{x},t)}{\partial \mathbf{x}} = \dot{\mathbf{F}}\mathbf{F}^{-1} \tag{1.14}$$

$\mathbf{L}$ can be decomposed into:

$$\mathbf{L} = \mathbf{D} + \mathbf{W} \tag{1.15}$$

where $\mathbf{D}$ is the symmetrical part and $\mathbf{W}$ is the skew-symmetric part of the gradient of velocity. The second order tensor

$$\mathbf{F}(\mathbf{X},t) := \frac{\partial \mathcal{X}(\mathbf{X},t)}{\partial \mathbf{X}} \tag{1.16}$$

is called the *deformation gradient* and it gives information on how the body is deformed locally. The *absolute value* of determinant of $\mathbf{F}$ at a point gives the ratio of the deformed volume to the undeformed volume of an infinitesimal parallelopiped at that point. The determinant of $\mathbf{F}$ will either be *always positive* or *always negative* throughout the body depending upon the reference configuration chosen. Since the

motion is one to one, determinant of $\mathbf{F}$ can never be zero.

Since $\mathbf{F}$ is invertible, we can use polar decomposition to get

$$\mathbf{F} = \mathbf{RU} = \mathbf{VR} \tag{1.17}$$

where $\mathbf{U}$ and $\mathbf{V}$ are symmetric positive definite tensors. $\mathbf{R}$ is an orthogonal tensor. Det($\mathbf{R}$) will carry the same sign throughout the motion at all points on the body. Henceforth we will assume that the reference configuration is one of the configurations occupied by the body during its motion. Hence det($\mathbf{F}$) and det($\mathbf{R}$) will always be greater than zero. Then $\mathbf{R}$ is a proper rotation and (1.17) tells us that every deformation can be decomposed locally as a pure stretch followed by a pure rotation or a pure rotation followed by a pure stretch. $\mathbf{U}$ and $\mathbf{V}$ have the same eigenvalues but different eigenvectors. In fact, if $\mathbf{u}$ is an eigenvector of $\mathbf{U}$ then $\mathbf{Ru}$ is an eigenvector of $\mathbf{V}$. This means that the material filaments along the eigenvectors of $\mathbf{U}$ in the undeformed configuration is mapped into material filaments along the eigenvectors of $\mathbf{V}$ in the deformed configuration.

The *right* and *left Cauchy-Green stretch tensors* are defined by:

$$\mathbf{C} := \mathbf{U}^2 = \mathbf{F}^T\mathbf{F} \tag{1.18}$$

$$\mathbf{B} := \mathbf{V}^2 = \mathbf{F}\mathbf{F}^T \tag{1.19}$$

The *Green-St.Venant strain tensor*($\mathbf{E}$) and the *Almansi-Hamel strain tensor* ($\mathbf{e}$) are defined in terms of $\mathbf{B}$ and $\mathbf{C}$.

$$\mathbf{E} := \frac{\mathbf{C}-\mathbf{I}}{2} \tag{1.20}$$

$$\mathbf{e} := \frac{\mathbf{I}-\mathbf{B}^{-1}}{2} \tag{1.21}$$

It is convenient to write the strain tensors in terms of the displacement $\mathbf{u}\,(\mathbf{X}, t)$ that

the particles may undergo.

$$\mathbf{u}(\mathbf{X}, t) := \mathbf{x}(\mathbf{X}, t) - \mathbf{X} \tag{1.22}$$

It immediately follows that,

$$\begin{aligned}
\mathbf{F} &= \mathbf{I} + \nabla\mathbf{u} && (1.23)\\
\mathbf{F^{-1}} &= \mathbf{I} - \mathrm{grad}\mathbf{u} && (1.24)\\
\mathbf{C} &= \mathbf{I} + \nabla\mathbf{u} + \nabla\mathbf{u^T} + \nabla\mathbf{u^T}\nabla\mathbf{u} && (1.25)\\
\mathbf{B}^{-1} &= \mathbf{I} - \mathrm{grad}\mathbf{u} - (\mathrm{grad}\mathbf{u})^{\mathbf{T}} + (\mathrm{grad}\mathbf{u})^{\mathbf{T}}\mathrm{grad}\mathbf{u} && (1.26)
\end{aligned}$$

$$\begin{aligned}
\mathbf{E} &= \frac{1}{2}(\nabla\mathbf{u} + \nabla\mathbf{u^T} + \nabla\mathbf{u^T}\nabla\mathbf{u}) && (1.27)\\
\mathbf{e} &= \frac{1}{2}\left(\mathrm{grad}\mathbf{u} + (\mathrm{grad}\mathbf{u})^{\mathbf{T}} - (\mathrm{grad}\mathbf{u})^{\mathbf{T}}\mathrm{grad}\mathbf{u}\right) && (1.28)
\end{aligned}$$

1. Homogeneous deformation

A deformation of the form

$$\mathbf{x} = \mathbf{A}\mathbf{X} + \mathbf{a} \tag{1.29}$$

where $\mathbf{A}$ and $\mathbf{a}$ are functions of time only is called a homogeneous deformation. We can easily see that $\mathbf{A} = \mathbf{F}$. Homogeneous deformations maps straight lines in the reference configuration to straight lines in the deformed configuration; two parallel straight lines deform into two parallel straight lines. Biaxial extension, dilatation, and simple shear are examples of homogeneous deformations.

B. Kinetics

1. Stress tensor

Suppose we are interested in finding out the forces acting in the interior of a continuous body. Consider a part $\mathcal{P}$ of a body $\mathcal{B}$. $\mathcal{P}$ occupies a region $\mathcal{V}$ and is obtained by cutting an imaginary surface $\mathcal{S}$ through Ω_t which is the region occupied by a body $\mathcal{B}$ at time t. Let us assume that $\mathcal{V}$ and $\mathcal{S}$ possess sufficient smoothness and continuity properties. We make a distinction between *body forces* which are forces acting from a distance and *contact forces* which are forces due to the contact between two surfaces.

Let us assume that the effect of all the forces acting along a surface can be adequately represented by a single vector field defined over the surface. We also assume that the effect of body forces can be represented by another vector field defined over the *region* $\mathcal{V}$. It is possible for *couples* as well as forces to be transmitted across a surface. But we consider only the latter.

We define the traction vector at a point $\mathbf{x}$ as

$$\mathbf{t}(\mathbf{x}, t, \mathcal{S}) := \lim_{\delta a \to 0} \frac{\delta \mathbf{f}}{\delta a} \tag{1.30}$$

where δa is the area of an element of $\mathcal{S}$ containing $\mathbf{x}$ and $\delta \mathbf{f}$ is the surface force transmitted across δa from the inside to the outside of the region $\mathcal{V}$ at time t. Thus traction vector $\mathbf{t}$ at a point will be different for different surfaces. Let us make an additional assumption that $\mathbf{t}$ at $\mathbf{x}$ depends on $\mathcal{S}$ only through its outward normal $\mathbf{n}$ at $\mathbf{x}$. It has been proved by Cauchy that the traction vector $\mathbf{t}(\mathbf{x}, t, \mathbf{n})$ at any spatial position $\mathbf{x}$ and time t on any surface with normal $\mathbf{n}$ is uniquely determined by the traction vectors at $\mathbf{x}$ and time t on any three linearly independent planes. $\mathbf{t}(\mathbf{x},t, \mathbf{n})$

has the following properties.

$$\mathbf{t}(\mathbf{x}, t, \mathbf{n}) = -\mathbf{t}(\mathbf{x}, t, -\mathbf{n}) \tag{1.31}$$

$$\mathbf{t}(\mathbf{x}, t, \mathbf{n}) = \mathbf{T}^{\mathbf{T}}(\mathbf{x},t)\mathbf{n} \tag{1.32}$$

Equation (1.31) is called the *Cauchy's Reciprocal theorem.* It is analogous to Newton's third law in particle dynamics. Equation (1.32) is called the *Existence theorem* or *Cauchy's Fundamental theorem.* It basically states that the traction vector is linearly related to the normal vector on the surface. The tensor field $\mathbf{T}(\mathbf{x}, t)$ is called the Cauchy stress tensor. The components T_{ij} of the stress tensor $\mathbf{T}$ in cartesian coordinates denotes the component of the traction vector in the direction of $\mathbf{e}_j$ on a plane whose normal is $\mathbf{e}_i$. Note that the Cauchy stress tensor will be symmetric for *non-polar* bodies due to the balance of angular momentum.

The stress tensor $\mathbf{T}$ is an Eulerian measure of stress. There are two other measures of stress. The *first Piola-Kirchoff stress tensor* enables us to calculate the traction vector in the current configuration measured per unit area of the corresponding element in the reference configuration. Since an infinitesimal area in the reference configuration ($d\mathbf{A}$) is deformed into an infinitesimal area in the current configuration ($d\mathbf{a}$) by $d\mathbf{a} = det(\mathbf{F})\mathbf{F}^{-\mathbf{T}}d\mathbf{A}$, the first Piola-Kirchoff stress tensor is given by:

$$\mathbf{S} = det(\mathbf{F})\mathbf{F}^{-1}\mathbf{T} \tag{1.33}$$

The *second Piola-Kirchhoff stress tensor* is defined by:

$$\tilde{\mathbf{S}} = det(\mathbf{F})\mathbf{F}^{-1}\mathbf{T}\mathbf{F}^{-\mathbf{T}} \tag{1.34}$$

When acted on a unit normal in the reference configuration, the second Piola-Kirchoff stress tensor gives a pseudo traction vector ($\tilde{\mathbf{t}} = \mathbf{F}^{-1}\mathbf{t}$). Second Piola-Kirchoff stress

tensor is a Lagrangean measure of stress. First Piola-Kirchhoff stress tensor is not symmetric whereas second Piola-Kirchhoff stress tensor is symmetric provided the Cauchy stress tensor is symmetric.

2. Balance of mass, linear momentum and angular momentum

There are some physical quantities such as mass, electric charge and momentum which are conserved during the motion of a body regardless of the material class which the body may belong to. It is desirable to distinguish between such equations from the equations which describe the behavior of a particular materials or classes of materials (*constitutive equations*).

Balance of mass expresses the fact that the mass of any part of a body remain unaltered during the course of motion of the body.

$$\int_{\Omega} \rho dV = \int_{\Omega_0} \rho dV_0 \tag{1.35}$$

where Ω and ρ are the material volume occupied by the body and it's density in the current configuration and Ω_0 and ρ_0 are it's volume an density in the reference configuration. If the integrands are continuous, this reduces to the Lagrangean form of the conservation of mass:

$$\rho_0 = \rho_0 \; det(\mathbf{F}) \tag{1.36}$$

The Eulerian local form of conservation of mass is given by:

$$\frac{\partial \rho}{\partial t} + \mathrm{div}(\rho \mathbf{v}) = 0 \tag{1.37}$$

If the material undergoes an isochoric motion, (1.37) reduces to:

$$\mathrm{div}(\mathbf{v}) = 0 \tag{1.38}$$

An *incompressible material* is one which can undergo only isochoric motions.

The rate of change of linear momentum of the particles which instantaneously lie within a fixed region Ω is proportional to the resultant force applied to the material occupying Ω.

$$\frac{D}{Dt}\int_{\Omega}\rho\mathbf{v}dV = \int_{\Omega}\rho\mathbf{b}dV + \int_{\partial\Omega}\mathbf{t}(\mathbf{x},t,\mathbf{n})dS \tag{1.39}$$

where $\mathbf{b}$ is the body force per unit mass of the body and $\mathbf{t}(\mathbf{x},t,\mathbf{n})$ is the traction vector acting on the surface of Ω. If the integrands are continuous this will reduce to:

$$\mathrm{div}(\mathbf{T}) + \rho\mathbf{b} = \rho\mathbf{a} \tag{1.40}$$

where $\mathbf{a}$ is the acceleration vector. Equation (1.40) represents the Eulerian form of the balance of linear momentum for a continuum. The Lagrangean form of the above equation is

$$\mathrm{Div}\mathbf{S}^{\mathbf{T}} + \rho_0\mathbf{b} = \rho_0\ddot{\mathbf{x}} \tag{1.41}$$

If $\mathbf{x}$ is the position vector from an arbitrarily chosen origin, then the conservation of angular momentum for a continuum gives

$$\frac{D}{Dt}\int_{\Omega}\rho\mathbf{x}\times\mathbf{v}dV = \int_{\Omega}\rho\mathbf{x}\times\mathbf{b}dV + \int_{\partial\Omega}\mathbf{x}\times\mathbf{t}(\mathbf{x},t,\mathbf{n})dS \tag{1.42}$$

This leads to $\mathbf{T} = \mathbf{T}^{\mathbf{T}}$ in the absence of body couples.

3. Conservation of energy

The kinetic energy (K) and internal energy (E) of a body occupying a region Ω at an instant of time t is given by:

$$K = \frac{1}{2}\int_{\Omega}\rho\mathbf{v}.\mathbf{v}dV \tag{1.43}$$

$$E = \int_{\Omega}\rho e dV \tag{1.44}$$

where e is the internal energy density. If $\mathbf{q}$ denotes the heat-flux vector, then the mathematical formulation of the conservation of energy takes the form

$$\frac{D}{Dt}\int_{\Omega}\rho(\frac{1}{2}\mathbf{v}.\mathbf{v}+e)dV=\int_{\Omega}\rho\mathbf{b}.\mathbf{v}dV+\int_{\partial\Omega}(\mathbf{t}(\mathbf{x},t,\mathbf{n}).\mathbf{v}-\mathbf{q}.\mathbf{n})dS \tag{1.45}$$

From the conservation of linear momentum and the symmetry of the Cauchy stress tensor we arrive at the local Eulerian form of the conservation of energy.

$$\rho\frac{De}{Dt}=\mathbf{T}.\mathbf{D}-\text{grad}\mathbf{q} \tag{1.46}$$

where $\mathbf{D}$ is the symmetric part of the spatial gradient of velocity.

Second law of thermodynamics gives additional constraints on the motion of the body. Since temperature is not of concern for the problem under consideration, we will omit a full thermodynamic formulation required for a general problem in continuum mechanics.

C. Constitutive Equations

Constitutive equations are particular to individual materials, or classes of materials, and they serve to distinguish one material from another. It specifies how the response of a particular class material may differ from another class of material in response to a given stimuli. It specifies the dependence of stress in a body on kinematical variables such as strain tensor or rate of deformation tensor.

1. Elastic body

One commonly used constitutive equation is that the stress tensor is a single valued function of the deformation gradient tensor.

$$\mathbf{T}=\mathbf{f}(\mathbf{F}) \tag{1.47}$$

Materials which satisfy (1.47) are said to be Cauchy elastic. If, in addition to (1.47), we suppose that the whole of the stress power is absorbed into, or derived from, a strain energy function W depending only on $\mathbf{F}$, the material is said to be *Green elastic* or *hyperelastic*.

$$\frac{D}{Dt}\int_{\Omega}\frac{\rho}{\rho_0}W dV = \int_{\Omega}\mathbf{T}.\mathbf{D}dV \tag{1.48}$$

Since (1.48) holds for all parts of the body and since the integrand is continuous, we get,

$$\frac{\rho}{\rho_0}\frac{DW}{Dt} = \mathbf{T}.\mathbf{D} \tag{1.49}$$

2. Material frame indifference

Consider two motions given below.

$$\mathbf{x} = \mathcal{X}(\mathbf{X}, t) \tag{1.50}$$

$$\hat{\mathbf{x}} = \mathbf{Q}(t)\mathcal{X}(\mathbf{X}, t) + \mathbf{c}(t) \tag{1.51}$$

Equation (1.51) describes a motion in which each particle is in the same position as in (1.50), relative to the rest of the body, but at each instant of time, the body has been rotated and translated, as a rigid body from its position in (1.50). Since the relative positions of the particles in both the motions are the same, we expect that W at a particle $\mathbf{X}$ is same in both motions at each instant of time. Mathematically this is equivalent to the requirement that W should be invariant under transformations of (1.50) to arbitrary moving right handed reference frames. This is called the *principle of material frame indifference*. Physically this means that two observers, even if they are in relative motion, will observe the same stress and strain fields in a given body.

The deformation gradient for the motion given by (1.51) is

$$\hat{\mathbf{F}} = \mathbf{QF} \tag{1.52}$$

Since W should be invariant with respect to rigid body motions,

$$W(\mathbf{F}) = W(\mathbf{QF}) \tag{1.53}$$

Since (1.53) holds for all $\mathbf{Q}$ including $\mathbf{R^T}$, W can depend on $\mathbf{F}$ only through $\mathbf{C}$.

$$W(\mathbf{F}) = \tilde{W}(\mathbf{C}) \tag{1.54}$$

Now equation (1.49) reduce to

$$\frac{\rho}{\rho_0}\frac{DW}{Dt} = \frac{\rho}{\rho_0}\frac{\partial W}{\partial \mathbf{C}}\frac{D}{Dt}(\mathbf{C}) = \mathbf{T}.\mathbf{D} \tag{1.55}$$

This gives

$$\mathbf{T} = \frac{\rho}{\rho_0}\mathbf{F}\left\{\left(\frac{\partial W}{\partial \mathbf{C}}\right) + \left(\frac{\partial W}{\partial \mathbf{C}}\right)^T\right\}\mathbf{F^T} \tag{1.56}$$

$$\mathbf{S} = \left\{\left(\frac{\partial W}{\partial \mathbf{C}}\right) + \left(\frac{\partial W}{\partial \mathbf{C}}\right)^T\right\}\mathbf{F^T} \tag{1.57}$$

3. Isotropy

If the mechanical response of a material does not depend on the orientation of the body with respect to the testing apparatus, the body is said to be *isotropic*. Consider two motions given by

$$\mathbf{x} = \mathcal{X}(\mathbf{X}, t) \tag{1.58}$$

$$\bar{\mathbf{x}} = \mathcal{X}(\mathbf{QX}, t) \tag{1.59}$$

If $\mathbf{x} = \bar{\mathbf{x}}$ for all $\mathbf{Q}$ then the material is said to be isotropic. Since the left Cauchy Green stretch tensor of (1.59) is related to that of (1.58) by $\bar{\mathbf{C}} = \mathbf{QCQ^T}$, we have, for an isotropic material,

$$W(\mathbf{C}) = \tilde{W}(\mathbf{QCQ^T}) \tag{1.60}$$

for all $\mathbf{Q}$. Then it follows that W is dependent on $\mathbf{C}$ only through the principal invariants of $\mathbf{C}$ or $\mathbf{B}$. Using (1.56) and the material frame indifference of $\mathbf{T}$, we can express $\mathbf{T}$ as

$$\mathbf{T} = \bar{\mathbf{f}}(\mathbf{B}) = f_0\mathbf{I} + f_1\mathbf{B} + f_{-1}\mathbf{B}^{-1} \tag{1.61}$$

where f_0, f_1 and f_{-1} are scalar functions of the invariants of $\mathbf{B}$. So far we have been dealing with compressible elastic solids. The stress tensor for an incompressible, isotropic, elastic solid has the form

$$\mathbf{T} = -p\mathbf{I} + 2\frac{\partial W}{\partial I_1}\mathbf{B} - 2\frac{\partial W}{\partial I_2}\mathbf{B}^{-1} \tag{1.62}$$

where p is an arbitrary scalar, I_1 and I_2 are the first and second invariants of $\mathbf{B}$.

4. Neo-Hookean material

For an incompressible material, the third invariant of $\mathbf{B}$ is 1 and hence

$$W = W(I_1, I_2) \tag{1.63}$$

Two simple forms of W suggested are one by Treolar

$$W = C_1(I_1 - 3) \tag{1.64}$$

where C_1 is a constant and the other one by Mooney

$$W = C_1(I_1 - 3) + C_2(I_2 - 3) \tag{1.65}$$

where C_1 and C_2 are constants. Materials which have a strain energy function satisfying (1.64) are called *neo-Hookean*. Materials which admit strain energy function of the form (1.65) are called *Mooney-Rivlin* materials. The stress tensor for neo-Hookean

and Mooney-Rivlin materials are of the form

$$\mathbf{T} = -p\mathbf{I} + 2C_1\mathbf{B} \qquad \text{(neo-Hookean)} \tag{1.66}$$

$$\mathbf{T} = -p\mathbf{I} + 2C_1\mathbf{B} - 2C_2\mathbf{B}^{-1} \qquad \text{(Mooney-Rivlin)} \tag{1.67}$$

CHAPTER II

CONSTANT AXIAL DISPLACEMENT RATE EXPERIMENTS OF ASPHALT CONCRETE SPECIMENS

A. Introduction

The response of the asphalt concrete specimens to constant displacement rate tests are measured at different confinement pressures in the experiment. The method of preparation of the asphalt concrete samples and the experimental procedure are presented. The axial force required to keep the constant displacement rate was measured and documented. The experiments were carried out for three different confinement pressures and four different displacement rates. Two different aggregates, namely Limestone and Granite were used for making the asphalt concrete samples. Results exhibit a peak stress in the experiment after which the force required to keep the constant displacment rate decays down to a constant value. This behavior is akin to that of dense granular specimens.

B. Sample Preparation

The preparation of test samples require utmost care and patience to ensure identical samples. Each step in the preparation process is crucial in determining the final response of the asphalt concrete specimens. For instance a reduction of aggregate fines of 3 % can produce a change in fatigue life of up to 300 % (Harvey and Monismith, 1993). The American Society for Testing and Materials (ASTM) has laid down detailed guide lines and testing procedures in order to standardize the testing procedure and the methods of peraparation. For example, ASTM D5-97 relates with the test method for penetration of bituminous materials whereas ASTM D1073-99 deals with

the specification for fine aggregate for bituminous mixtures. We followed the ASTM guidelines in the preparation of the test specimens.

Broadly, the preparation of the sample can be classified into the following:

i) Separation of aggregates into different aggregate size fractions

ii) Mix design

iii) Prepare batch mixes

iv) Preheat the batch mixes and asphalt

v) Batch mixing of asphalt and aggregate

vi) Oven aging

vii) Compaction using a gyratory compactor

viii) Air void determination

1. Aggregate separation

The aggregates used in the highway construction are largely obtained from local supplies of natural rock. This aggregate obtained from the quarry will range from very fine soil to large sized rocks. The properties of the final test sample will largely be determined by the overall size of the aggregates and the relative percentages of various sizes of aggregates in the sample. In order to ensure the same relative percentages of sizes of aggregates in the final sample, one need to blend the aggregates keeping the relative percentage of aggregate sizes constant. Hence it is important that one should first separate the aggregates into different sized particles.

Aggregates are separated into different sized fractions through sieving. Sieves typically used for sieve analysis are: 2 inches, 1 1/2 inches, 1 inch, 3/4 inch, 1/2 inch, 3/8 inch, No. 4, No. 8, No. 16, No. 30, No. 50, No. 100 and No. 200. A 3/8 inch sieve has openings equal to 3/8 inch. A No. 8 sieve has 8 openings per inch. A No.8 sieve size will be smaller than 1/8 inch, since the diameter of the wire should also be

taken into consideration when calculating the sieve size. The sizes of successive sieves usually differ by a factor of 2. So when plotted on a logarithmic scale, the distance between adjacent sieve sizes are equal.

2. Mix design

The objective of a mix design is to determine the right combination of asphalt cement and aggregate that will give a stable and strong pavement structure. Mix design involves selecting the appropriate blend of aggregate sources to produce a proper gradation of mineral aggregate, and selecting the type and amount of asphalt to be used as a binder for that gradation.

Aggregate gradation is the distribution of particle sizes expressed as a percent of the total weight. The gradation of an aggregate is normally expressed as total percent passing various sieve sizes. Gradation of an aggregate can be graphically represented by a gradation curve for which the ordinate is the total percent by weight passing a given size on an arithmetic scale, while the abscissa is the particle size plotted to a logarithmic scale. The gradation of an aggregate is determined by a sieve analysis. Standard proecdures for a dry sieve analysis are given in ASTM C136.

Gradation is one of the most important properties of the aggregate. It influences all the important properties of the asphalt concrete specimen including its strenght, durability, permeability, workability, moisture susceptibility etc. It might seem reasonable to assume that the best gradation is the one that gives the densest particle packing. This densest packing will provide increased stability through increased interparticle contacts and reduced air voids in the aggregate matrix. However a sufficient amount of air voids is required in the asphalt concrete to incorporate enough asphalt cement to ensure durability. Also some amount of air voids is necessary in the mixture to avoid bleeding and rutting of the pavements. Another unwanted effect of the

densest packing is that the mixture will be more sensitive to slight changes in the asphalt content.

One of the best known gradations for maximum density is the Fuller's curve proposed by Fuller and Thompson. The equation for Fuller's maximum density curve is:

$$P = 100(d/D)^n \tag{2.1}$$

where d is the diameter of the sieve size, P is the total percent passing, and D is the maximum size of the aggregate. Studies by Fuller and Thompson showed that the maximum density can be obtained when $n = 0.5$.

The Federal Highway Administration introduced an aggregate grading chart which is based on the Fuller gradation but uses a 0.45 exponent in the equation. The maximum density line in this chart is easily obtained by drawing a straight line from the origin at the lower left of the chart to the actual percentage point of the nominal maximum size. the nominal maximum size is defined as the largest sieve size in the specification upon which any material is retained.

As said before, one may not want the maximum density gradation of aggregates to provide adequate film thickness for maximum durability without bleeding. Hence deviations from the maximum density curves are necessary in order to increase the total voids in the mineral aggregate (VMA). Minimum VMA requirements have been suggested to take this into account. This will vary with the maximum nominal aggregate size. Some asphalt paving agencies prefer that the gradation be approximately parallel to the maximum density grading, and offset from it a few points above or below that line. The requirement for minimum VMA is necessary to ensure that there are sufficient voids in the aggregate to allow enough asphalt to be added to provide a durable mix and sufficient air voids to maintain stability.

Most specifications for HMA (Hot Mix Asphalt) require well or dense graded aggregate gradations with the middle portion of the curves approximately parallel to the maximum density curves. ASTM D 3515 recommends some gradation limits to be used with asphalt mixtures. This is shown in table I. For the most part, the maximum density curve for a 3/4 inch maximum size aggregate fits inside these limits.

A large number of blending methods have been developed to obtain a desired gradation. The suitability of these methods depends on the types of specification and the number of aggregates involved. The basic formula for expressing the combination is

$$p = Aa + Bb + Cc + \dots \tag{2.2}$$

where, p = the percent of material passing a given sieve for the combined aggregates A, B, C, ...

A, B, C, ... = the percent of material passing a given sieve for each aggregate A, B, C,...

a, b, c, ... = proportions of aggregates A, B, C, ... to be used in the blend, $a + b + c, \dots = 1.00$.

The most common method of determining the proportions of aggregate to use to meet specification requirements is through trial and error. A trial blend is selected and calculations are made using equation (2.2) to determine the percent passing each sieve size for the blend. This grading is then compared with the specification requirements. The process is repeated for the critical sieves until a satisfactory or optimum blend is obtained.

An aggregate gradation was obtained which will meet the specification requirements for the both the limestone and granite aggregates to be used for making the

Table I. ASTM D 3515 Gradation specification for dense mixtures

Sieve Size	Dense Mixtures								
	Mix Designation and Nominal Maximum Size of Aggregate								
	2 inch	1 1/2 inch	1 inch	3/4 inch	1/2 inch	3/8 inch	No. 4	No. 8	No. 16
Grading of Total Aggregate (Coarse Plus Fine Plus Filler if Required) Amounts Finer than Each Laboratory Sieve (Square Opening), Percent by Weight									
2 1/2 inch	100	-	-	-	-	-	-	-	-
2 inch	90 to 100	100	-	-	-	-	-	-	-
1 1/2 inch	-	90 to 100	100	-	-	-	-	-	-
1 inch	60 to 80	-	90 to 100	100	-	-	-	-	-
3/4 inch	-	56 to 80	-	90 to 100	100	-	-	-	-
1/2 inch	35 to 65	-	56 to 80	-	90 to 100	100	-	-	-
3/8 inch	-	-	-	56 to 80	-	90 to 100	100	-	-
No. 4	17 to 47	23 to 53	29 to 59	35 to 65	44 to 74	55 to 85	80 to 100	-	100
No. 8	10 to 36	15 to 41	19 to 45	23 to 49	28 to 58	32 to 67	65 to 100	-	95 to 100
No. 16	-	-	-	-	-	-	40 to 80	-	85 to 100
No. 30	-	-	-	-	-	-	25 to 65	-	70 to 95
No. 50	3 to 15	4 to 16	5 to 17	5 to 19	5 to 21	7 to 23	7 to 40	-	45 to 75
No. 100	-	-	-	-	-	-	3 to 20	-	20 to 40
No. 200	0 to 5	0 to 6	1 to 7	2 to 8	2 to 10	2 to 10	2 to 10	-	9 to 20

Table II. Gradation of the mixes

Mix	**Limestone**	**Granite**
Sieve Size,mm	**Percent Passing**	
12.5	98.8	98.8
9.5	79.5	79.5
4.75	46.2	46.2
2.36	31.6	31.6
1.18	24.5	24.5
0.6	17.8	17.8
0.3	11.2	11.2
0.15	6.3	6.3
0.075	1.5	1.5
Pan	0	0

samples. This is shown in table II. The gradation curve is shown in figure 1. The asphalt content was fixed as 4.85 percent of the weight of the mix.

3. Preparation of batch mixes

After the mix design the amount of aggregates required to make one sample is determined. This is obtained by making a trial sample or from past experience. A sligthly higher quantity of aggregates is used to take care of the losses which may occur when transferring and mixing. Once the quantity of aggregates required to make a sample is determined, the required quantity of the different fractions are obtained from the mix design. Then each fraction of aggregate is carefully weighed and mixed together to obtain the batch mix.

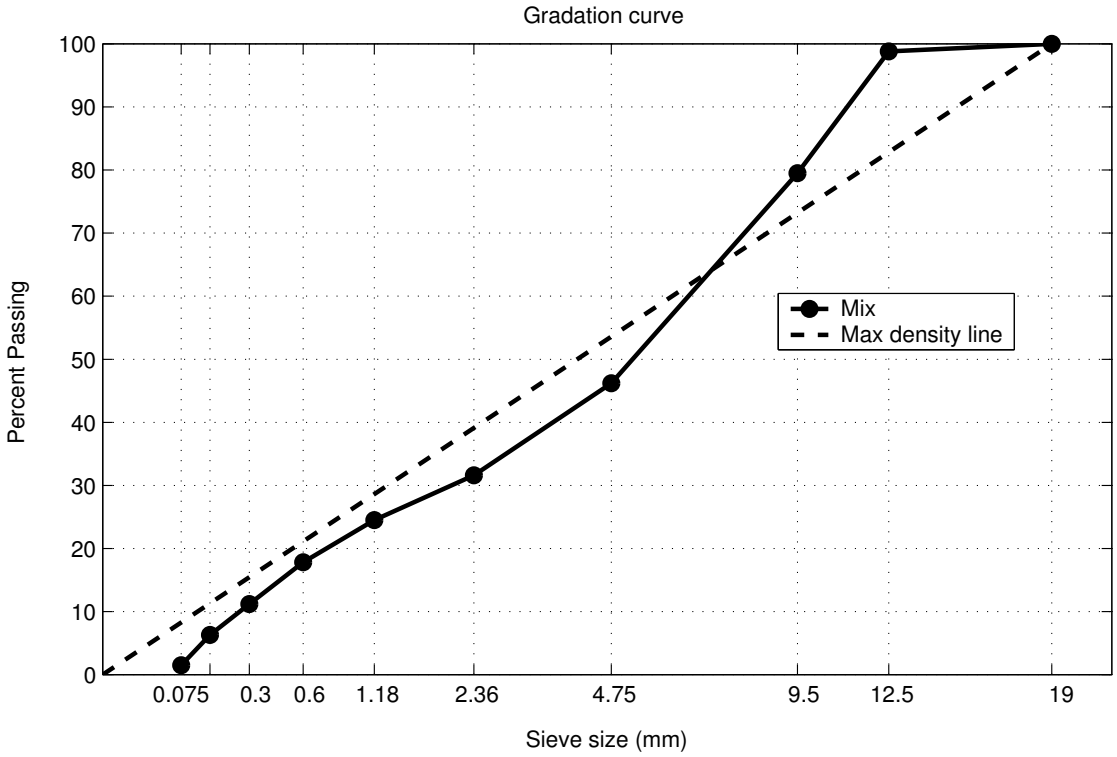

Fig. 1. Gradation used for the aggregates

4. Preheat batch mixes and asphalt to mixing temperature

The batch mix and the asphalt is heated to a mixing temperature of 155^0C. The mixing temperature is the temperature at which the kinematic viscosity of asphalt is 170 ± 20 centistokes. (Centistoke is the viscosity of a liquid in centipoise divided by the density of the liquid at the same temperature. One centipoise is 1/100 th of a poise (1 poise = 1 dyne sec per square centimeter). Water at 68.4 F has an absolute viscosity of one centipoise). The batch mix is kept in the oven at the mixing temperature for at least 4 hours. The asphalt is kept at the mixing temperature for 1 hour. Similarly all the mixing tools and equipment is also preheated to the mixing temperature.

5. Mixing

Once the batch mix is preheated to the mixing temperature, the aggregate is transferred to the preheated mixing bowl. The required amount of asphalt as determined by the binder content in the mix design is carefully poured into the mixing bowl. Extreme care has to be taken at this stage since even a slight increase or decrease in the asphalt content will drastically change the properties of the asphalt concrete specimen. Also care should be taken so as to minimize the loss of asphalt which adheres to the walls of the bowl. The batch mix is mixed with the hot asphalt at the mixing temperature using a mechanical mixer (see figure 2)

6. Oven aging

Once the mixing is completed, the mix is spread out on a relatively wide pan and kept inside the oven at the compaction temperature (135^0C) for 2 hours.. Care should be taken out so as not to lose the fines sticking to the sides of the mixing bowl in

Fig. 2. Mechanical mixer for mixing asphalt and the aggregates

the process. The compaction temperature is the temperature at which the kinematic viscosity of asphalt is 280 ± 30 centistokes. Also the mould and any other equipment used in the compaction process are also kept in the oven at this time.

7. Compaction

After oven aging, the required amount of mix is filled in the mould in three stages. After each stage the mix is hand compacted by poking it with a spatula 20 times. The amount of mix required is fixed by trial and error so as to get the required height of the final compacted specimen. Once the mould is filled, the mix is compacted using a servopac gyratory compactor. The mix is compacted till the air voids in the mix reduces to the required value. In the experiment, the target air voids was 7%. The samples made were of 4 inches diameter and 6 inches height. The mould for the preparation of 4 inch by 6 inch sample is shown in figure 3.

The superpave gyratory compactor has been designed to compact HMA samples

Fig. 3. Mould used in the preparation of the samples

to a density similar to that obtained in the field under traffic. It also tends to orient the aggregate particles similar to that observed in the field. Although the Superpave gyratory has some similarities to other gyratory compactors, it is a unique piece of equipent. There are three parameters that control the compaction effort on the Superpave machine. These settings are vertical pressure, angle of gyration and number of gyrations. For the Superpave procedure, the vertical pressure is set at 600 kPa and the angle of gyration is set at 1.25 degrees. The gyrations are applied at a rate of 30 revolutions per minute. The picture of the superpave gyratory compactor used to compact the mix is shown in figure 4. The final compacted specimen is shown in figure 5 and a cut cross section of the finished sample is shown in figure 6.

Fig. 4. Superpave gyratory compactor

8. Determination of air voids

For determining the air voids, it is first necessary to calcualte both ethe theoretical maximum specific gravity (Rice specific gravity) of the mix and also the bulk specific gravity of the compacted asphalt concrete specimen. The ratio of the weight in air of a unit volume of an uncompacted bituminous paving mixture (without air voids) at a stated temperature to the weight of an equal volume of a gas-free distilled water at a stated temperature is called the Rice Specific Gravity of the mixture. The test method for finding the theoretical maximum specific gravity of bituminous paving mixtures is described in ASTM D 2041. The theoretical maximum specific gravity

Fig. 5. Compacted specimen

can be determined by the following equation:

$$G_{mm} = \frac{A}{A - C} \tag{2.3}$$

where, G_{mm} = rice specific gravity of the asphalt mix, A = mass of oven dry sample in air and C = mass of water displaced by the sample.

The compacted specimens will have air voids in it, and hence the bulk specific gravity of the specimen with the air voids will be less than the rice specific gravity of the mix. The bulk specific gravity of the sample is the ration of the weight of a unit volume of a compacted specimen (including permeable air voids) at 25^0 C to the weight of an equal volume of gas-free distilled water at the same temperature. The detailed procedure for carrying out this test is described in ASTM D 2726. The compacted specimen is dryed in air for 2-3 days. The dry weight of the specimen in air is taken (A). The specimen is immersed in a water bath at 25^0 C for 4 minutes and

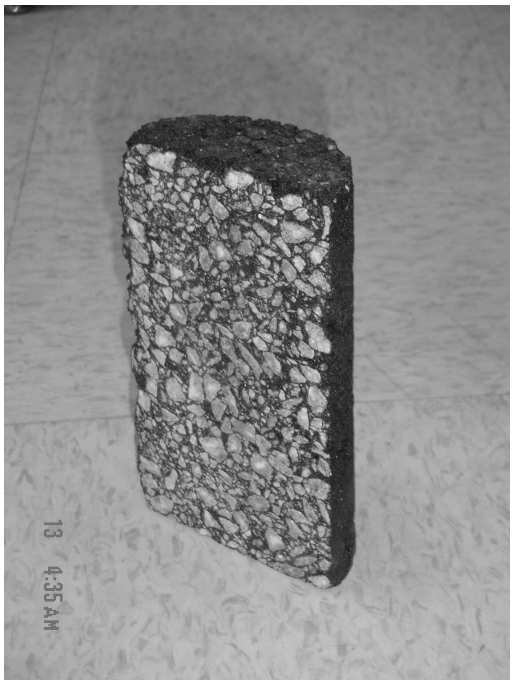

Fig. 6. Cross section of a granite sample

the weight of the specimen in water is determined (C). The specimen is taken out of water, and blotted quickly with a damp towel so as to surface dry the specimen. Then determine the weight of this surface dried specimen by weighing in air (B). Then the bulk specific gravity (G_{mb}) of the sample is given by:

$$G_{mb} = \frac{A}{B - C}. \tag{2.4}$$

The percent of air voids in the specimen can be determined from G_{mb} and G_{mm}:

$$\text{Percent air voids} = \left(1 - \frac{G_{mb}}{G_{mm}}\right) 100. \tag{2.5}$$

Once the actual air voids in the sample is determined, it is compared with the target air voids. Even though the specimen is compacted for the target air voids, the actual air voids in the specimen can be different from this target air voids. If there is too much deviation between the actual air voids and target air voids, the sample

is thrown and a new sample is made. After measuring the air voids, the sample is again air dried for 7 days before conducting the experiment.

C. Constant Displacement Rate Experiments

In the experiment, the sample is subjected to a hydrostatic confining pressure. An axial load is applied so that the top ram moves at a constant displacment rate. The force required to maintain this displacement rate is recorded. A table showing the different confinement pressures and displacement rates used for both type of aggregates is shown in table III. A schematic of the experiment is showin in figure 7.

The experiment was carried out using an MTS machine. All the tests were conducted at 130^0 F. The sample is kept at the testing temperature for 2 hours prior to the test to ensure that the whole sample reaches a steady state temperature. The MTS machine has a temperature chamber which will keep the testing environment at the requisite temperature. During testing, the sample is placed in a triaxial cell and is kept inside the temperature chamber. MTS triaxial cells are configurable for a wide range of tests including triaxial asphalt resarch, soil resilient modulus, dynamics foundation research as well as liquefaction. Air was used as a confining fluid to

Table III. Materials, confinement pressures and displacement rates used in the experiment

Material - Limestone		Material - Georgia Granite	
Confinement Pressure	Disp. rates	Confinement Pressure	Disp. rates
0 psi	0.1 mm/min		0.1 mm/min
15 psi	0.5 mm/min	15 psi	0.5 mm/min
30 psi	2.5 mm/min	30 psi	2.5 mm/min
	12.5 mm/min		12.5 mm/min

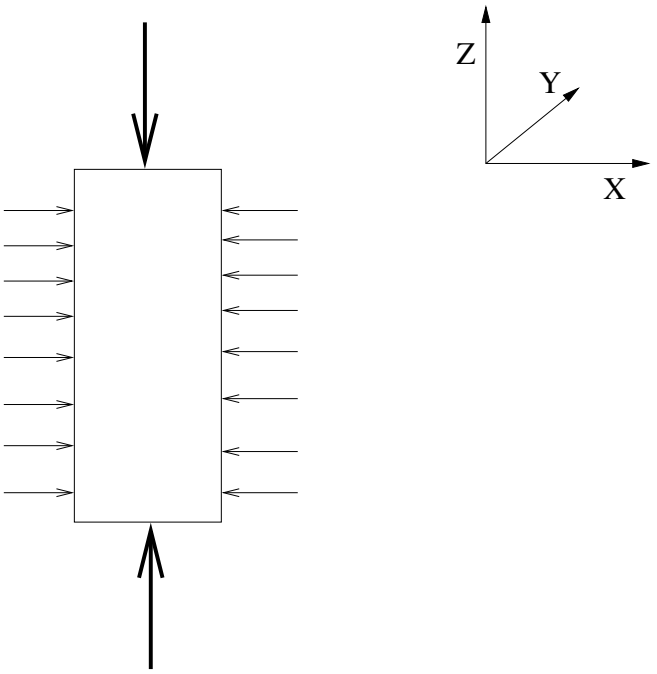

Fig. 7. Schematic of the experiment

generate the confining pressure. A picture of the MTS machine with the temperature chamber is shown in figure 8 and without the temperature chamber is shown in figure 9.

The sample is placed in the triaxial cell and the cell is placed inside temperature chamber. The confinement pressure is brought to a requisite value. The top ram is moved at constant rate. The apparatus is computer controlled and the force required to maintain this displacement rate is recorded. A typical experimental result is shown in figure 10.

Fig. 8. MTS machine with the temperature chamber

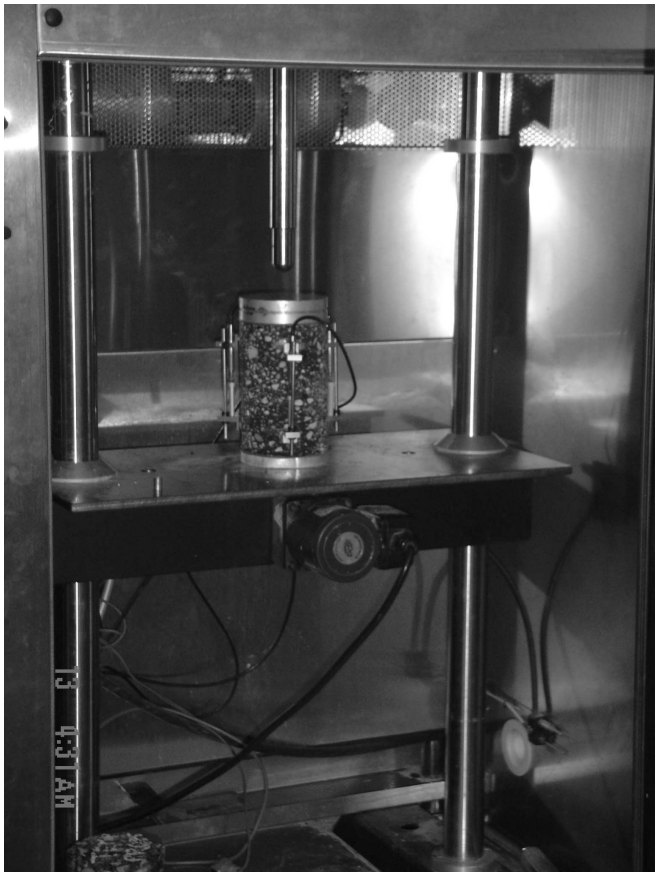

Fig. 9. MTS machine with temperature chamber removed

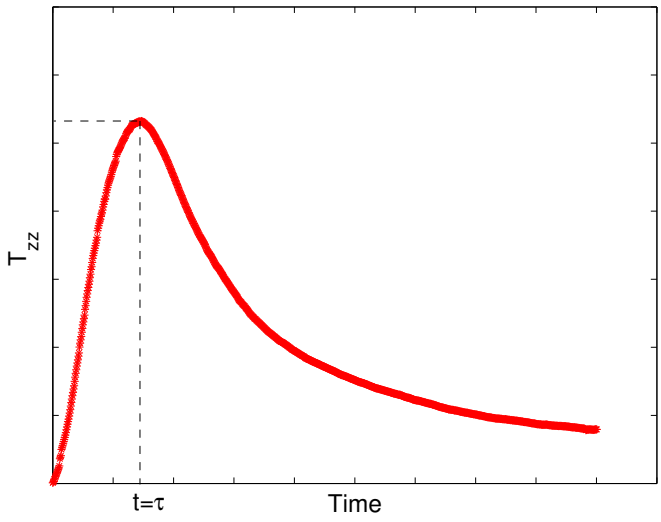

Fig. 10. Typical experimental result

CHAPTER III

AN INCOMPRESSIBLE CONSTITUTIVE MODEL FOR ASPHALT MIXTURES

This study is concerned with the constitutive modeling of asphalt concrete mixtures. The response of the asphalt concrete pavement depends on its internal structure. The internal structure of the asphalt concrete mixture evolves during the loading process. Here we develop a one constituent model for asphalt concrete mixture by associating different natural configurations (stress-free configurations) with distinct internal structures of the body. The evolution of the natural configurations is determined using a thermodynamic criterion, namely the maximization of the rate of dissipation. Making appropriate assumptions concerning the manner in which the body stores and dissipates energy, the constitutive relations for the stress is deduced. Constant displacement rate experiments are carried out at different confinement pressures on asphalt concrete specimens made of two different aggregates - granite and limestone. The efficacy of the model in predicting the mechanical response of asphalt concrete mixtures is shown by corroborating the model predictions with the experimental results.

A. Introduction

Asphalt concrete exhibits nonlinear response even at small strains and the response of the material to different types of loading (tension and compression) is quite different. In addition to this, the response of asphalt concrete is more sensitive to variations in temperature than to the changes in magnitude of the load.

The response of asphalt mixtures depends on the type and percentage of asphalt and aggregates. Asphalt from different crude sources have different chemical compositions and hence different properties. The properties of asphalt are highly dependent

on the type of refining process used. Also the structure of asphalt keeps on changing from the time it leaves the refinery to the final mixing in the hot mix asphalt plant due to repeated heating and cooling during its transport. Depending on the temperature and the type of loading, asphalt can respond like brittle-elastic solid, viscoelastic solid, viscoelastic fluid or a Newtonian fluid. In general, the viscosity of asphalt can be a function of the pressure[1] (see Saal and Koens [4]). In addition to all this, asphalt is extremely sensitive to temperature.

Asphalt concrete is made up of different sizes and fractions of aggregates and this will give rise to air voids in the asphalt concrete during the manufacturing process. The properties of asphalt concrete depend on the type of aggregates, the distribution of the different sizes of aggregate particles, the relative percentage of each of the components and also on the percentage and distribution of air voids.

The initial microstructure of an asphalt concrete mix is largely determined by the manufacturing process. Due to the influence of different activities at the microlevel and also due to the interactions with the environment, there is a progressive change in the microstructure of asphalt concrete. The change in microstructure occurs due to the interaction at the constituent interface or within the constituents themselves. Micro-mechanical activities like reduction of air voids due to traffic densification, debonding and possible rebonding of aggregate contact points under dynamic traffic loads etc., act at the constituent interfaces. The changes in the rheological and microstructural properties of asphalt during its life time and aggregate disintegration are some of the micro-mechanical activities occurring within the constituents. Hence, there is a change in the internal structure of asphalt concrete during its lifetime. This change in internal structure will give rise to a change in the mechanical response of

[1]By pressure here we mean the mean normal stress.

asphalt concrete during its life time. From this discussion it should be clear that one needs a model which will take into account the evolution of the internal structure for modeling asphalt concrete.

Studies assuming asphalt concrete to be viscoelastic use either a spring-dashpot analogy in the form of a Burgers' model (Burgers [5], Lee et al. [6], Monismith and Secor [7] etc.) or some other ad hoc form of viscoelastic constitutive equation (Huang [8], Kim and Little [9]). Huschek [10] modeled asphalt concrete as a three phase system consisting of regions characterized by viscosity, modulus of elasticity and modulus of plasticity. Van der Poel [11] modeled asphalt concrete as concentrated solutions of elastic spheres in an elastic medium. Other models have been proposed that appeal to a "correspondence principle" proposed by Schapery to generate non-linear viscoelastic models from non-linear elastic models (see Park et al.[12]). But it has been shown recently that the models generated by appealing to the correspondence principle cannot satisfy the balance of angular momentum (see Rajagopal and Srinivasa [13]). Studies which take into consideration the microstructure of asphalt concrete have also been carried out. But they either neglect the evolution of the microstructure or take it into account by means of some "shift factors". Nijboer [14] uses the analogy of soil mechanics for modeling asphalt concrete. According to his model, the deformation resistance of asphalt concrete is comprised of an initial resistance, internal friction and viscous resistance. Hills [15] developed models which explains the long term creep behavior of asphalt by characterizing the internal structure of the mix by means of the asphalt thickness. Boutin and Auriault [16] use the analogy of a porous media saturated by a viscoelastic fluid to describe asphalt concrete behavior. Florea [17, 18] uses a viscoplastic potential for developing an elastic/viscoplastic model for asphalt concrete. With the advent of computer tomography and other imaging techniques additional information about the internal structure of asphalt concrete can be obtained.

Masad et al. [19, 20] studied the effect of compaction on the internal structure of asphalt concrete. Masad and Button [21] used a imaging technique to measure the aggregate angularity and texture in asphalt concrete. Recently Murali Krishnan and Rajagopal [22] have modeled asphalt concrete based on a thermodynamic framework which takes into account the effect of microstructure and its evolution.

Most of the traditional methods of modeling asphalt concrete have not considered in detail the change in the microstructure of asphalt concrete as the material deforms, and assume that the Cauchy stress tensor is dependent upon the deformation gradient measured from a single reference configuration. For a material like asphalt concrete whose constitutive behavior is dependent on the internal structure and its change, this would not be correct. Here we will develop a model using a thermodynamical framework which takes into account the evolution of the internal structure of the material. This framework has been used to explain the material response of a large class of materials including multinetwork theory for polymers (Rajagopal and Wineman [23]), traditional plasticity (Rajagopal and Srinivasa [24, 25]), twinning (Rajagopal and Srinivasa [26]), viscoelastic liquids (Rajagopal and Srinivasa [27]) and growth of biological materials (Humphrey and Rajagopal [28]). This model is based on the notion of natural configurations, the preferred natural configuration corresponding to the preferred stress free configuration associated with the current configuration occupied by the body. The natural configurations evolve as the material is deformed, and this change in the natural configuration is associated with the dissipative response of the material. An irreversible thermo-mechanical process is characterized by a positive rate of entropy production. The entropy production can be due to different mechanisms, for e.g., due to phase change, conversion of mechanical working into energy in its thermal form (heat), chemical reactions, heat conduction etc. In this work we use the term rate of dissipation synonymously with the rate of entropy production due

to mechanical working (strictly speaking the rate of dissipation is the product of the rate of entropy production, density and the absolute temperature). The evolution of the natural configurations is determined by a 'maximum rate of dissipation' criterion subject to the constraint that the difference between the stress power and the rate of change of stored energy is equal to the rate of dissipation. A variety of energetically consistent rate type models can be developed by choosing different forms for the stored energy and the rate of dissipation for the material.

The specific influence of different sizes and shapes of aggregates on the overall mechanical behavior of asphalt concrete is difficult to understand completely. In the present work, we will make no attempt to take into account the influence of each of these parameters separately. We will develop a phenomenological model that will capture all these factors in a global sense. However, the framework developed here allows one to easily incorporate these individual components into the model once the specifics of the influence of these components on the behavior of asphalt concrete are obtained. For example if one knows the effect of angularity on the stored energy of the specimen and on the rate of dissipation, one can incorporate those by explicitly taking these into account in the stored energy function and rate of dissipation function in the model.

In their work Murali Krishnan and Rajagopal [22] used a two constituent constrained model for asphalt concrete. In this work we model asphalt concrete as a single constituent. That this itself is effective to capture the behavior of asphalt concrete shows the efficacy of this model. Also, in this study we assume that the rate of dissipation is a function of the mean normal stress. The physical motivation in using such a model is explained later. Using this model we are able to effectively capture the response of asphalt concrete under different confinement pressures. In this work we model the response of asphalt concrete under constant displacement rate

tests as opposed to the creep tests modeled by Murali Krishnan and Rajagopal. As can be seen from the experimental results, the axial stress increases, attains a peak value and then decreases in a constant displacement rate test. The model was able to predict reasonably well this peak stress attained in a constant displacement rate test for various confinement pressures.

We will first introduce the notion of natural configurations and use it to develop a thermodynamically consistent model for asphalt concrete. Constant displacement rate tests on asphalt concrete specimens in triaxial compression have been conducted as part of this study. We then use the developed model to corroborate the experimental results, and we find that the predictions of the model agree reasonably well with the experimental results. It is important to recognize that just one set of material parameters is used to corroborate all the experimental data.

B. Preliminaries

Consider a body B in a configuration $\kappa_R(B)$. For ease of notation, we shall use κ_R to denote $\kappa_R(B)$. Let $\mathbf{X}$ denote a typical position of a material point in κ_R. Let κ_t denote the configuration occupied by the body B at time t. The motion of the body is defined as the one-to-one mapping which assigns to each point $\mathbf{X}$ in κ_R a corresponding point $\mathbf{x}$ in κ_t:

$$\mathbf{x} = \boldsymbol{\chi}_{\kappa_R}(\mathbf{X}, t). \tag{3.1}$$

The deformation gradient $\mathbf{F}_{\kappa_R}$ is defined through:

$$\mathbf{F}_{\kappa_R} = \frac{\partial \boldsymbol{\chi}_{\kappa_R}}{\partial \mathbf{X}}. \tag{3.2}$$

The left and right Cauchy-Green stretch tensors $\mathbf{B}_{\kappa_R}$ and $\mathbf{C}_{\kappa_R}$ are defined through:

$$\mathbf{B}_{\kappa_R} = \mathbf{F}_{\kappa_R}\mathbf{F}_{\kappa_R}^{\mathrm{T}}, \quad \mathbf{C}_{\kappa_R} = \mathbf{F}_{\kappa_R}^{\mathrm{T}}\mathbf{F}_{\kappa_R}. \tag{3.3}$$

Asphalt concrete is a mixture of continuously graded aggregates, filler and asphalt. To model asphalt concrete as a mixture (see Rajagopal and Tao [29]) consisting of different aggregate sizes, asphalt and air voids is extremely difficult. However one can look at the overall mechanical behavior of asphalt concrete as made up of the mechanical behavior of asphalt mastic (asphalt and filler particles) and aggregate matrix (Murali Krishnan and Rajagopal [22], Wood and Goetz [30] etc.). The aggregate matrix acts as a skeleton in which the voids are filled with asphalt mastic and the air voids. The asphalt mastic acts as a lubricant which allows for the relative motion of the aggregate matrix. Such an approach is used in the work of Murali Krishnan and Rajagopal [22]. They used a constrained two constituent model which allowed them to take into account the properties of asphalt mastic and aggregate matrix separately in the model. However, in this work we will model asphalt concrete as a single continuum. The stored energy function and the rate of dissipation function we choose will capture the properties of asphalt mastic and aggregate matrix in a global sense. We will demonstrate that this one constituent model can successfully corroborate the experimental results.

Any acceptable process has to satisfy the appropriate balance laws. The appropriate balance laws for the problem at hand are the conservation of mass, linear and angular momentum and energy. The conservation of mass is given by

$$\dot{\rho} + \rho \, \mathrm{div}(\mathbf{v}) = 0, \tag{3.4}$$

where ρ is the density and $\mathbf{v}$ is the velocity of the material.

We assume the asphalt mixture consisting of aggregate particles and asphalt to be incompressible. This assumption simplifies the problem at hand. In actuality density changes do occur in the bulk of the material (Huang [8]). The density change can be taken into account by appropriately modifying the theory. If we assume the

asphalt mixture to be incompressible, the conservation of mass reduces to

$$\mathrm{div}(\mathbf{v}) = 0. \tag{3.5}$$

The conservation of linear momentum is given by

$$\rho\left[\frac{\partial \mathbf{v}}{\partial t} + (\nabla \mathbf{v})\mathbf{v}\right] = \mathrm{div}\mathbf{T} + \rho\mathbf{g}, \tag{3.6}$$

where $\mathbf{g}$ is the acceleration due to gravity and $\mathbf{T}$ is the Cauchy stress tensor. In the absence of internal couples, conservation of angular momentum implies that the Cauchy stress tensor is symmetric. The conservation of energy gives:

$$\rho\dot{\epsilon} + \mathrm{div}\mathbf{q} = \mathbf{T}\cdot\mathbf{L} + \rho\mathrm{r}, \tag{3.7}$$

where ϵ is the internal energy, $\mathbf{q}$ is the heat flux vector and r is the radiant heating.

The second law of thermodynamics is often used in continuum mechanics in the form of the Clausius-Duhem inequality (see Truesdell and Noll [2]). In the present work we will introduce the second law in the form of an equality by introducing a balance law for entropy. This approach is similar to that of Green and Naghdi [31] and Rajagopal and Srinivasa [25]. The balance law for entropy then takes the form

$$\rho\dot{\zeta} + \mathrm{div}\left(\frac{\mathbf{q}}{\theta}\right) = \rho\frac{\mathrm{r}}{\theta} + \rho\Xi, \quad \Xi \geq 0, \tag{3.8}$$

where ζ is the entropy, θ is the absolute temperature and Ξ is the rate of entropy production. Combining the balance of energy and the balance of entropy gives the reduced energy-dissipation equation:

$$\mathbf{T}\cdot\mathbf{L} - \rho\dot{\psi} - \rho\zeta\dot{\theta} - \frac{\mathbf{q}\cdot\mathrm{grad}\theta}{\theta} = \rho\theta\Xi = \xi \geq 0, \tag{3.9}$$

where ψ is the Helmholtz potential and is given by $\psi = \epsilon - \theta\zeta$ and ξ is the rate of dissipation. We shall assume that the rate of dissipation can be split into two parts,

one pertaining to heat conduction and the other related to the rate at which work is converted into energy in its thermal form. Assuming that the rate of dissipation due to heat conduction is given by

$$\xi_c = -\frac{\mathbf{q} \cdot \text{grad}\theta}{\theta} \geq 0, \tag{3.10}$$

we can rewrite (3.9) as:

$$\mathbf{T} \cdot \mathbf{L} - \rho\dot{\psi} - \rho\zeta\dot{\theta} = \xi_d \geq 0. \tag{3.11}$$

In this work, we use the reduced energy-dissipation equation in the above form to place restrictions on the constitutive equations.

C. Modeling of Asphalt Concrete

Corresponding to each current configuration κ_t we associate a natural configuration $\kappa_{p(t)}$. In figure 11, κ_R is a reference configuration, κ_t is the configuration currently occupied by the material and $\kappa_{p(t)}$ is the natural configuration associated with the material that is currently in the configuration κ_t. The preferred natural configuration $\kappa_{p(t)}$ corresponds to the preferred stress free configuration associated with the current configuration κ_t occupied by the body at time t, i.e., this is the configuration the body attains on the removal of the external stimuli, given a class of admissible processes. For a more detailed discussion of natural configurations the readers are referred to the papers by Rajagopal [32], Rajagopal and Srinivasa [27, 24, 25] and Rao and Rajagopal [33]. Most real materials can exist in a variety of stress free configurations and these configurations are not necessarily related to each other by rigid body motions. It is possible for materials to possess more than one natural configuration (see Rajagopal and Srinivasa [26, 27, 34], Rao and Rajagopal [33]). In polymeric materials with more than one relaxation mechanism, it is common to use models with more than

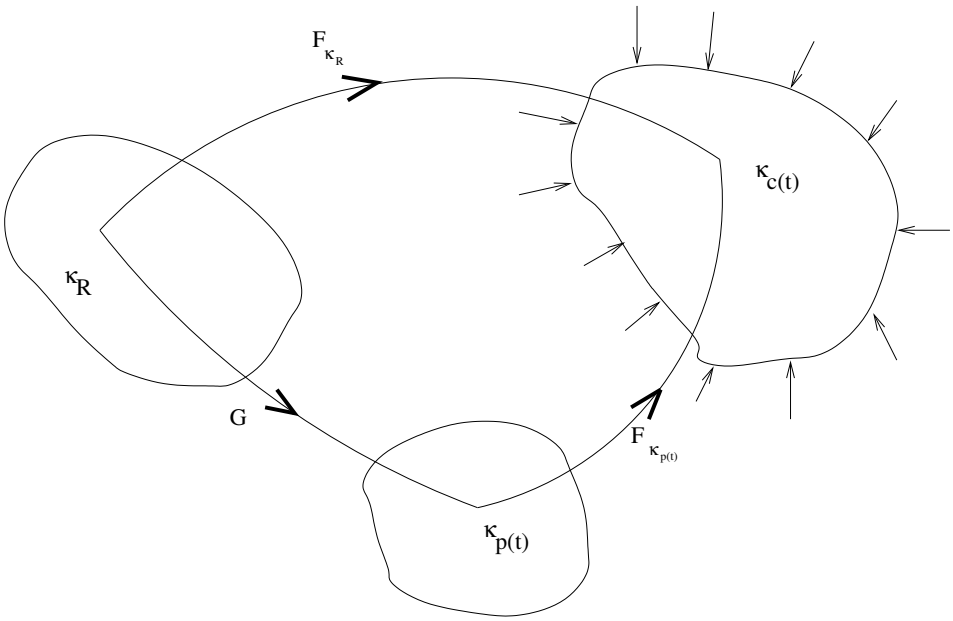

Fig. 11. Natural configuration associated with the current configuration

one relaxation time. These models with multiple relaxation times are equivalent to viscoelastic fluid models with multiple sets of natural configuration. Murali Krishnan and Rajagopal [35]) assign more than one relaxation mechanism for asphalt concrete, one pertaining to the movement of the aggregate particles and the other pertaining to asphalt mastic (see also Wood and Goetz [30]). But in this work we shall assume just one relaxation mechanism which will effectively capture the overall relaxation of the asphalt mixture. The relaxation mechanism of the model is determined by the evolution of the natural configuration which in turn is determined by the rate of dissipation function. Since we are assuming only one relaxation mechanism, we shall associate only one natural configuration ($\kappa_{p(t)}$) corresponding to each current configuration (κ_t).

We assume that the asphalt mixture has an instantaneous elastic response from the natural configuration $\kappa_{p(t)}$. The gradient of the mapping from $\kappa_{p(t)}$ to κ_t is defined as $\mathbf{F}_{\kappa_{p(t)}}$. The natural configuration $\kappa_{p(t)}$ is not fixed as in the case of an elastic solid

but evolves as the material is deformed. This change in the natural configuration is associated with the dissipative response of the material. We define $\mathbf{G}$ to be the mapping between the tangent spaces of κ_R and the natural configuration $\kappa_{p(t)}$, i.e.,

$$\mathbf{G} = \mathbf{F}_{\kappa_R \to \kappa_{p(t)}} = \mathbf{F}^{-1}_{\kappa_{p(t)}} \mathbf{F}_{\kappa_R}. \tag{3.12}$$

We define:

$$\mathbf{B}_{\kappa_{p(t)}} = \mathbf{F}_{\kappa_{p(t)}} \mathbf{F}^{T}_{\kappa_{p(t)}}. \tag{3.13}$$

We define the velocity gradient $\mathbf{L}$ in the conventional way and introduce a corresponding velocity gradient $\mathbf{L}_{\kappa_{p(t)}}$ through (Rajagopal and Srinivasa [27]),

$$\mathbf{L} = \dot{\mathbf{F}}_{\kappa_R} \mathbf{F}^{-1}_{\kappa_R}, \tag{3.14}$$

$$\mathbf{L}_{\kappa_{p(t)}} = \dot{\mathbf{G}} \mathbf{G}^{-1}. \tag{3.15}$$

Also,

$$\mathbf{D}_{\kappa_{p(t)}} = \frac{1}{2}(\mathbf{L}_{\kappa_{p(t)}} + \mathbf{L}^{T}_{\kappa_{p(t)}}), \tag{3.16}$$

$$\mathbf{D} = \frac{1}{2}(\mathbf{L} + \mathbf{L}^{T}). \tag{3.17}$$

We define the Oldroyd derivative of $\mathbf{B}_{\kappa_{p(t)}}$ as:

$$\overset{\nabla}{\mathbf{B}} := \dot{\mathbf{B}}_{\kappa_{p(t)}} - \mathbf{L}\mathbf{B}_{\kappa_{p(t)}} - \mathbf{B}_{\kappa_{p(t)}}\mathbf{L}^{T} = -2\mathbf{F}_{\kappa_{p(t)}} \mathbf{D}_{\kappa_{p(t)}} \mathbf{F}^{T}_{\kappa_{p(t)}}, \tag{3.18}$$

where the inverted triangle denotes the upper convected Oldroyd derivative and the superposed dot is the material time derivative. Specifying $\mathbf{D}_{\kappa_{p(t)}}$ amounts to prescribing the manner in which the underlying natural configurations evolve. We shall assume that the motion associated with the natural configurations are also isochoric, i.e.,

$$tr(\mathbf{D}_{\kappa_{p(t)}}) = 0. \tag{3.19}$$

Since asphalt concrete is a mixture of different sized aggregate particles and asphalt, it exhibits anisotropic behavior. The initial anisotropy of an asphalt concrete specimen depends on the aggregate characteristics, aggregate gradation and the compaction method used to prepare the specimen (Masad et al. [19, 20]). Since the internal structure of asphalt concrete keeps on evolving during loading, the anisotropy of the material also evolves with it.

As we observed before, the initial anisotropy and the evolution of the anisotropy in an asphalt concrete specimen is highly dependent on the aggregate characteristics, aggregate gradation, the compaction method used and the testing condition. One big obstacle in taking into account anisotropy in modeling asphalt concrete is the lack of experimental data. The modern tools of X-Ray Computed Tomography (CT) and Image Analysis Techniques (IAT) look more promising in this regard. Even if one knows that the relative aggregate orientation is horizontal in a specimen prepared using a gyratory compactor one still does not have the experimental data which can correlate this with the response of the specimen. This gets further complicated by the fact that the internal structure and the anisotropy of the material keep on evolving during the loading process. Similarly one should have enough experimental data to conclude how the aggregate characteristics, gradation etc., affects the anisotropy of the final compacted specimen. It is imperative to resolve the above issues before one can take anisotropy into account in modeling asphalt concrete.

The anisotropy can be taken into account in modeling asphalt concrete using the framework developed here. One needs to take into account not only the initial anisotropy but also its evolution as the material deforms. The anisotropy can be built into the framework by requiring the stored energy and the rate of dissipation function to depend on the directions of anisotropy also. Here for simplicity we model asphalt concrete as an isotropic material.

The internal energy and the entropy are assumed to depend on the temperature θ and the first two invariants of $\mathbf{B}_{\kappa_{p(t)}}$: $I_{\kappa_{p(t)}}, II_{\kappa_{p(t)}}$.

$$\epsilon = \epsilon(\theta, I_{\kappa_{p(t)}}, II_{\kappa_{p(t)}}), \tag{3.20}$$

$$\zeta = \zeta(\theta, I_{\kappa_{p(t)}}, II_{\kappa_{p(t)}}), \tag{3.21}$$

where $I_{\kappa_{p(t)}} = \mathrm{tr}(\mathbf{B}_{\kappa_{p(t)}}), II_{\kappa_{p(t)}} = \mathrm{tr}(\mathbf{B}_{\kappa_{p(t)}}{}^2)$. Hence the Helmholtz potential has the form:

$$\psi = \psi(\theta, I_{\kappa_{p(t)}}, II_{\kappa_{p(t)}}). \tag{3.22}$$

The above assumptions are tantamount to assuming that the instantaneous elastic response is that of an incompressible material that is isotropic with respect to $\kappa_{p(t)}$.

Since asphalt concrete is a mixture of aggregate particles of various sizes bound together by asphalt, a higher confinement pressure will increase the resistance to deformation. The pressure in the lateral direction will mobilize more aggregate interlock and hence the deformation resistance of asphalt concrete is a function of the confinement pressure. The fact that the confinement pressure will increase the resistance to deformation in well known (see Endersby [36], Nijboer [14]). Since the rate of dissipation is a measure of the rate at which work is converted to energy in its thermal form, it should in some way reflect this dependence on the confinement pressure. Hence we assume the following form for the rate of dissipation function:

$$\xi = \xi(\theta, \mathbf{B}_{\kappa_{p(t)}}, \mathbf{D}_{\kappa_{p(t)}}, tr(\mathbf{T})). \tag{3.23}$$

The dependence of the rate of dissipation on the pressure is not new. In general, the rate of dissipation of a fluid is dependent on the viscosity of the fluid see Stokes [37], Bridgman [38]). While the dependence of viscosity on pressure is not immediately obvious in common flows like the flow of water in a pipe, it can have significant effect

when the change in pressure is sufficiently large (Hron et al. [39]). It is possible that for liquids such as water, the effect of change in pressure on density is not significant over a wide range of pressures but viscosity can change significantly (even exponently) with pressure. Extensive experiments have been carried out to find the effect of pressure on the viscosity of various fluids (Bridgman [38]). Recently several experiments have been carried out which also document the dependence of viscosity on pressure (mean normal stress) (see Cutler et al. [40], Griest et al. [41], Johnson and Cameron [42] and Johnson and Tevaarwerk [43]).

Now we shall give specific forms for constitutive equations. For the internal energy we assume that, it is a linear function of temperature and that the change in internal energy due to deformation is dependent on the first invariant of $\mathbf{B}_{\kappa_{p(t)}}$.

$$\epsilon = C\theta + A + f(I_{\kappa_{p(t)}}), \tag{3.24}$$

$$\zeta = C\ln(\theta) + \mathrm{B}. \tag{3.25}$$

where $I_{\kappa_{p(t)}} = \mathrm{tr}(\mathbf{B}_{\kappa_{p(t)}})$.

We assume the following form for the rate of dissipation function:

$$\xi = \eta_1(\mathbf{B}_{\kappa_{p(t)}}, \mathrm{tr}(\mathbf{T}))\mathbf{D}_{\kappa_{\mathrm{p(t)}}} \cdot \mathbf{B}_{\kappa_{\mathrm{p(t)}}}\mathbf{D}_{\kappa_{\mathrm{p(t)}}}. \tag{3.26}$$

Here $\eta_1(\mathbf{B}_{\kappa_{p(t)}})$ is the viscosity of the material.

Substituting (4.24) and (4.25) into (3.9), we get:

$$\mathbf{T} \cdot \mathbf{L} - \rho\dot{f}(I_{\kappa_{p(t)}}) = \xi. \tag{3.27}$$

Since we are assuming asphalt concrete to be isotropic, we can choose, without any loss of generality, the natural configurations $\kappa_{p(t)}$ to be such that

$$\mathbf{F}_{\kappa_{p(t)}} = \mathbf{V}_{\kappa_{p(t)}}. \tag{3.28}$$

Using (4.10) for $\dot{\mathbf{B}}_{\kappa_{p(t)}}$ and using (3.28), we get,

$$\left[\mathbf{T} - 2\rho\frac{\partial f}{\partial I_{\kappa_p(t)}}\mathbf{B}_{\kappa_{p(t)}}\right]\cdot\mathbf{D} = \left[\eta_1(\mathbf{B}_{\kappa_{p(t)}}, \mathrm{tr}(\mathbf{T}))\mathbf{B}_{\kappa_{p(t)}}\mathbf{D}_{\kappa_{p(t)}} - 2\rho\frac{\partial f}{\partial I_{\kappa_p(t)}}\mathbf{B}_{\kappa_{p(t)}}\right]\cdot\mathbf{D}_{\kappa_{p(t)}}. \tag{3.29}$$

Since we are looking for forms that are sufficient to satisfy the above equation, and since we are assuming that the material is incompressible, we can stipulate

$$\mathbf{T} = -p\mathbf{I} + 2\rho\frac{\partial f}{\partial I_{\kappa_p(t)}}\mathbf{B}_{\kappa_{p(t)}}. \tag{3.30}$$

We will choose the specific form

$$f(I_{\kappa_p(t)}) = \frac{1}{2\rho}\mu(I_{\kappa_p(t)})(I_{\kappa_p(t)} - 3) \tag{3.31}$$

for $f(I_{\kappa_p(t)})$. This means that we are assuming that the storage of energy due to deformation in the material is similar to that of a neo-Hookean material. We shall choose

$$\mu_1(I_{\kappa_{p(t)}}) = \mu(I_{\kappa_{p(t)}}) + (I_{\kappa_{p(t)}} - 3)\frac{\partial\mu(I_{\kappa_{p(t)}})}{\partial I_{\kappa_{p(t)}}}. \tag{3.32}$$

Then (3.30) becomes

$$\mathbf{T} = -p\mathbf{I} + \mu_1(I_{\kappa_{p(t)}})\mathbf{B}_{\kappa_{p(t)}}. \tag{3.33}$$

Note that since $tr(\mathbf{D}_{\kappa_{p(t)}}) = 0$ (natural configuration is also one of the possible configurations that the body can occupy),

$$\mathbf{T}\cdot\mathbf{D}_{\kappa_{p(t)}} = \eta_1(\mathbf{B}_{\kappa_{p(t)}}, tr(\mathbf{T}))\mathbf{B}_{\kappa_{p(t)}}\mathbf{D}_{\kappa_{p(t)}}\cdot\mathbf{D}_{\kappa_{p(t)}} = \xi. \tag{3.34}$$

Equation (4.27) imposes a constraint in the evolution of natural configurations. At this point, we do not know how the natural configurations evolve. We assume that for a fixed $\mathbf{B}_{\kappa_{p(t)}}$ and $\mathbf{D}$, $\mathbf{D}_{\kappa_{p(t)}}$ should be such that it maximizes the rate of entropy production. We maximize ξ subject to the constraints (4.27) and $tr(\mathbf{D}_{\kappa_{p(t)}}) = 0$. One

could also keep $\mathbf{B}_{\kappa_{p(t)}}$ fixed and maximize ξ with respect to both $\mathbf{D}$ and $\mathbf{D}_{\kappa_{p(t)}}$ (see Rajagopal and Srinivasa [44]).

This gives

$$\mathbf{V}_{\kappa_{p(t)}}\mathbf{D}_{\kappa_{p(t)}}\mathbf{V}_{\kappa_{p(t)}} = \frac{\mu_1(I_{\kappa_{p(t)}})}{\eta_1(\mathbf{B}_{\kappa_{p(t)}}, tr(\mathbf{T}))}\left[\mathbf{B}_{\kappa_{p(t)}} - \lambda\mathbf{I}\right]. \tag{3.35}$$

Taking the dot product of (3.35) with $\mathbf{B}^{-1}_{\kappa_{p(t)}}$ and noting that $tr(\mathbf{V}_{\kappa_{p(t)}}\mathbf{D}_{\kappa_{p(t)}}\mathbf{V}^{-1}_{\kappa_{p(t)}}) = tr(\mathbf{D}_{\kappa_{p(t)}}) = 0$,

$$\lambda = \frac{3}{tr(\mathbf{B}^{-1}_{\kappa_{p(t)}})}. \tag{3.36}$$

So (4.10) becomes

$$-\frac{1}{2}\overset{\nabla}{\mathbf{B}} = \frac{\mu_1(I_{\kappa_{p(t)}})}{\eta_1(\mathbf{B}_{\kappa_{p(t)}}, tr(\mathbf{T}))}\left[\mathbf{B}_{\kappa_{p(t)}} - \lambda\mathbf{I}\right]. \tag{3.37}$$

Hence the evolution equation is given by (4.43) and the stress is given by (4.26). So far we have not assumed any form for the functions $\mu_1(I_{\kappa_{p(t)}})$, or $\eta_1(\mathbf{B}_{\kappa_{p(t)}}, tr(\mathbf{T}))$.

D. Experiment - Constant axial displacement rate testing of asphalt mixtures

There are different kinds of tests used in the industry to measure the response characteristics of asphalt concrete. One is the performance test which measures a mixture response characteristic or parameter that is closely related to the occurrence of a particular pavement distress. NCHRP 465 [45] details some of the performance test methods and asphalt concrete mixture responses that are related to two types of pavement distress - permanent deformation and fracture. The others are tests in which some material property is sought to be measured. In the experiment that was carried out,the main purpose was to corroborate the model with the experimental data.

The triaxial test in its present form owes much to Buisman [46] who used it for testing sand and clay and to Stanton and Hveem [47] who used it for characterizing asphalt pavement materials. If one were to confine a fluid in a cylinder and apply a

vertical load, then the lateral pressure must equal the normal stress in the vertical direction. On the other hand if the material is rigid, then there is no need for any confining pressure to balance the vertical load (Endersby [36]). Hence the amount of confinement pressure required to balance a given vertical load measures in some sense the strength of the material. This is the central notion used in the triaxial test. The hypothesis postulated by Haar and von Karman [48], that the intermediate principal stress is either equal to the major or the minor principal stress, is intuitively used in triaxial testing. In the triaxial test, the stresses acting on the specimen closely approach the system of stresses existing in a flexible pavement when it is supporting a load.

Table IV. Mix design factors for the mixes

Mix	**Limestone**	**Granite**
Binder Type	PG 64-22	PG 64-22
Binder Content, %	4.85	4.86
Maximum Specific Gravity	2.47	2.471
Avg. Measure Air void, %	6.7	6.89
SD of Air Voids	0.25	0.30
Specimen Height, mm	157.5	157.5
Specimen Diameter, mm	101.6	101.6

In practice, the triaxial test is used to study the permanent deformation of pavements. The rate at which permanent deformation accumulates increases rapidly at higher temperatures. Hence any laboratory testing to study permanent deformation of asphalt concrete must be conducted at temperatures simulating the highest temperatures in the actual pavement service. Also, the permanent deformation of an asphalt concrete pavement depends on the rate at which it is deformed. In the exper-

iment conducted, the response of the asphalt mixture was studied at different axial displacement rates.

Table V. Gradation of limestone and granite mixes

Mix	**Limestone**	**Granite**
Sieve Size,mm	**Percent Passing**	
12.5	98.8	98.8
9.5	79.5	79.5
4.75	46.2	46.2
2.36	31.6	31.6
1.18	24.5	24.5
0.6	17.8	17.8
0.3	11.2	11.2
0.15	6.3	6.3
0.075	1.5	1.5
Pan	0	0

In the experiments conducted in this study, a simple triaxial compression test at a constant displacement rate is used to capture the response characteristics of asphalt mixtures (see figure 12). Cylindrical test specimens of asphalt concrete of 4 in (101.6 mm) diameter and 6.2 in (157.5 mm) height were compacted using a ServoPac gyratory compactor (see table IV). Two different mixes with different aggregate types (granite and limestone) were used to make the specimens. The gradations of the different aggregates are shown in table V. The same gradation was used for both the aggregate types. The target air void content was 7 percent. The specimens were subjected to a compressive load in the axial direction at a given confinement pressure such that the axial displacement rate is kept constant. The axial force required to

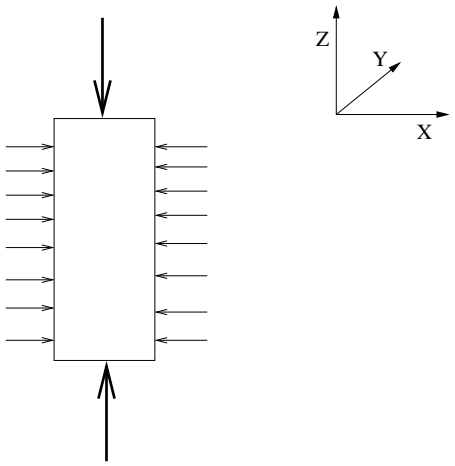

Fig. 12. Experiment

maintain the given displacement rate is measured. The experiment was carried out at four displacement rates (0.1 mm/min, 0.5 mm/min, 2.5 mm/min and 12.5 mm/min) at three confining pressures (0 psi, 15 psi, 30 psi) at a temperature of 130^0 F (see table VI). Each experiment was repeated with at least two samples. A typical experimental result is shown in figure 13.

Table VI. Table showing the different materials, confinement pressures and displacement rates used

Material - Limestone		Material - Georgia Granite	
Confinement Pressure	Disp. rates	Confinement Pressure	Disp. rates
0 psi	0.1 mm/min		0.1 mm/min
15 psi	0.5 mm/min	15 psi	0.5 mm/min
30 psi	2.5 mm/min	30 psi	2.5 mm/min
	12.5 mm/min		12.5 mm/min

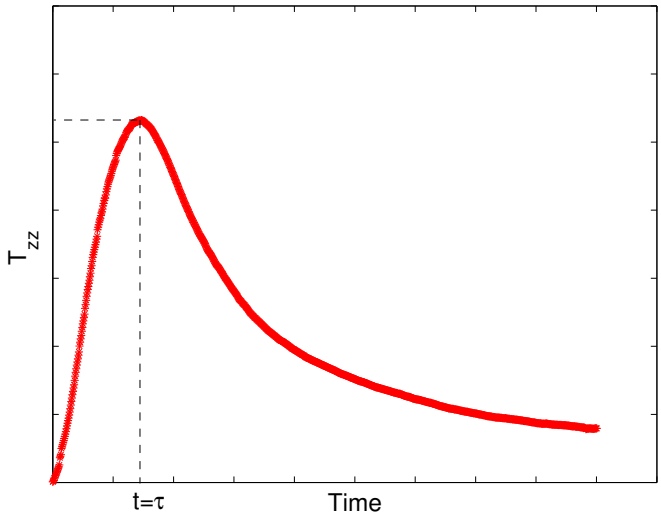

Fig. 13. Typical experimental result

E. Corroboration of the model with the experimental data

For simplicity, we will assume that the deformation is homogeneous and is given by

$$r = \frac{1}{\sqrt{\Lambda(t)}}R,\ \theta = \Theta,\ z = \Lambda(t)Z \tag{3.38}$$

in cylindrical polar co-ordinates.

The assumption that the deformation is homogeneous can be called into question for the following reason: the deformation field is not valid towards the end of the specimen because of the end effects. End restraint was long recognized as the cause for strong inhomogeneous responses, such as barreling and localization of deformations (Bishop and Henkel [49], Sowers [50], Roscoe et al. [51]). This is a question of concern and every effort was taken during the experiment to minimize the end effects. Both the ends of the specimen were covered with a double layer of elastic rubber membrane with a layer of silicone grease between the rubber membranes. This will considerably reduce the end effects and will ensure that only vertical forces are transmitted from the ram to the specimen during testing (Rowe and Barden [52], Bishop and Green

[53]).

Towards the end of the experiment the specimen starts barreling out which is clearly an inhomogeneous deformation. But the time scale associated with the inhomogeneous deformation is very short compared to that of the rest of the experiment and it is reasonable to assume that the entire deformation is homogeneous.

The deformation gradient is given by

$$\mathbf{F}_{\kappa_R} = \text{diag}\left(\frac{1}{\sqrt{\Lambda}},\ \frac{1}{\sqrt{\Lambda}},\ \Lambda\right). \tag{3.39}$$

Note that $\det(\mathbf{F}_{\kappa_R})$=1 for the assumed deformation field. The left Cauchy-Green stretch tensor and the velocity gradient are given by

$$\mathbf{B}_{\kappa_R} = \text{diag}\left(\frac{1}{\Lambda},\ \frac{1}{\Lambda},\ \Lambda^2\right),\quad \mathbf{L} = \mathbf{D} = \frac{\dot{\Lambda}}{\Lambda}\text{diag}\left(-\frac{1}{2},\ -\frac{1}{2},\ 1\right). \tag{3.40}$$

Let's assume that $\mathbf{B}_{\kappa_{p(t)}}$ has the form:

$$\mathbf{B}_{\kappa_{p(t)}} = \text{diag}\left(B_{\kappa_{p(t)}rr},\ B_{\kappa_{p(t)}\theta\theta},\ B_{\kappa_{p(t)}zz}\right). \tag{3.41}$$

The constitutive equation is given by (4.26):

$$\mathbf{T} = -p\mathbf{I} + \mu_1(I_{\kappa_p(t)})\mathbf{B}_{\kappa_{p(t)}}. \tag{3.42}$$

We shall assume that $\mathbf{B}_{\kappa_{p(t)}}$ is a function of time only and $B_{\kappa_{p(t)}rr},\ B_{\kappa_{p(t)}\theta\theta},\ B_{\kappa_{p(t)}zz}$ are not functions of $r,\ \theta$ or z. Eliminating p from (4.46), we obtain

$$T_{rr} - T_{\theta\theta} = \mu_1(I_{\kappa_{p(t)}})\left(B_{\kappa_{p(t)}rr} - B_{\kappa_{p(t)}\theta\theta}\right), \tag{3.43}$$

$$T_{zz} - T_{rr} = \mu_1(I_{\kappa_{p(t)}})\left(B_{\kappa_{p(t)}zz} - B_{\kappa_{p(t)}rr}\right). \tag{3.44}$$

Since $\det(\mathbf{B}_{\kappa_{p(t)}}) = 1$, $\mathrm{tr}(\mathbf{B}^{-1}_{\kappa_{p(t)}})$ can be written as

$$\begin{aligned} tr(\mathbf{B}^{-1}_{\kappa_{p(t)}}) &= \frac{1}{B_{\kappa_{p(t)}rr}} + \frac{1}{B_{\kappa_{p(t)}\theta\theta}} + \frac{1}{B_{\kappa_{p(t)}zz}} \\ &= B_{\kappa_{p(t)}rr}B_{\kappa_{p(t)}\theta\theta} + B_{\kappa_{p(t)}rr}B_{\kappa_{p(t)}zz} + B_{\kappa_{p(t)}\theta\theta}B_{\kappa_{p(t)}zz}. \end{aligned} \tag{3.45}$$

The evolution equation (4.43) becomes

$$-\frac{1}{2}\left(\dot{B}_{\kappa_{p(t)}rr} + \frac{\dot{\Lambda}}{\Lambda}B_{\kappa_{p(t)}rr}\right) = \frac{\mu_1(I_{\kappa_{p(t)}})}{\eta_1(\mathbf{B}_{\kappa_{p(t)}}, tr(\mathbf{T}))}\left(B_{\kappa_{p(t)}rr} - \frac{3}{tr(\mathbf{B}^{-1}_{\kappa_{p(t)}})}\right), \tag{3.46}$$

$$-\frac{1}{2}\left(\dot{B}_{\kappa_{p(t)}\theta\theta} + \frac{\dot{\Lambda}}{\Lambda}B_{\kappa_{p(t)}\theta\theta}\right) = \frac{\mu_1(I_{\kappa_{p(t)}})}{\eta_1(\mathbf{B}_{\kappa_{p(t)}}, tr(\mathbf{T}))}\left(B_{\kappa_{p(t)}\theta\theta} - \frac{3}{tr(\mathbf{B}^{-1}_{\kappa_{p(t)}})}\right), \tag{3.47}$$

$$-\frac{1}{2}\left(\dot{B}_{\kappa_{p(t)}zz} - 2\frac{\dot{\Lambda}}{\Lambda}B_{\kappa_{p(t)}zz}\right) = \frac{\mu_1(I_{\kappa_{p(t)}})}{\eta_1(\mathbf{B}_{\kappa_{p(t)}}, tr(\mathbf{T}))}\left(B_{\kappa_{p(t)}zz} - \frac{3}{tr(\mathbf{B}^{-1}_{\kappa_{p(t)}})}\right). \tag{3.48}$$

We have one more additional equation from incompressibility:

$$\det(\mathbf{B}_{\kappa_{\mathrm{p(t)}}}) = \mathrm{B}_{\kappa_{\mathrm{p(t)rr}}}\mathrm{B}_{\kappa_{\mathrm{p(t)}\theta\theta}}\mathrm{B}_{\kappa_{\mathrm{p(t)zz}}} = 1. \tag{3.49}$$

Hence we have six equations (3.43,4.50,4.52-4.55) and five unknowns ($T_{\theta\theta}$, T_{zz}, $B_{\kappa_{p(t)}rr}$, $B_{\kappa_{p(t)}\theta\theta}$, $B_{\kappa_{p(t)}zz}$). It looks like the system is over-constrained. But it can be easily shown that (3.48) is a linear combination of (4.52), (4.53) and (4.55). Thus, there are as many equations as unknowns. For solving this problem, we will use a form for $\mathbf{B}_{\kappa_{p(t)}}$ which is similar to $\mathbf{B}_{\kappa_R}$.

$$\mathbf{B}_{\kappa_{p(t)}} = \mathrm{diag}\left(B(t),\ B(t),\ \frac{1}{B(t)^2}\right). \tag{3.50}$$

It is easy to see that the above form for $\mathbf{B}_{\kappa_{p(t)}}$ will satisfy (4.55) and that equations (4.52, 4.53, 3.48) will reduce to a single ordinary differential equation for $B(t)$.

The physical and chemical properties of the aggregates influences the response of the final asphalt concrete specimen (Stephens and Sinha [54] etc.,). Basic physical and mechanical properties (such as density, porosity, mechanical response) and

physicochemical properties (such as water adsorption, adhesion, stripping) are functions of the composition and structure of the minerals in the aggregate. Aggregate mineralogy has a strong influence on adhesion and moisture damage of the asphalt pavement. Aggregates with certain mineral types bind better with asphalt cement. For example, carbonate aggregates (limestone) bonds better with asphalt cement than siliceous aggregates like gravel. Most aggregates tend to be either basic or acidic in nature. Siliceous aggregates such as sandstone, quartz and siliceous gravel become negatively charged in the presence of water, while limestone and other calcareous materials become positively charged in the presence of water. The nature of electric charges on the aggregate surface when in contact with water has a strong influence on the aggregate asphalt adhesion and its resistance to moisture damage. Another important property of the aggregates which will influence the properties of the asphalt concrete is the aggregate shape (Campen and Smith [55], Wedding and Gaynor [56], Herrin and Goetz [57]). Granite aggregates are much more angular and sharp cornered than natural gravels containing rounded particles. The angular-shaped particles exhibit greater interlock and internal friction, and hence result in greater strength and resistance to deformation than asphalt concrete made of rounded particles. The surface texture also influences the properties of asphalt mixture (Vallerga et al. [58]). Smooth-textured aggregates like river gravel are easier to coat with asphalt film, but the asphalt cement forms stronger bonds with rough-textured aggregates like granite. From this discussion it is very clear that asphalt concrete made with one type of aggregate stores and dissipates energy in a very different way from that made with another type of aggregate because of the large difference in the way in which the aggregates interact amongst themselves and with the asphalt mastic. Hence one would expect different forms for the stored energy and rate of dissipation functions for asphalt concrete made with each of these different aggregates. The mechanical response

of a material is determined by the way in which it stores and dissipates energy and hence we would expect the response of specimens made with different aggregates to be different.

Gradation is the most important property of the aggregate which influences the properties of the asphalt concrete. Almost all the important properties of the asphalt concrete are determined, to a large extent by the gradation of the aggregates (Hveem [59], Krutz and Sebaaly [60], Chen and Liao [61], Kim et al. [62]). This is especially true with the aggregate fines. For example, a reduction of aggregate fines of 3 % produced a change in the fatigue life of the pavement of the order of more than 300 % (Harvey and Monismith [63]). In this experiment, we have used the same gradation for both the limestone and granite mixes, so that we can compare their mechanical responses. Binder content is another important parameter which will affect the properties of asphalt concrete. Here, we have used a binder content of 4.85 % for limestone and 4.86 % for granite mixes.

If one sees the experimental data in figure 13, it is very clear that there is a change in the material response after the stress reaches a peak value at $t = \tau$. The displacement rate is a constant throughout the experiment but the response characteristics of the specimen changes after time τ. The experimental behavior is similar to that of dense granular soil specimens, in which the stress rises to a peak value and then drops to a constant value (Baladi and Wu [64], Holtz and Kovacs [65]). This is in contrast to specimens made of initially loose granular soil. The increase in strength for dense granular soils is due to the interlocking of soil particles with each other. The same analogy can be extended to the triaxial testing of compacted asphalt mixture specimens.The initial displacement of the specimen is contributed more by the smaller sized aggregate particles moving in to the space initially occupied by the asphalt mastic. More aggregate to aggregate contact is achieved at this stage and

the whole aggregate skeleton readjusts itself to form a better interlock. At the peak stress, the optimum aggregate interlock is achieved. Any further deformation causes the aggregate interlock to break down and causes the larger aggregate particles to roll and slide past one another. From this point onward, the viscous nature of the asphalt mastic plays a more prominent role in the deformation resistance of the specimen. Hence, it can be clearly seen that there is a distinct change in the way the internal structure evolves during the experiment after the stress reaches the peak value. The form for the stored energy function and the rate of dissipation function has to change after the stress reaches the peak value (at t=τ), to capture this change in the evolution of the internal structure.

To find the time τ at which the switch in the model takes place, the following condition has been used:

$$\overset{\nabla}{\mathbf{B}} + \mathbf{B}_{\kappa_{p(t)}}\mathbf{L}^T + \mathbf{L}\mathbf{B}_{\kappa_{p(t)}} = \mathbf{0}. \tag{3.51}$$

This amounts to requiring that $\dot{\mathbf{B}}_{\kappa_{p(t)}} = \mathbf{0}$. This is the stage corresponding to the optimum interlock. Till this point the material deforms in such a way as to get a better interlock between the aggregate particles. The stored energy and rate of dissipation used for the model so far has captured this kind of interaction between the aggregate particles and between the aggregate particles and the asphalt mastic, in a global sense. Hence the fact that $\dot{\mathbf{B}}_{\kappa_{p(t)}} = \mathbf{0}$ tells us that this kind of deformation is coming to an end and further deformation is caused by a different mechanism. From this point onwards, the mechanics of deformation and deformation resistance of the specimen changes, which will be reflected in the model by a new form for stored energy and rate of dissipation. The material builds up resistance up to the point $t = \tau$ through the development of aggregate interlock. After this point, the asphalt mastic plays a more prominent role in the deformation resistance of the specimen. A similar

behavior is exhibited by asphalt concrete during a compression test and tension test. The aggregate matrix takes most of the load in the compression test due to aggregate interlock, while the asphalt mastic takes most of the load in a tension test (see Murali Krishnan and Rajagopal [22]).

At this stage, let us give specific forms for the functions $\mu_1(I_{\kappa_{p(t)}})$ and $\eta_1(\mathbf{B}_{\kappa_{p(t)}})$.

Limestone

For $t \leq \tau$:

$$\mu_1(I_{\kappa_{p(t)}}) = \bar{\mu}_1 \left(1 + \frac{1}{1 + exp(-a(I_{\kappa_{p(t)}} - 3 - b))}\right), \tag{3.52}$$

$$\frac{\mu_1}{\eta_1} = c\left(1 + \frac{d}{n}(I_{\kappa_{p(t)}} - 3)\right)^{n-1} \left(\frac{g(I_{\kappa_{p(t)}} - 3)^f}{tr(\mathbf{T})}\right)^m, \tag{3.53}$$

where $\bar{\mu}_1,\ a,\ b$ are material constants related to the shear modulus of the material and $c,\ d,\ f,\ g,\ n,\ m$ are material constants related to the relaxation time of the material. Also $\dfrac{\mu_1}{\eta_1}$ is related to the relaxation time of the material.

For $t > \tau$:

$$\mu_1(I_{\kappa_p(t)}) = ((\mu_1)_\tau - \beta_1)exp(\alpha_1(I_{\kappa_p(t)} - I_{\kappa_p(t)_\tau})) + \beta_1, \tag{3.54}$$

$$\frac{\mu_1}{\eta_1} = \left(\frac{\mu_1}{\eta_1}\right)_\tau, \tag{3.55}$$

where $\alpha_1 = \alpha_1(I_{\kappa_p(t)_\tau} - 3)$, $\beta_1 = \beta_1(I_{\kappa_p(t)_\tau} - 3)$.

Georgia Granite

For $t \leq \tau$:

$$\mu_1(I_{\kappa_{p(t)}}) = \bar{\mu}_1 \left(1 + \frac{1}{1 + exp(-a(I_{\kappa_{p(t)}} - 3 - b))}\right), \tag{3.56}$$

$$\frac{\mu_1}{\eta_1} = c\left(1 + \frac{d}{n}(I_{\kappa_{p(t)}} - 3)\right)^{n-1} \left(\frac{g(I_{\kappa_{p(t)}} - 3)^f}{tr(\mathbf{T}) - q}\right)^m, \tag{3.57}$$

where $\bar{\mu}_1,\ a,\ b,\ c,\ d,\ f,\ g,\ n,\ m$ are material constants.

For $t > \tau$:

$$\mu_1(I_{\kappa_p(t)}) = \alpha_2\left(x^{\beta_2} - x_\tau^{\beta_2}\right) + \mu_{1_\tau}, \tag{3.58}$$

$$\frac{\mu_1}{\eta_1} = \left(\frac{\mu_1}{\eta_1}\right)_\tau, \tag{3.59}$$

where $x = I_{\kappa_p(t)} - 3,\ \alpha_2 = \alpha_2(I_{\kappa_p(t)_\tau} - 3),\ \beta_2 = \beta_2(I_{\kappa_p(t)_\tau} - 3)$.

Table VII. Material constants used in modeling

Aggregate material	Limestone	Granite
$\bar{\mu_1}$	1.5x10$^7(N/m^2)$	1.86x10$^7(N/m^2)$
a	1x10^4	1x10^4
b	2x10^{-4}	0
c	1.5x10^{-5} s^{-1}	2x10^{-6} s^{-1}
d	6x10^4	6x10^4
n	6	6
f	0.7047	0.57
g	2.352x10$^8(N/m^2)$	1.12x10$^8(N/m^2)$
m	4	35
q	-	2.9x10$^5(N/m^2)$

The term $\dfrac{\mu_1}{\eta_1}$ is related to the relaxation time of the material. This means that the relaxation time of the asphalt keeps changing till $t = \tau$ according to (4.57) for limestone and (4.60) for granite, but after that it becomes a constant equal to the relaxation time at $t = \tau$. Similarly the 'shear modulus', μ_1 associated with the instantaneous elastic response of asphalt concrete increases as given by (3.52) till $t = \tau$ and then it starts decreasing as given by (4.58) for limestone and (3.58) for granite. This is to be expected since till $t = \tau$, the aggregate interlock builds up and

afterwards it breaks down and more of the load is carried by the asphalt mastic.

Table VII shows the different material constants used for the model. Figures 14-21 shows the comparison of the predictions of the model with the experimental results. The '*' shows the experimental data points and the solid line depicts the predictions of the model. As one can see, the model corroborates with the experimental results reasonably well. In figure 16, the experimental data corresponding to a confinement pressure of 15 psi in the time period from 25 to 45 seconds does not show the same trend as the rest of the experiments. The model captures the trend of the experiments reasonably well. Also the model is able to predict the peak stress developed in the material for different confinement pressures. One would expect the deformation resistance of the asphalt concrete specimen to increase with an increase in confinement pressure. Also one would expect the granite specimens to have a higher resistance to deformation as compared to the limestone specimens. These are in conformity with the experimental results and the model successfully captures both the change in material properties and the increase in resistance to deformation with an increase in confinement pressure for both the granite and limestone specimens.

F. Conclusions

In this paper we have used a general thermodynamic framework to construct models to describe the behavior of asphalt mixtures. The internal structure of asphalt concrete evolves as the material deforms. The framework used and the models developed here take into account this evolution of the internal structure of asphalt concrete. The response of the body is defined through a set of response functions from various natural configurations that the body can take. The maximization of the rate of dissipation is used to obtain the equations for the evolution of the underlying natural

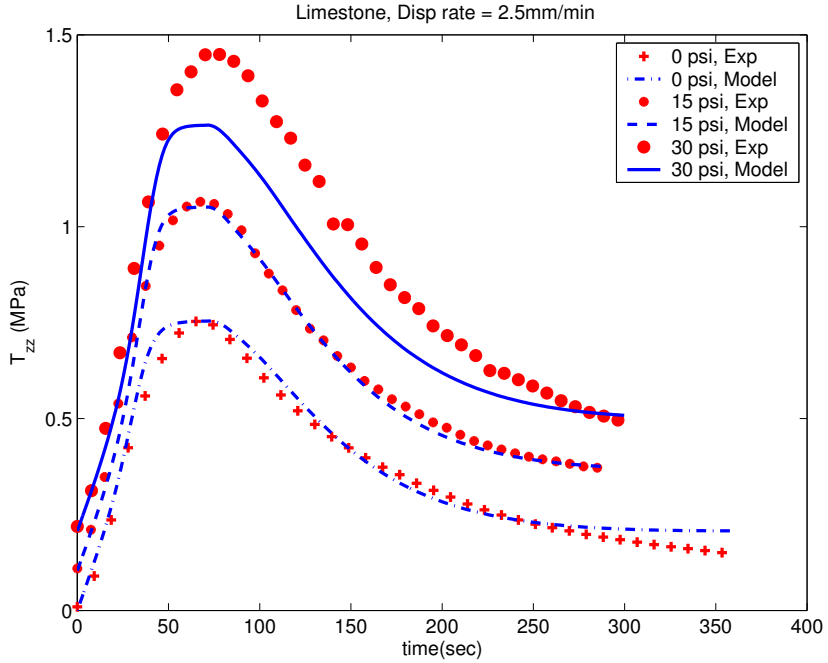

Fig. 14. Limestone, Disp rate = 2.5 mm/min (Incompressible)

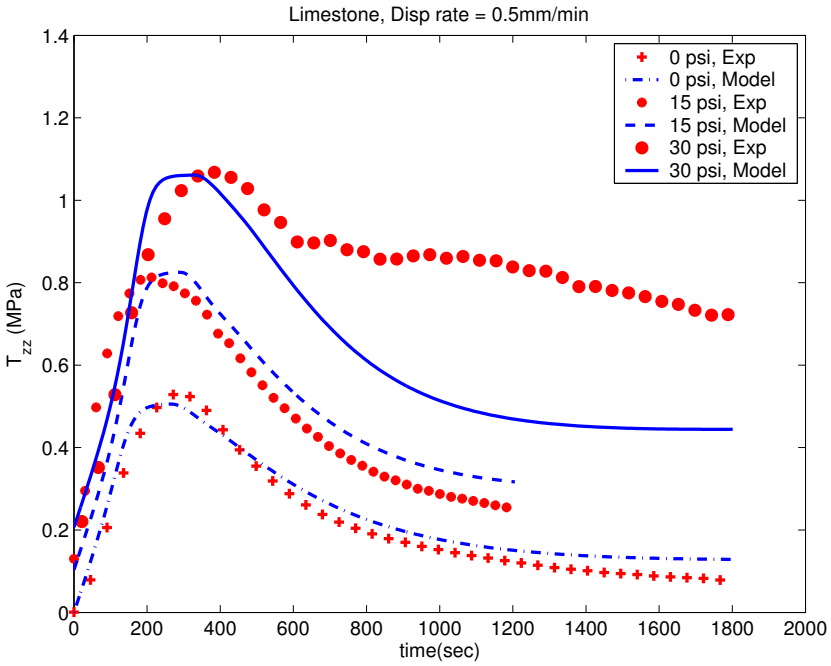

Fig. 15. Limestone, Disp rate = 0.5 mm/min (Incompressible)

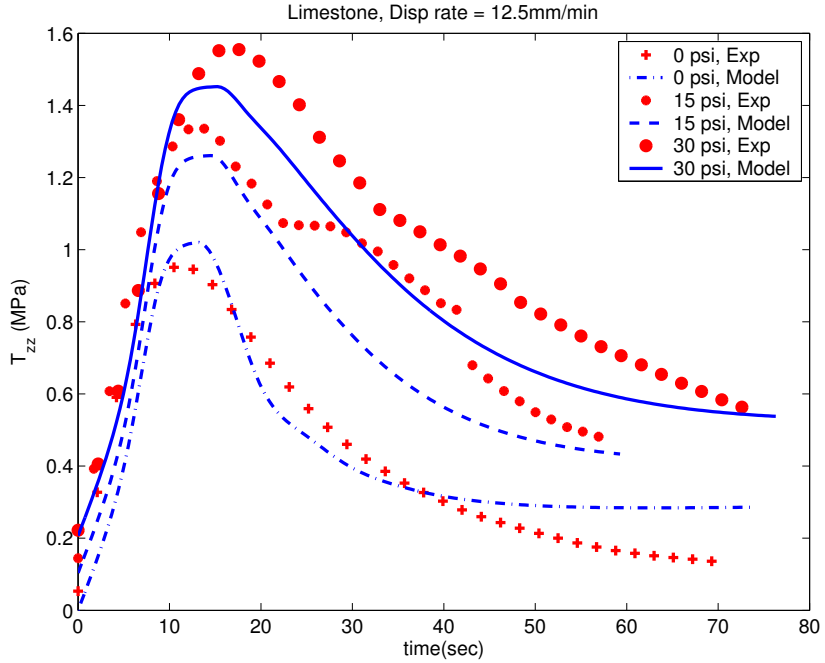

Fig. 16. Limestone, Disp rate = 12.5 mm/min (Incompressible)

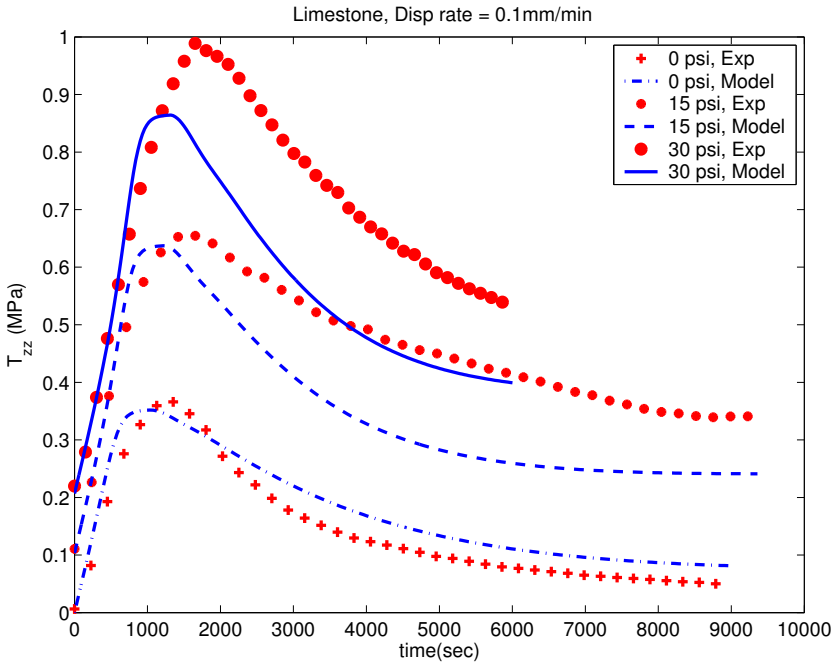

Fig. 17. Limestone, Disp rate = 0.1 mm/min (Incompressible)

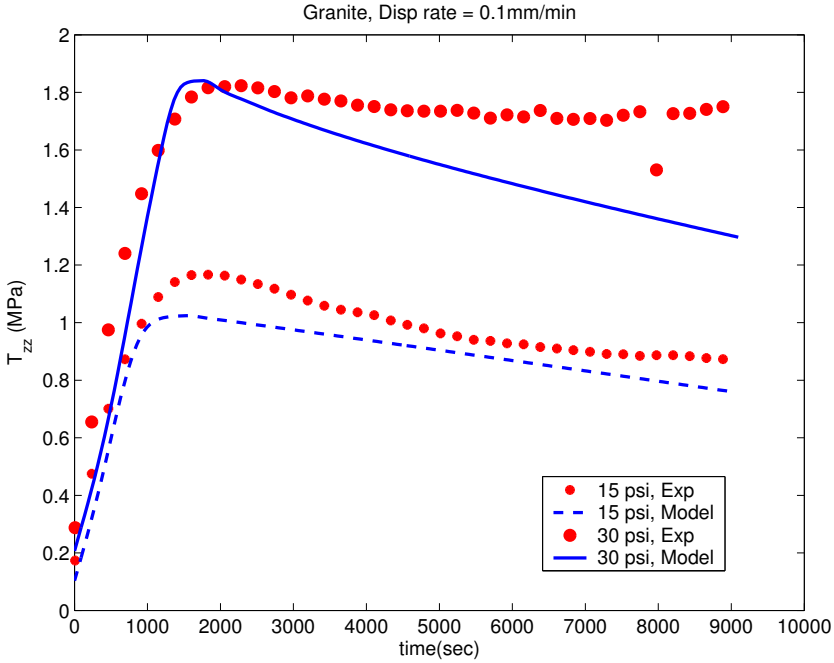

Fig. 18. Granite, Disp rate = 0.1 mm/min (Incompressible)

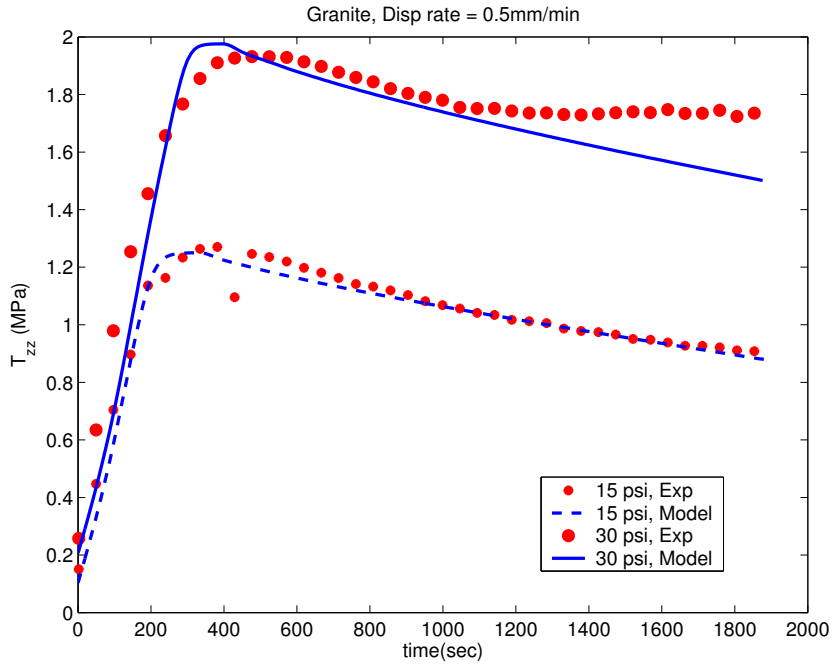

Fig. 19. Granite, Disp rate = 0.5 mm/min (Incompressible)

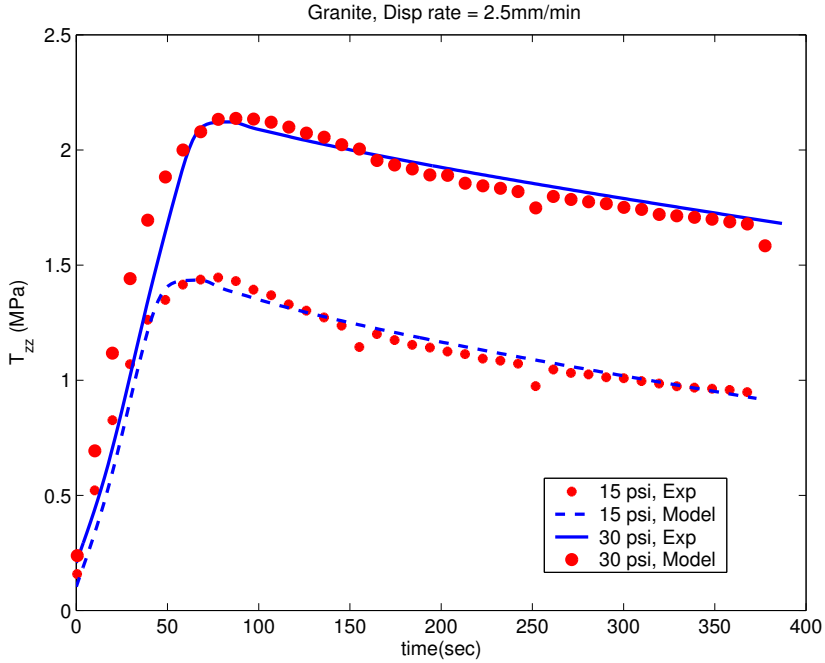

Fig. 20. Granite, Disp rate = 2.5 mm/min (Incompressible)

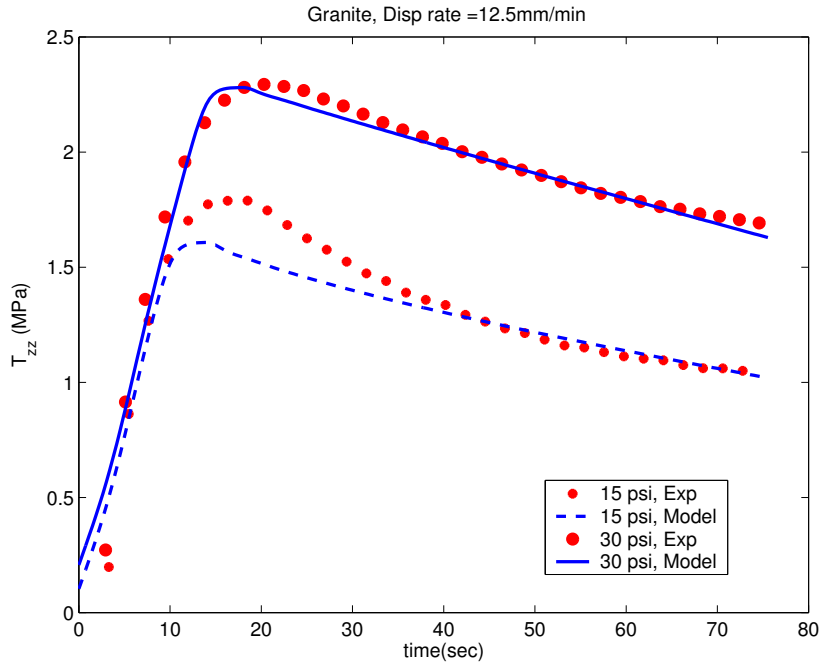

Fig. 21. Granite, Disp rate = 12.5 mm/min (Incompressible)

configurations. Using appropriate choices for the Helmholtz potential, rate of dissipation etc., we try to capture the complex internal processes and interactions in the asphalt concrete.

We demonstrate the efficacy of the model by corroborating with the experimental results of constant displacement rate tests on asphalt concrete specimens. The model is general enough to capture the response of asphalt concrete at different confinement pressures and displacement rates. By choosing different forms for the material parameters related to the shear modulus and relaxation time of the material, we could model the experimental data for two different types of aggregates - limestone and granite. The change in the form for the material parameters were needed to take into account the different ways in which these aggregates interact with themselves and with the asphalt mastic. In the experiment, for a constant displacement rate, the stress reaches a peak value and then drops down gradually to a lower value. The interaction mechanism to provide deformation resistance changes after the stress reaches the peak value. Here, we have used the criterion (4.56) to switch from one type of response to another to reflect the change in the interaction mechanism. Using this switching criterion, the model was able to successfully predict the peak stress developed in the material. It is important to recognize that the material parameters that are used for the corroboration are the same for all the experiments, for a particular kind of material, i.e., the same set of material parameters are able to describe a large class of experiments.

G. Acknowledgment

We thank Dr. J. Murali Krishnan for his many helpful comments and discussions.

CHAPTER IV

A COMPRESSIBLE MODEL FOR ASPHALT MIXTURES

In this study we develop a compressible model for asphalt concrete. Asphalt concrete is a compressible material. The density of an asphalt cocrete pavement changes due to the repeated application of traffic loads. We develop a one constituent compressible model for asphalt concrete by associating different natural configurations with distinct internal structures of the body. Finally, the model predictions are corroborated with the experimental results.

A. Introduction

Asphalt concrete is a mixture of asphalt and aggregates continuously graded from a maximum size of 25 mm to a fine filler of about 0.075 mm in size. Since asphalt concrete is made of granular materials which are bound to together by a viscoelastic fluid, it exhibits different behavior in the presence of different loading and environmental conditions. Asphalt from different crude sources has completely different properties. The method of separation of asphalt from the crude and the processing method has an important influence on the mechanical response of asphalt. In addition to this, asphalt is extremely sensitive to temperature. The interaction between the aggregate particles is highly influenced by the size, shape, angularity and surface roughness of the constituent particles. Since the behavior of asphalt concrete depends on the non-linear interaction between the aggregate particles themselves and with asphalt, it is an extremely difficult material to model.

The density of an asphalt concrete pavement changes during the life time of the pavement. This change in density is primarily due to the compaction effects due to moving traffic loads. The consolidation in asphalt concrete occurs via two mecha-

nisms: 1 D densification and consolidation in minearal aggregate which is identified as plastic flow in the mineral aggregates. When the reduction in air voids take place without significant deformation of asphalt, it is termed as densification. Pavement performance studies ([66]) have indicated that the consolidation mechanism perdominates when the air voids are less than 3 %. In the reduced air voids space, there is a build up of high pore pressure and some amount of asphalt is forced to flow into the voids. This will ultimately result in the reduction of relative distance between the aggregate particles. This flow of asphalt into the voids will result in over-lubrication, which in turn affects the strength and shear properties of the asphalt mixture. On the same hand, air voids in excess of 8 % will result in high air and water permeability that will lead to durability problems.

From the previous discussion it is clear that density plays a crucial role in the construction of asphalt mixtures. The voids in an asphalt mixture are directly related to density. Thus density must be closely controlled to insure that the voids stay within an acceptable range. There has been much work that has shown that the initial in-place voids should be no more than approximately 8 percent and the percentage of voids should never fall below approximately 3 percent during the life time of the pavement.

Ford ([67]) showed in a study that asphalt mixtures should be designed and constructed so that in-pace air voids stay above 2.5 percent. As long as the voids are above 2.5 percent, he showed that the expected rut depth would be no greater than 10/32 inch. Brown and Cross [68] showed that significant rutting was likely to occur once the air voids reduces to 3 percent. Huber ([69]) in a study of rutting in Canada reached a similar conclusion. Zube ([70]) showed that asphalt mixtures were impermeable to water as long as the air voids content was below 8 percent. The permeability increased rapidly as the air void content increased above 8 percent.

Brown and Brownfield ([71]) and Santucci and other ([72]) reached similar conclusions in other studies. A recent study of air voids and its change in the pavement was conducted by Harmelink and Aschenbrener ([73]).

From the previous studies, it is apparent that a mixture that is properly designed and compacted should contain enough air voids to prevent rutting due to plastic flow but low enough air voids to prevent permeability of air and water. Since density of asphalt mixture varies throughout its life the voids must be low enough initially to prevent permeability of air and water and high enough after a few years of traffic to prevent plastc flow.

Some authors have used a mixture theory approach to capture the initial air voids and its change in the asphalt concrete pavement. Murali Krishnan and Lakshmana Rao ([74]) modeled asphalt concrete as a three constituent mixture consisting of asphalt, aggregate matrix and air. Constitutive relations for each constituent is assumed to depend only on the kinematical quantities of each constituent. A similar approach was presented by Wang et al. ([75]) where they modeled asphalt concrete as a two constituent mixture consisting of asphalt mixture and air voids. In this work we use a compressible one constituent model for asphalt concrete. We do not take into account air voids directly in the model. However the model captures the change in density of the asphalt concrete mixture which is closely related to the change in the air voids of the mixture.

B. Preliminaries

Consider a body B in a configuration $\kappa_R(B)$. For ease of notation, we shall use κ_R to mean $\kappa_R(B)$. Let $\mathbf{X}$ denote a typical position of a material point in κ_R. Let $\kappa_c(t)$ denote the configuration occupied by the body B at time t. Motion is defined as the

one-to-one mapping which assigns to each point $\mathbf{X}$ in κ_R a corresponding point $\mathbf{x}$ in κ_c:

$$\mathbf{x} = \boldsymbol{\chi}_{\kappa_R}(\mathbf{X}, t). \tag{4.1}$$

The deformation gradient $\mathbf{F}_{\kappa_R}$ is defined through:

$$\mathbf{F}_{\kappa_R} = \frac{\partial \boldsymbol{\chi}_{\kappa_R}}{\partial \mathbf{X}}. \tag{4.2}$$

The left and right Cauchy-Green stretch tensors $\mathbf{B}_{\kappa_R}$ and $\mathbf{C}_{\kappa_R}$ are defined through:

$$\mathbf{B}_{\kappa_R} = \mathbf{F}_{\kappa_R}\mathbf{F}_{\kappa_R}^{\mathrm{T}}, \quad \mathbf{C}_{\kappa_R} = \mathbf{F}_{\kappa_R}^{\mathrm{T}}\mathbf{F}_{\kappa_R}. \tag{4.3}$$

Any acceptable process has to satisfy the appropriate balance laws. The appropriate balance laws for the problem at hand are the conservation of mass, linear and angular momentum and energy. The conservation of mass is given by

$$\dot{\rho} + \rho \ \mathrm{div}(\mathbf{v}) = 0, \tag{4.4}$$

where ρ is the density and $\mathbf{v}$ is the velocity of the material. The conservation of linear momentum is

$$\rho \left[\frac{\partial \mathbf{v}}{\partial t} + (\nabla \mathbf{v})\mathbf{v} \right] = \mathrm{div}\mathbf{T} + \rho \mathbf{g}, \tag{4.5}$$

where $\mathbf{g}$ is the acceleration due to gravity and $\mathbf{T}$ is the Cauchy stress tensor. In the absence of internal couples, conservation of angular momentum implies that the stress tensor is symmetric. The conservation of energy gives:

$$\rho\dot{\epsilon} + \mathrm{div}\mathbf{q} = \mathbf{T} \cdot \mathbf{L} + \rho \mathrm{r}, \tag{4.6}$$

where ϵ is the internal energy, $\mathbf{q}$ is the heat flux vector and r is the radiant heating.

The second law of thermodynamics is often used in continuum mechanics in the form of the Clausius-Duhem inequality (see Truesdell and Noll [2]). In the present

work we will introduce the second law in the form of an equality by introducing a balance law for entropy. This approach is similar to that of Green and Naghdi [31] and Rajagopal and Srinivasa [25]. The balance law for entropy then takes the form

$$\rho\dot{\zeta} + \mathrm{div}\left(\frac{\mathbf{q}}{\theta}\right) = \rho\frac{\mathrm{r}}{\theta} + \rho\Xi, \quad \Xi \geq 0, \tag{4.7}$$

where ζ is the entropy, θ is the absolute temperature and Ξ is the rate of entropy production. Combining the balance of energy and the balance of entropy gives the reduced energy-dissipation equation:

$$\mathbf{T}\cdot\mathbf{L} - \rho\dot{\psi} - \rho\zeta\dot{\theta} - \frac{\mathbf{q}\cdot\mathrm{grad}\theta}{\theta} = \rho\theta\Xi = \xi \geq 0, \tag{4.8}$$

where ψ is the Helmholtz potential and is given by $\psi = \epsilon - \theta\zeta$ and ξ is the rate of dissipation. It is usually assumed that the rate of dissipation can be split into two parts, one pertaining to heat conduction and the other related to the rate at which work is converted into thermal energy. Assuming that the rate of dissipation due to heat conduction is given by

$$\xi_c = -\frac{\mathbf{q}\cdot\mathrm{grad}\theta}{\theta} \geq 0, \tag{4.9}$$

we can rewrite (4.8) as:

$$\mathbf{T}\cdot\mathbf{L} - \rho\dot{\psi} - \rho\zeta\dot{\theta} = \xi_d \geq 0. \tag{4.10}$$

In this work, we use the reduced energy equation in the above form to place restrictions on the constitutive equations.

C. Modeling of Asphalt Concrete

Corresponding to each current configuration $\kappa_c(t)$ we associate a natural configuration $\kappa_p(t)$. In figure 1, κ_R is a reference configuration, κ_t is the configuration currently

occupied by the material and $\kappa_{p(t)}$ is the natural configuration associated with the material that is currently in the configuration κ_t. The natural configuration $\kappa_{p(t)}$ corresponds to the stress free configuration associated with the current configuration κ_t occupied by the body at time t. For further discussion on natural configuration the readers are referred to the papers by Rajagopal and Srinivasa [27, 24, 25].

In this work we shall assume just one relaxation mechanism which will effectively capture the overall relaxation of the asphalt mixture. Since we are assuming only one relaxation mechanism, we shall associate only one natural configuration $(\kappa_{p(t)})$ corresponding to each current configuration $(\kappa_c(t))$.

We assume that the asphalt mixture has an instantaneous elastic response from the natural configuration $\kappa_{p(t)}$. The gradient of the mapping from $\kappa_{p(t)}$ to κ_t is defined as $\mathbf{F}_{\kappa_{p(t)}}$. The natural configuration $\kappa_{p(t)}$ is not fixed as in the case of an elastic solid but evolves as the material is deformed. This change in the natural configuration is associated with the dissipative response of the material. We define $\mathbf{G}$ to be the mapping between the tangent spaces of κ_R and the natural configuration $\kappa_{p(t)}$,

$$\mathbf{G} = \mathbf{F}_{\kappa_R \to \kappa_{p(t)}} = \mathbf{F}^{-1}_{\kappa_{p(t)}} \mathbf{F}_{\kappa_R}. \tag{4.11}$$

We define:

$$\mathbf{B}_{\kappa_{p(t)}} = \mathbf{F}_{\kappa_{p(t)}} \mathbf{F}^{T}_{\kappa_{p(t)}}. \tag{4.12}$$

We define the velocity gradient $\mathbf{L}$ in the conventional way and introduce a corresponding velocity gradient $\mathbf{L}_{\kappa_{p(t)}}$ associated with the natural configuration (Rajagopal and Srinivasa [27]),

$$\mathbf{L} = \dot{\mathbf{F}}_{\kappa_R} \mathbf{F}^{-1}_{\kappa_R}, \tag{4.13}$$

$$\mathbf{L}_{\kappa_{p(t)}} = \dot{\mathbf{G}} \mathbf{G}^{-1}. \tag{4.14}$$

Also,

$$\mathbf{D}_{\kappa_{p(t)}} = \frac{1}{2}(\mathbf{L}_{\kappa_{p(t)}} + \mathbf{L}^T_{\kappa_{p(t)}}), \tag{4.15}$$

$$\mathbf{D} = \frac{1}{2}(\mathbf{L} + \mathbf{L}^T). \tag{4.16}$$

We define the Oldroyd derivative of $\mathbf{B}_{\kappa_{p(t)}}$ as:

$$\overset{\nabla}{\mathbf{B}} := \dot{\mathbf{B}}_{\kappa_{p(t)}} - \mathbf{L}\mathbf{B}_{\kappa_{p(t)}} - \mathbf{B}_{\kappa_{p(t)}}\mathbf{L}^T = -2\mathbf{F}_{\kappa_{p(t)}}\mathbf{D}_{\kappa_{p(t)}}\mathbf{F}^T_{\kappa_{p(t)}}, \tag{4.17}$$

where the inverted triangle denotes the upper convected Oldroyd derivative and the dot is the material time derivative. Specifying $\mathbf{D}_{\kappa_{p(t)}}$ amounts to prescribing the manner in which the underlying natural configurations evolve. We will assume that the evolution of the natural configurations is isotropic:

$$\mathrm{tr}(\mathbf{D}_{\kappa_{p(t)}}) = 0. \tag{4.18}$$

The internal energy and the entropy is assumed to depend on the temperature θ and the invariants of $\mathbf{B}_{\kappa_{p(t)}}$: $I_{\kappa_{p(t)}}$, $II_{\kappa_{p(t)}}$, $III_{\kappa_{p(t)}}$.

$$\epsilon = \epsilon(\theta, I_{\kappa_{p(t)}}, II_{\kappa_{p(t)}}, III_{\kappa_{p(t)}}) \tag{4.19}$$

$$\zeta = \zeta(\theta, I_{\kappa_{p(t)}}, II_{\kappa_{p(t)}}, III_{\kappa_{p(t)}}), \tag{4.20}$$

where $I_{\kappa_{p(t)}} = \mathrm{tr}(\mathbf{B}_{\kappa_{p(t)}}), II_{\kappa_{p(t)}} = \mathrm{tr}({\mathbf{B}_{\kappa_{p(t)}}}^2), III_{\kappa_{p(t)}} = \mathrm{det}\mathbf{B}_{\kappa_{\mathrm{p(t)}}}$. Hence the Helmholtz potential has the form:

$$\psi = \psi(\theta, I_{\kappa_{p(t)}}, II_{\kappa_{p(t)}}, III_{\kappa_{p(t)}}). \tag{4.21}$$

Assuming that the increase in confinement pressure will increase the mean normal stress in the speimen, we assume the following form for the rate of dissipation function:

$$\xi_d = \xi_d(\theta, \mathbf{B}_{\kappa_{p(t)}}, \mathbf{D}_{\kappa_{p(t)}}, tr(\mathbf{T})). \tag{4.22}$$

Now we shall give specific forms for constitutive equations. We shall give the following form for the stored energy and entropy for the model.

$$\epsilon = C\theta + A + W(I_{\kappa_{p(t)}}, II_{\kappa_{p(t)}}, III_{\kappa_{p(t)}}) \tag{4.23}$$

$$\zeta = C\ln(\theta) + \mathrm{B}. \tag{4.24}$$

From (4.23) and (4.24) it follows that (since $\psi = \epsilon - \theta\zeta$)

$$\dot{\psi} + \zeta\dot{\theta} = \dot{W}(I_{\kappa_p(t)}, II_{\kappa_{p(t)}}, III_{\kappa_{p(t)}}). \tag{4.25}$$

Substituting (4.25) into (4.10), we get:

$$\mathbf{T}\cdot\mathbf{L} - \rho\left[\frac{\partial W}{\partial I_{\kappa_p(t)}}\mathbf{I} + 2\frac{\partial W}{\partial II_{\kappa_{p(t)}}}\mathbf{B}_{\kappa_{p(t)}} + \frac{\partial W}{\partial III_{\kappa_{p(t)}}}III_{\kappa_{p(t)}}\mathbf{B}^{-\mathrm{T}}_{\kappa_{p(t)}}\right]\cdot\dot{\mathbf{B}}_{\kappa_{p(t)}} = \xi_d \tag{4.26}$$

Since we are assuming asphalt concrete to be isotropic, we can choose, without any loss of generality, the natural configurations $\kappa_{p(t)}$ to be such that

$$\mathbf{F}_{\kappa_{p(t)}} = \mathbf{V}_{\kappa_{p(t)}}. \tag{4.27}$$

Substituting for $\dot{\mathbf{B}}_{\kappa_{p(t)}}$ from (4.17) and using (4.27) we get,

$$\mathbf{I}\cdot\dot{\mathbf{B}}_{\kappa_{p(t)}} = 2\mathbf{B}_{\kappa_{p(t)}}\cdot(\mathbf{D} - \mathbf{D}_{\kappa_{p(t)}}), \tag{4.28}$$

$$\mathbf{B}_{\kappa_{p(t)}}\cdot\dot{\mathbf{B}}_{\kappa_{p(t)}} = 2\mathbf{B}^2_{\kappa_{p(t)}}\cdot(\mathbf{D} - \mathbf{D}_{\kappa_{p(t)}}), \tag{4.29}$$

$$\mathbf{B}^{-\mathrm{T}}_{\kappa_{p(t)}}\cdot\dot{\mathbf{B}}_{\kappa_{p(t)}} = 2\mathbf{I}\cdot(\mathbf{D} - \mathbf{D}_{\kappa_{p(t)}}). \tag{4.30}$$

Using these in (4.26) gives

$$\mathbf{T}\cdot\mathbf{D} - 2\rho\left[W_1\mathbf{B}_{\kappa_{p(t)}} + 2W_2\mathbf{B}^2_{\kappa_{p(t)}} + \det(\mathbf{B}_{\kappa_{p(t)}})W_3\mathbf{I}\right]\cdot\left(\mathbf{D} - \mathbf{D}_{\kappa_{p(t)}}\right) \tag{4.31}$$

where $W_1 = \dfrac{\partial W}{\partial I_{\kappa_{p(t)}}},\ W_2 = \dfrac{\partial W}{\partial II_{\kappa_{p(t)}}},\ W_3 = \dfrac{\partial W}{\partial III_{\kappa_{p(t)}}}$. We can rewrite (4.31) as:

$$\left[\mathbf{T} - 2\rho\left(W_1\mathbf{B}_{\kappa_{p(t)}} + 2W_2\mathbf{B}^2_{\kappa_{p(t)}} + \det(\mathbf{B}_{\kappa_{p(t)}})W_3\mathbf{I}\right)\right]\cdot\mathbf{D} = \tag{4.32}$$

$$\xi_d(\mathbf{B}_{\kappa_{p(t)}}, \mathbf{D}_{\kappa_{p(t)}}, tr(\mathbf{T})) - 2\rho\left(W_1\mathbf{B}_{\kappa_{p(t)}} + 2W_2\mathbf{B}^2_{\kappa_{p(t)}} + \det(\mathbf{B}_{\kappa_{p(t)}})W_3\mathbf{I}\right)\cdot\mathbf{D}_{\kappa_{p(t)}}$$

Since we are looking for forms sufficient to satisfy the above equation, we stipulate that

$$\mathbf{T} = 2\rho\left(W_1\mathbf{B}_{\kappa_{p(t)}} + 2W_2\mathbf{B}^2_{\kappa_{p(t)}} + \det(\mathbf{B}_{\kappa_{p(t)}})W_3\mathbf{I}\right). \tag{4.33}$$

This will give,

$$\xi_d = \mathbf{T}\cdot\mathbf{D}_{\kappa_{p(t)}}. \tag{4.34}$$

Equation (4.34) imposes a constraint in the evolution of natural configurations. We will pick the following form for ξ_d:

$$\xi_d = \eta(\mathbf{B}_{\kappa_{p(t)}}, \mathrm{tr}(\mathbf{T}))\mathbf{D}_{\kappa_{\mathrm{p(t)}}}\cdot\mathbf{B}_{\kappa_{\mathrm{p(t)}}}\mathbf{D}_{\kappa_{\mathrm{p(t)}}}. \tag{4.35}$$

The material parameter η is related to the 'viscosity' of the material. At this point, we do not know how the natural configurations evolve. We assume that for a fixed $\mathbf{B}_{\kappa_{p(t)}}$ and $\mathbf{D}$, $\mathbf{D}_{\kappa_{p(t)}}$ should be such that it maximizes the rate of entropy production. We maximize ξ_d subject to the constraint (4.34) and (4.18). This gives

$$f = \xi_d - \lambda_1(\xi_d - \mathbf{T}\cdot\mathbf{D}_{\kappa_{p(t)}}) - \lambda_2\mathrm{tr}(\mathbf{D}_{\kappa_{p(t)}}), \tag{4.36}$$

$$\frac{\partial f}{\partial\mathbf{D}_{\kappa_{p(t)}}} = (1-\lambda_1)\frac{\partial\xi_d}{\partial\mathbf{D}_{\kappa_{p(t)}}} + \lambda_1\mathbf{T} - \lambda_2\mathbf{I} = 0. \tag{4.37}$$

This gives

$$\mathbf{T} = \frac{1-\lambda_1}{-\lambda_1}\frac{\partial\xi_d}{\partial\mathbf{D}_{\kappa_{p(t)}}} + \frac{\lambda_2}{\lambda_1}\mathbf{I} = \beta\frac{\partial\xi_d}{\partial\mathbf{D}_{\kappa_{p(t)}}} + \lambda_3\mathbf{I}. \tag{4.38}$$

Now if ξ_d is given by (4.35), then

$$\xi_d = \frac{1}{2}\frac{\partial \xi_d}{\partial \mathbf{D}_{\kappa_{p(t)}}} \cdot \mathbf{D}_{\kappa_{p(t)}}. \tag{4.39}$$

Therefore $\beta = 1/2$ and

$$\mathbf{T} = \frac{1}{2}\frac{\partial \xi_d}{\partial \mathbf{D}_{\kappa_{p(t)}}} + \lambda_3 \mathbf{I}. \tag{4.40}$$

Substituting (4.33) and (4.35) into (4.45), pre-multiplying by $\mathbf{V}^{-1}_{\kappa_{p(t)}}$ and postmultiplying by $\mathbf{V}_{\kappa_{p(t)}}$, we get,

$$\mathbf{V}_{\kappa_{p(t)}}\mathbf{D}_{\kappa_{p(t)}}\mathbf{V}_{\kappa_{p(t)}} = \frac{2\rho}{\eta}\left(W_1\mathbf{B}_{\kappa_{p(t)}} + 2W_2\mathbf{B}^2_{\kappa_{p(t)}} + W_3 \mathrm{det}\mathbf{B}_{\kappa_{p(t)}}\mathbf{I}\right) - \lambda\mathbf{I}, \tag{4.41}$$

where $\lambda = \lambda_1/\eta$. Substituting (4.33) and (4.36) into (4.35), pre-multiplying by $\mathbf{V}^{-1}_{\kappa_{p(t)}}$ and postmultiplying by $\mathbf{V}_{\kappa_{p(t)}}$, we get,

$$\mathbf{V}_{\kappa_{p(t)}}\mathbf{D}_{\kappa_{p(t)}}\mathbf{V}_{\kappa_{p(t)}} = \frac{2\rho}{\eta}\left(W_1\mathbf{B}_{\kappa_{p(t)}} + 2W_2\mathbf{B}^2_{\kappa_{p(t)}} + W_3 \mathrm{det}\mathbf{B}_{\kappa_{p(t)}}\mathbf{I}\right) - \lambda\mathbf{I}, \tag{4.42}$$

where $\lambda = \beta/\eta$. Taking dot product of (4.42) with $\mathbf{B}^{-1}_{\kappa_{p(t)}}$ and noting that $tr(\mathbf{V}_{\kappa_{p(t)}}\mathbf{D}_{\kappa_{p(t)}}\mathbf{V}^{-1}_{\kappa_{p(t)}}) \;=\; tr(\mathbf{D}_{\kappa_{p(t)}}) \;=\; 0$,

$$\lambda = \frac{2\rho}{\eta \mathrm{tr}(\mathbf{B}^{-1}_{\kappa_{p(t)}})}\left(3W_1 + 2W_2 \mathrm{tr}(\mathbf{B}_{\kappa_{p(t)}}) + W_3 \mathrm{det}\mathbf{B}_{\kappa_{p(t)}} \mathrm{tr}(\mathbf{B}^{-1}_{\kappa_{p(t)}})\right). \tag{4.43}$$

So (4.17) becomes

$$-\frac{1}{2}\overset{\nabla}{\mathbf{B}} = \frac{2\rho}{\eta}\left(W_1\mathbf{B}_{\kappa_{p(t)}} + 2W_2\mathbf{B}^2_{\kappa_{p(t)}} + W_3 \mathrm{det}\mathbf{B}_{\kappa_{p(t)}}\mathbf{I}\right) - \lambda\mathbf{I}, \tag{4.44}$$

where λ is given by (4.43). Substituting this back in (4.44), we get,

$$-\frac{1}{2}\overset{\nabla}{\mathbf{B}} = \frac{2\rho}{\eta}\left[W_1\left(\mathbf{B}_{\kappa_{p(t)}} - \frac{3}{\mathrm{tr}(\mathbf{B}^{-1}_{\kappa_{p(t)}})}\mathbf{I}\right) + 2W_2\left(\mathbf{B}^2_{\kappa_{p(t)}} - \frac{\mathrm{tr}(\mathbf{B}_{\kappa_{p(t)}})}{\mathrm{tr}(\mathbf{B}^{-1}_{\kappa_{p(t)}})}\mathbf{I}\right)\right]. \tag{4.45}$$

Hence the evolution equation is given by (4.45)[1] and the stress is given by (4.33).

[1]The evolution equation does not depend on W_3. This is probably because we

D. Corroboration of the Model with the Experimental Data

For simplicity, we will assume that the deformation is homogeneous and is given by

$$r = \Lambda_1(t)R,\ \theta = \Theta,\ z = \Lambda_2(t)Z \tag{4.46}$$

in cylindrical polar co-ordinates. The deformation gradient is given by

$$\mathbf{F}_{\kappa_R} = \mathrm{diag}\Big(\Lambda_1,\ \Lambda_1,\ \Lambda_2\Big). \tag{4.47}$$

The left Cauchy-Green stretch tensor and the velocity gradient are given by

$$\mathbf{B}_{\kappa_R} = \mathrm{diag}\Big(\Lambda_1^2,\ \Lambda_1^2,\ \Lambda_2^2\Big),\quad \mathbf{L} = \mathbf{D} = \mathrm{diag}\left(\frac{\dot{\Lambda}_1}{\Lambda_1},\ \frac{\dot{\Lambda}_1}{\Lambda_1},\ \frac{\dot{\Lambda}_2}{\Lambda_2}\right). \tag{4.48}$$

We will assume that $\mathbf{B}_{\kappa_{p(t)}}$ is a function of time only and has the form: Let's assume that $\mathbf{B}_{\kappa_{p(t)}}$ has the form which is similar to $\mathbf{B}_{\kappa_R}$.

$$\mathbf{B}_{\kappa_{p(t)}} = \mathrm{diag}\Big(B_1(t),\ B_1(t),\ B_2(t)\Big). \tag{4.49}$$

Then $\mathrm{tr}(\mathbf{B}^{-1}_{\kappa_{p(t)}}) = \dfrac{B_1 + 2B_2}{B_1 B_2}$ and the evolution equation (4.45) will reduce to

$$-\frac{1}{2}\left(\dot{B}_1 - 2\frac{\dot{\Lambda}_1}{\Lambda_1}B_1\right) = \frac{2\rho B_1}{\eta(B_1+2B_2)}\left[W_1(B_1-B_2) + 2W_2(B_1^2 - B_2^2)\right], \tag{4.50}$$

$$-\frac{1}{2}\left(\dot{B}_2 - 2\frac{\dot{\Lambda}_2}{\Lambda_2}B_2\right) = \frac{-4\rho B_2}{\eta(B_1+2B_2)}\left[W_1(B_1-B_2) + 2W_2(B_1^2 - B_2^2)\right]. \tag{4.51}$$

If $\eta \neq 0$, we get

$$\frac{\dot{B}_1}{B_1} + \frac{1}{2}\frac{\dot{B}_2}{B_2} = 2\frac{\dot{\Lambda}_1}{\Lambda_1} + \frac{\dot{\Lambda}_2}{\Lambda_2}. \tag{4.52}$$

Solving,

$$B_1 B_2^{1/2} = K\Lambda_1^2\Lambda_2, \tag{4.53}$$

---

assumed that evolution of natural configurations is isochoric.

where K is a constant. $K = \dfrac{B_1(0)B_2(0)^{1/2}}{\Lambda_1(0)^2\Lambda_2(0)}$. Note from (4.46) and (3.43) that $III_{\kappa_{p(t)}} = B_1^2 B_2$ and $\det\mathbf{B}_{\kappa_R} = \Lambda_1^4\Lambda_2^2$. Therefore, $III_{\kappa_{p(t)}} = K^2\det\mathbf{B}_{\kappa_R}$. Also,

$$\rho = \frac{K\rho_0}{III_{\kappa_{p(t)}}^{1/2}}, \tag{4.54}$$

$$\frac{\partial\rho}{\partial III_{\kappa_{p(t)}}} = -\frac{1}{2}\frac{\rho}{III_{\kappa_{p(t)}}}. \tag{4.55}$$

The constitutive equation (4.33) will reduce to:

$$T_{zz} - T_{rr} = 2\rho\Big\{W_1\left(B_2 - B_1\right) + 2W_2(B_2^2 - B_1^2)\Big\}. \tag{4.56}$$

Now we will give a specific form for W.

Limestone

For $t < \tau$:

We shall choose

$$W_1 = \frac{\mu}{2\rho}, \tag{4.57}$$

$$W_2 = 0, \tag{4.58}$$

$$W_3 = \frac{\mu}{4\rho III_{\kappa_{p(t)}}}(I_{\kappa_p(t)} - 5). \tag{4.59}$$

Here μ is a constant and is equal to 2.8e7 Pa. The 'viscosity' η is given by $\eta = \eta(tr(\mathbf{T}), det(\mathbf{T}))$. Since $W_2 = 0$, (4.51) reduces to

$$-\frac{1}{2}\left(\dot{B}_2 - 2\frac{\dot{\Lambda}_2}{\Lambda_2}B_2\right) = \frac{-4\rho B_2}{\eta(B_1 + 2B_2)}\left[W_1(B_1 - B_2)\right]. \tag{4.60}$$

Also (4.33) reduces to:

$$T_{rr} = 2\rho(W_1 B_1 + B_1^2 B_2 W_3). \tag{4.61}$$

T_{rr} is a constant, and one can solve for B_1 in (4.61) as a function of B_2. So one can substitute B_1 back in (4.60) and solve the differential equation for B_2. After that

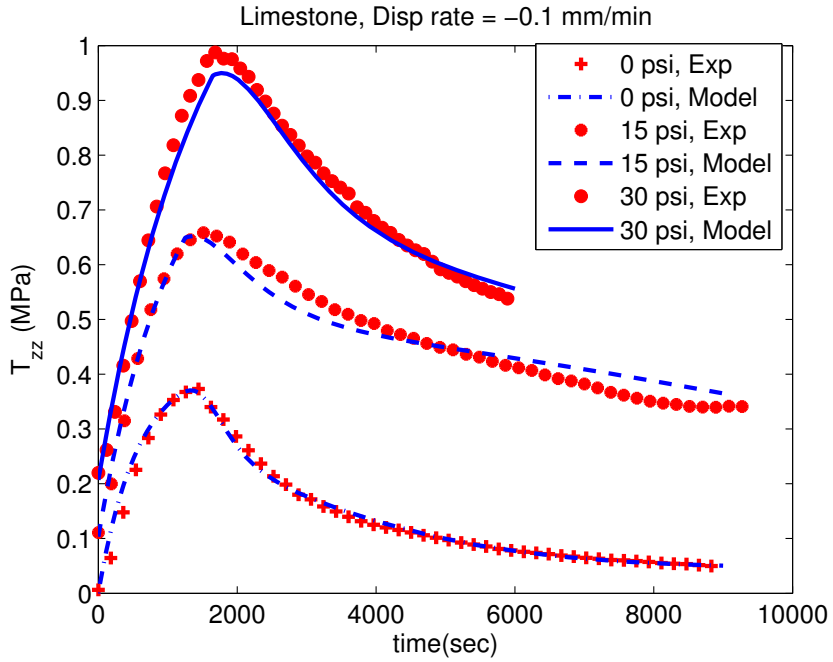

Fig. 22. Limestone, Disp rate = -0.1 mm/min (Compressible)

using (4.56) T_{zz} is calculated.

For $t > \tau$:

$$W_1 = \frac{1}{2\rho}\left[c\ exp(a(I_{\kappa_p(t)} - I_{\kappa_{p(t)_\tau}} + b)) + d\right], \tag{4.62}$$

$$W_2 = 0, \tag{4.63}$$

$$W_3 = \frac{1}{4\rho III_{\kappa_{p(t)}}}\left[\frac{c}{a}exp(a(I_{\kappa_p(t)} - I_{\kappa_{p(t)_\tau}} + b)) + dI_{\kappa_p(t)} + e\right]. \tag{4.64}$$

Here $a,\ b,\ c$ are functions of $I_{\kappa_{p(t)_\tau}}$ and $III_{\kappa_{p(t)_\tau}}$.

The switching criterion is determined by

$$\mathrm{tr}\mathbf{D} - \alpha(I_{\kappa_p(t)} - 3 - \beta)^m = 0 \tag{4.65}$$

where $\alpha = 2e11,\ \beta = \beta(tr(\mathbf{T}), det(\mathbf{T})),\ m = 7.905$. The model predictions are compared with the experimental results in figures 22 through 25.

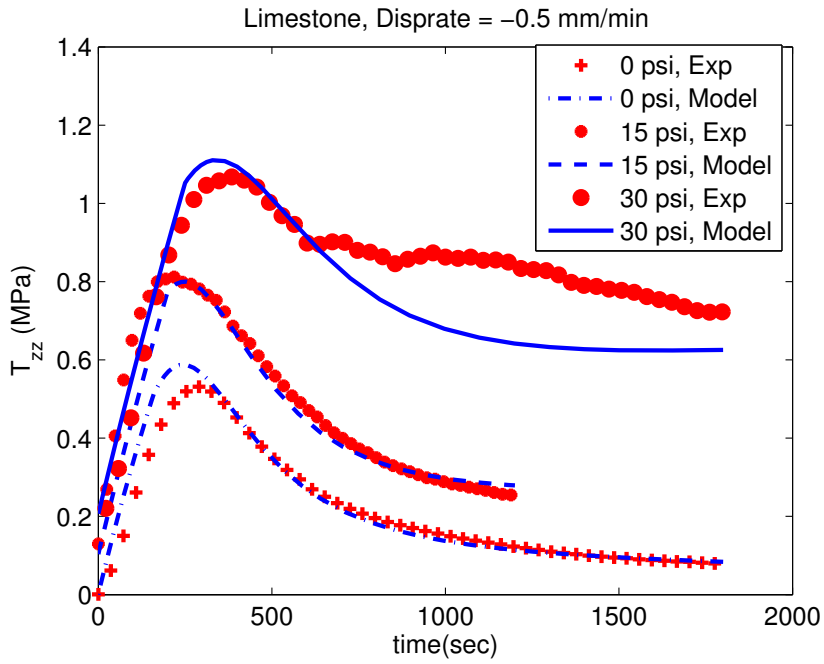

Fig. 23. Limestone, Disp rate = -0.5 mm/min (Compressible)

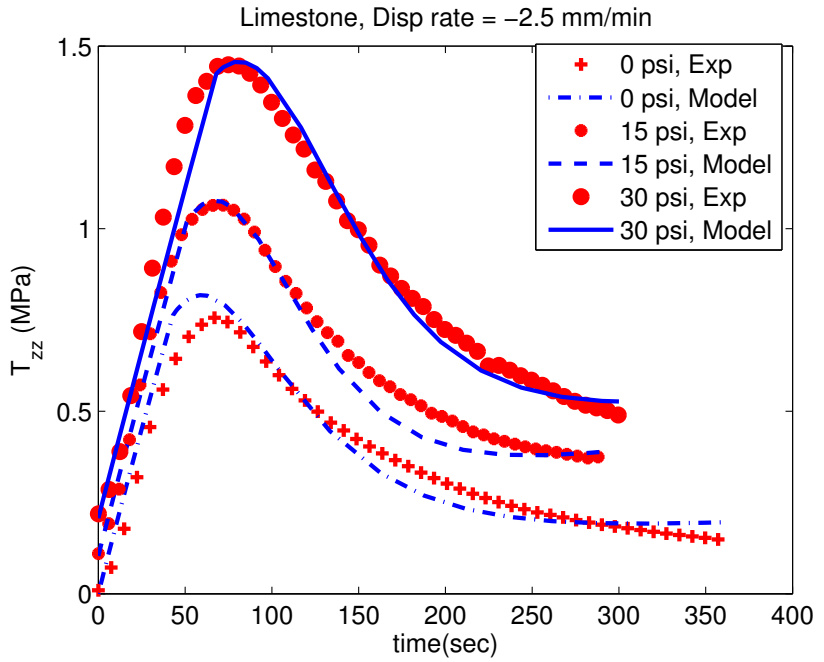

Fig. 24. Limestone, Disp rate = -2.5 mm/min (Compressible)

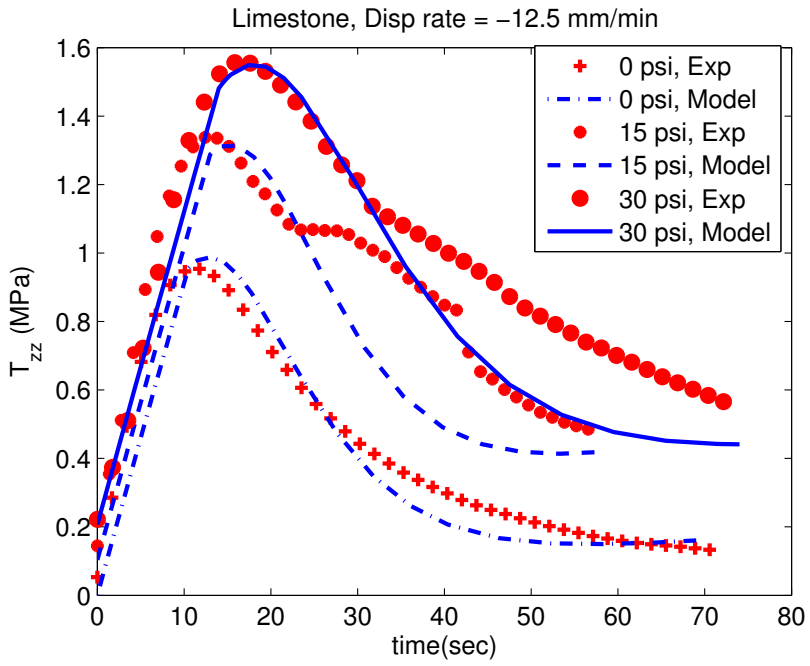

Fig. 25. Limestone, Disp rate = -12.5 mm/min (Compressible)

CHAPTER V

CONCLUDING REMARKS AND DISCUSSION

A. Summary

The aim of this dissertation was to conduct constant displacement rate experiments for asphalt concrete at various confinement pressures and to develop a continuum model which will describe the experimental results. To this end a series of experiments were carried out at different confinement pressures and displacement rates on cylindrical samples of asphalt concrete. The experiments were repeated for two different aggregate samples. A general framework was used using the idea of multiple natural configurations and the maximization of the rate of dissipation to generate models for asphalt concrete. The frame-work is general enough that models capable of describing the behavior of asphalt concrete for different confinement pressure and displacement rates are easily generated. An incompressible model and a compressible model were developed and were used to corroborate the experimental data.

Experiments were carried out at different confinement pressures and displacement rates on cylindrical samples of asphalt concrete. Two different aggregates were used to make the samples - limestone and granite. The aggregates were first sieved and seperated to different size distributions. Then using a mix design methodology, specific percentage by weight of different sized aggregates and asphalt are mixed using a mechanical mixer. The mix is then compacted to cylindrical samples of 4 inch diameter and 6 inch height using a gyratory compactor. The specimens are finally tested in a MTS machine at a constant displacement rate. To this end, the specimen is first enclosed in a triaxial cell and the desired confinement pressure is achieved by adjusting the pressure of air inside the triaxial cell. The specimen is loaded axially

and the displacement of the ram is controlled using a computer so that a constant displacment rate is obtained. The axial force required to keep this constant displacement rate is measured as a function of time and recorded. The experiment is conducted for three different confinement pressures namely 0 psi, 15 psi and 30 psi and also at 4 different displacement rates - 0.1 mm/min, 0.5 mm/min, 2.5 mm/min, 12.5 mm/min. The experiments were carried out for samples made of two different aggregates - limestone and granite.

A general framework has been developed to construct specific models to describe the behavior of asphalt concrete. The framework is built on the idea of evolving natural configurations and the maximization of the rate of dissipation. By specifying different forms for the internal energy, entropy and rate of dissipation, different models are constructed. The evolution of the natural configuration is determined by the maximization of the rate of dissipation function and the constitutive equation is obtained from the reduced energy-dissipation equation. Since asphalt concrete made from different aggregates stores and dissipates energy in very different ways, different forms were used for the stored energy and the rate of dissipation for asphalt concrete made from the two different aggregates.

Using the above framework, first an incompressible model was developed. In this model, asphalt concrete was assumed to be incompressible. The predictions of the theory were tested by corroborating the model predictions with the experimental data. A switching criteria was used to switch the model to capture the change in material behavior after the stress reached a peak value. This is done in order to capture the change in the way in which the internal structure of the material evolves once the material reaches a peak value.

Asphalt concrete is a compressible material and a compressible model was generated using the above framework which will take this factor into account. The model

predictions were corroborated with the experimental data for limestone and better predictions were obtained using the compressible model. Similar to the incompressible model, a switching criteria was used to switch the model to capture the change in response of the material after the stress reached a peak value. Both the models were able to caputre the peak stress developed in the material.

B. Recommendations for Future Work

In this work we have developed both a compressible and an incompressible model for asphalt concrete. This work can be further improved and can be used to model other experimental data. Some specific recommendations to improve the model developed in this dissertation are as follows:

Asphalt concrete is composed of different sized aggregate particles and asphalt and hence it exhibits anisotropic behavior. Using the framework developed it is possible to model the anisotropic behavior of asphalt concrete. The anisotropy of asphalt concrete evolves as the material deforms. This is due to the fact that the relative orientation and the distance between the aggregate particles changes during the deformation process. The anisotropy can be built into the framework by requiring the stored energy and the rate of dissipation function to depend on the directions of anisotropy also. One big obstacle in taking into account anisotropy in modeling asphalt concrete is the lack of experimental data. Even if one knows the relative orientation of the aggregate particles at the start of the experiment one does not have enough experimental data to correlate this with the response of the material. Also we should have enough experimental data to correlate the evolution of anisotropy and its effect on the behavior of the asphalt concrete.

Asphalt concrete in pavements are subjected to traffic loads by moving vehicles.

Hence the load on the pavement is not constant. On the contrary, it is more similar to a cyclic loading. Experiments have been carried out by various researchers in the laboratory which simulates the cyclic loading due to traffic. In a cyclic loading experiment, the boundary conditions are different from that of the experiment done here. It is a traction controlled experiment as opposed to the displacement controlled experiment (axial) done in this work. Also there is a repeated loading and unloading of the specimen and hence the boundary conditions are going to change with time. The model developed in this work could be extended to model this kind of experimental data.

Another pheneomenon which occurs in the pavement is healing. Healing refers to the coalescence of microcracks so that it 'heals' itself. This has a significant impact on the pavement performance. In fact the traffic in an airport runway is determined by the healing period of the asphalt concrete. The framework developed is general enough to take into account the effect of healing in asphalt concrete. But one needs to know the specifics as to how healing affects the energy storage and rate of dissipation in the material.

The ultimate success of a model is how well it can describe the material in real life situation. Asphalt concrete is a very complex material it behaves very differently under different loading, temperature and environmental conditions. For example, it behaves quite differently in tension and in compression. The moisture, temperature, its reaction with athmospheric air etc., will cause its behavior to change over time. The response of asphalt concrete is highly dependent on the compaction process, the shape, type and distribution of the aggregate materials and the type and amount of asphalt used in making the pavement. To take all these into account in modeling a material is extremely difficult. The specific models developed in this work using the framework seems to be the right step in this direction. But it may probably require

a lot more work before it can be put into real life applications.

In conclusion, constant displacement rate experiments were done on asphalt concrete specimens to study the behavior of asphalt concrete. We developed a general framework to study asphalt concrete in a full thermodynamic setting. Specific incompressible and compressible models were developed using the framework. The efficacy of the models were illustrated by corroborating the model with the experimental results.

REFERENCES

[1] C. A. Truesdell, *A First Course in Rational Continuum Mechanics*, Pure and Applied Mathematics Series, Boston: Academic Press, 2 edition, 1991.

[2] C. Truesdell and W. Noll, *The Non-Linear Field Theories of Mechanics*, 3rd edition, Berlin: Springer-Verlag, 2004.

[3] C. Truesdell and R. A. Toupin, "The classical field theories," in *Handbuch der Physik*, vol. III, no.1. Berlin: Springer Verlag, 1960.

[4] R. N. J. Saal and G. Koens, "Investigation into the plastic properties of asphaltic bitumen," *Journal of Institute of Petroleum*, vol. 19, pp. 176–212, 1933.

[5] J. M. Burgers, "Mechanical considerations, model systems, phenomenological theories of relaxation and of viscosity," in *First report on viscosity and plasticity, 2nd edition*, pp. 21–33. Prepared by the Committee for the Study of Viscosity of the Academy of Sciences at Amsterdam, New York: Nordemann Publ., 1939.

[6] A. R. Lee and A. H. D. Marwick, "The mechanical properties of bituminous surfacing materials under constant stress," *J Soc Chem Indust*, vol. 56, pp. 146T–156T, 1937.

[7] C. L. Monismith and K. E. Secor, "Viscoelastic behavior of asphalt concrete pavements," in *Rep., Inst of Transportation and Traffic Engineering*. Univ of California, Berkeley, California, 1962.

[8] Y. H. Huang, "Deformation and volume change characteristics of a sand asphalt mixture under constant direct and triaxial compressive stresses," *Highway Research Record*, vol. 178, pp. 60–74, 1967.

[9] Y. R. Kim and D. N. Little, "One-dimensional constitutive modeling of asphalt concrete," *J. Eng. Mech. Div.*, vol. 116, pp. 751–772, 1990.

[10] S. Huschek, "The deformation behavior of asphalt concrete under triaxial compression," in *Proceedings of the Association of Asphalt Paving Technologists*, vol. 54, pp. 407–431. 1985.

[11] C. Van der Poel, "On the rheology of concentrated dispersions," *Rheologica Acta*, vol. 1, pp. 198–205, 1958.

[12] Sun Woo Park, Y. Richard Kim, and Richard A. Schapery, "A viscoelastic continuum damage model and its application to uniaxial behavior of asphalt concrete," *Mechanics of Materials*, vol. 24, pp. 241–255, 1996.

[13] K. R. Rajagopal and A. R. Srinivasa, "A note on a correspondence principle in non-linear viscoelastic materials," *International Journal of Fracture*, Submitted for publication.

[14] L. W. Nijboer, *Plasticity as a Factor in the Design of Dense Bituminous Road Carpets*, Amsterdam: Elsevier, 1948.

[15] J. F. Hills, "The creep of asphalt mixes," *J. Inst. Pet*, vol. 59, no. 3, pp. 247–262, 1973.

[16] C. Boutin and J. L. Auriault, "Dynamic behavior of porous media saturated by a viscoelastic fluid: Application to bituminous concretes," *Int. J. Eng. Sci*, vol. 28, pp. 1157–1181, 1990.

[17] D. Florea, "Associated elastic/viscoelastic model for bituminous concrete," *Int. J. Eng. Sci.*, vol. 32, pp. 79–86, 1994.

[18] D. Florea, "Nonassociated elastic/viscoelastic model for bituminous concrete," *Int. J. Eng. Sci.*, vol. 32, pp. 87–93, 1994.

[19] E. Masad, B. Muhunthan, N. Shashidhar, and T. Harman, "Aggregate orientation and segregation in asphalt concrete," *Geotechnical Special Publication, ASCE, GSP*, vol. 85, pp. 69–80, 1998.

[20] E. Masad, B. Muhunthan, N. Shashidhar, and T. Harman, "Effect of compaction procedure on the aggregate structure in asphalt concrete," *Transportation Research Record*, vol. 1681, pp. 179–185, 1999.

[21] E. Masad and J. W. Button, "Unified imaging approach for measuring aggregate angularity and texture," *Computer-aided Civil and Infrastructure Engineering*, vol. 15, pp. 272–280, 2000.

[22] J. Murali Krishnan and K. R. Rajagopal, "Thermodynamic framework for the constitutive modeling of asphalt concrete: Theory and applications," *Journal of Materials in Civil Engineering*, vol. 16, no. 2, pp. 155–166, April 2004.

[23] K. R. Rajagopal and A. S. Wineman, "A constitutive equation for nonlinear solids which undergo deformation induced microstructural changes," *International Journal of Plasticity*, vol. 8, pp. 385–395, 1992.

[24] K. R. Rajagopal and A. R. Srinivasa, "Mechanics of inelastic behavior of materials - part i: Theoretical underpinnings," *International Journal of Plasticity*, vol. 14, pp. 945–967, 1998.

[25] K. R. Rajagopal and A. R. Srinivasa, "Mechanics of inelastic behavior of materials - part ii: Inelastic response," *International Journal of Plasticity*, vol. 14, pp. 969–995, 1998.

[26] K. R. Rajagopal and A. R. Srinivasa, "On the inelastic behavior of solids-part i: Twinning," *International Journal of Plasticity*, vol. 6, pp. 969–995, 1995.

[27] K. R. Rajagopal and A. R. Srinivasa, "A thermodynamic framwork for rate type fluid models," *Journal of Non-Newtonian Fluid Mechanics*, vol. 88, pp. 207–227, 2000.

[28] J. D. Humphrey and K. R. Rajagopal, "A constrained mixture model for growth and remodeling of soft tissues," *Mathematical Models and Methods in Applied Sciences*, vol. 12, pp. 1–24, 2002.

[29] K. R. Rajagopal and L. Tao, *Mechanics of Mixtures*, Singapore: World Scientific, 1996.

[30] L. E. Wood and W. Goetz, "The rheological characteristics of a sand-asphalt mixture," in *Proceedings of the Association of Asphalt Paving Technologists*, vol. 28, pp. 211–229. 1959.

[31] A. E. Green and P. M. Naghdi, "On thermodynamics and the nature of the second law," in *Proceedings of the R. Soc. London, Ser. A*, vol. 357, pp. 253–270. 1977.

[32] K. R. Rajagopal, "Multiple configurations in continuum mechanics," *Report 6, Institute of Computational and Applied Mechanics*, University of Pittsburgh, PA, 1995.

[33] I. J. Rao and K. R. Rajagopal, "A thermodynamic framework for the study of crystallization in polymers," *Z. angew. Math. Phys. (ZAMP)*, vol. 53, pp. 365–406, 2002.

[34] K. R. Rajagopal and A. R. Srinivasa, "Modeling anisotropic fluids within the framework of bodies with multiple natural configurations," *Journal of Non-Newtonian Fluid Mechanics*, vol. 99, pp. 109–124, July 2001.

[35] J. Murali Krishnan and K. R. Rajagopal, "Triaxial testing and stress relaxation of asphalt concrete," *Mechanics of Materials*, vol. 36, pp. 849–864, 2004.

[36] V. A. Endersby, "The history and theory of triaxial testing, and the preparation of realistic test specimens - a report of the triaxial institute," in *Triaxial Testing of Soils and Bituminous mixtures, ASTM Special Technical Publication*, vol. 106, pp. 5–20. American Society of Testing and Materials, Philadelphia, 1951.

[37] G. G. Stokes, "On the theories of the internal friction of fluids in motion, and of the equilibrium and motion of elastic solids," *Trans. Camb. Phil. Soc.*, vol. 8, pp. 287–305, 1845.

[38] P. W. Bridgman, "The effect of pressure on the viscosity of forty-three pure liquids," in *Proceedings of American Academy of Arts and Sciences*, vol. 61, pp. 57–99. 1926.

[39] J. Hron, J. Malek, and K. R. Rajagopal, "Simple flows of fluids with pressure-dependent viscosities," in *Proceedings of the R. Soc. London A*, vol. 457, pp. 1603–1622. 2001.

[40] W. G. Cutler, R. H. McMickle, W. Webb, and R. W. Schiessler, "Study of the compressions of several high molecular weight hydrocarbons," *J. Chem. Phys.*, vol. 29, pp. 727–740, 1958.

[41] E. M. Griest, W. Webb, and R. W. Schiessler, "Effect of pressure on viscosity of higher hydrocarbons and their mixtures," *J. Chem. Phys.*, vol. 29, pp. 711–720,

1958.

[42] K. L. Johnson and R. Cameron, "Shear behavior of elastohydrodynamic oil films at high rolling contact pressures," in *Proceedings of the Instn. Mech. Engrs.*, vol. 182, pp. 307–319. 1967.

[43] K. L. Johnson and J. L. Tevaarwerk, "Shear behavior of elastohydrodynamic oil films," in *Proceedings of the R. Soc. London A*, vol. 356, pp. 215–236. 1977.

[44] K. R. Rajagopal and A. R. Srinivasa, "On the thermomechanics of materials that have multiple natural configurations, part i - viscoelasticity and classical plasticity," *Z. angew. Math. Phys. (ZAMP)*, vol. 55, no. 5, pp. 861–893, September 2004.

[45] M. W. Witczak, K. Kaloush, T. Pellinen, M. El-Basyouny, and H. Von Quintus, "Simple performance test for superpave mix design," *NCHRP*, vol. 465, pp. 1–105, 2002.

[46] A. S. Buisman, "Proefondervindelijke bepaling van de grens van inwendig evenwicht van een grondmassa," *De Ingenieur*, vol. 26, pp. B83–B88, June 1934.

[47] T. E. Stanton and F. N. Hveem, "Role of laboratory in the preliminary investigation and control of materials for low cost bituminous pavements," in *Proceedings of the Highway Research Board, Part II, R. W. Crum (Ed.)*, vol. 14, pp. 14–54. A Symposium on Research Features of Flexible-type Bituminous Roads, 1934.

[48] M. A. Haar and T. von Karman, "Zur theorie der spannungszusttande in plastischen und sandartigen medien," *Nachrichten der K. Gesellschaft der Wissenschaften zu Gottingen Mathematisch-physikalische Klasse K1*, pp. 204–218, 1909.

[49] A. W. Bishop and D. J. Henkel, *The Measurement of Soil Properties in the Triaxial Test*, London: Edward Arnold, 1957.

[50] G. H. Sowers, "Laboratory shear testing of soils," *Special Technical Publication 361, American Society for Testing and Materials*, pp. 3–21, 1963.

[51] K. H. Roscoe, A. N. Schofield, and A. Thurairajah, "Laboratory shear testing of soils," *Special Technical Publication 361, American Society for Testing and Materials*, pp. 111–128, 1963.

[52] P. W. Rowe and L. Barden, "The importance of free-ends in the triaxial test," *Journal of the Soil Mechanics and Foundation Division*, vol. 90, no. SM1, pp. 1–27, 1964.

[53] A. W. Bishop and G. E. Green, "The influence of end restraint on the compression strength of a cohesionless soil," *Geotechnique*, vol. 15, no. 3, pp. 243–266, 1965.

[54] J. E. Stephens and K. C. Sinha, "Effect of aggregate shape on bituminous mix characteristics," in *Proceedings of the Association of Asphalt Paving Technologists*, vol. 47, pp. 434–456. 1978.

[55] W. H. Campen and J. R. Smith, "A study of the role of angular aggregates in the development of stability in bituminous mixtures," in *Proceedings of the Association of Asphalt Paving Technologists*, vol. 17, pp. 114–142. 1948.

[56] P. A. Wedding and R. D. Gaynor, "The effects of using crushed gravel as the coarse and fine aggregate in dense graded bituminous mixtures," in *Proceedings of the Association of Asphalt Paving Technologists*, vol. 30, pp. 469–492. 1961.

[57] M. Herrin and W. H. Goetz, "Effect of aggregate shape on stability of bituminous mixes," in *Proceedings, Highway Research Board*, vol. 33, pp. 293–308. 1954.

[58] B. A. Vallerga, H. B. Seed, C. L. Monismith, and R. S. Cooper, "Effect of shape, size and surface roughness of aggregate particles on the strength of granular materials," *Special Technical Publication 212, ASTM*, pp. 63–76, September 1956.

[59] F. N. Hveem, "Gradation of mineral aggregates for dense graded bituminous mixtures," in *Proceedings of the Association of Asphalt Paving Technologists*, vol. 11, pp. 315–339. 1940.

[60] N. C. Krutz and P. E. Sebaaly, "The effect of aggregate gradation on permanent deformation of asphalt concrete," in *Proceedings of the Association of Asphalt Paving Technologists*, vol. 39, pp. 450–473. 1993.

[61] J. S. Chen and M. C. Liao, "Evaluation of internal resistance in hot-mix asphalt (hma) concrete," *Construction and Building Materials*, vol. 16, pp. 313–319, 2002.

[62] Y. R. Kim, N. Yim, and N. P. Khosla, "Effect of aggregate type and gradation on fatigue and permanent deformation of asphalt concrete," *Special Technical Publication 1147, ASTM*, pp. 310–328, 1992.

[63] J. Harvey and C. L. Monismith, "Effects of laboratory asphalt concrete specimen preparation variables on fatigue and permanent deformation test results using strategic highway research program a-003a proposed testing equipment," *Transportation Research Record 1417*, pp. 38–48, 1993.

[64] G. Y. Baladi and T. T. H. Wu, "Interpretation of triaxial test results of cohesionless soils: A new model," in *Advanced triaxial testing of soil and rock, ASTM STP*, vol. 977, pp. 567–581. American Society for Testing and Materials, Philadelphia, 1988.

[65] R. D. Holtz and W. D. Kovacs, *An Introduction to Geotechnical Engineering*, Englewood Cliffs, NJ: Prentice Hall, 1981.

[66] H. L. Von Quintus, J. A. Scherocman, C. S. Hughes, and T. W. Kennedy, "Asphalt aggregate mixture analysis system," *NCHRP Report 338*, 1991.

[67] M. C. Ford, "Pavement densification related to asphalt mix characteristics," *1988 Annual Meeting of the Transportation Resarch Board*, 1988.

[68] E. R. Brown and Steve Cross, "A study of in-place rutting of asphalt pavments," *1989 Annual Meeting of the Association of Asphalt Paving Technologists*, 1989.

[69] G. A. Huber and G. H. Heiman, "Effect of asphalt concrete parameters on rutting performance: A field investigation," in *Proceedings of Association of Asphalt Paving Technologists*, vol. 56, pp. 33–61. 1987.

[70] E. Zube, "Compaction studies of asphalt concrete pavement as related to the water permeability test," *41st Annual Meeting of the Highway Research Board*, 1962.

[71] E. R. Brown, R. Collins, and J. R. Brownfield, "Investigation of segregation of asphalt mixtures in state of Georgia," in *Transportation Research Record*, vol. 1217, pp. 1–8. TRB, National Research Council, Washington, D.C., 1989.

[72] L. E. Santucci, D. D. Allen, and R. L. Coats, "The effects of moisture and compaction on the quality of asphalt pavements," *Association of Asphalt Paving Technologists*, vol. 54, pp. 168–208, 1985.

[73] D. Harmelink and T. Aschenbrener, "In-place voids monitoring of hot mix asphalt pavements," *Report No.CDOT-DTD-R-2002-11, Colorado Department of Transporation Research Branch*, 2002.

[74] J. Murali Krishnan and C. Lakshmana Rao, "Mechanics of air voids reduction of asphalt concrete using mixture theory," *International Journal of Engineering Science*, vol. 38, pp. 1331–1354, 2000.

[75] L. Wang, X. Wang, L. Mohammad, and Y. Wang, "Asphalt aggregate mixture analysis system," *ASCE Journal of Materials in Civil Engineering*, vol. 16, no. 2, pp. 167–174, 2004.

APPENDIX A

EXPERIMENTAL DATA

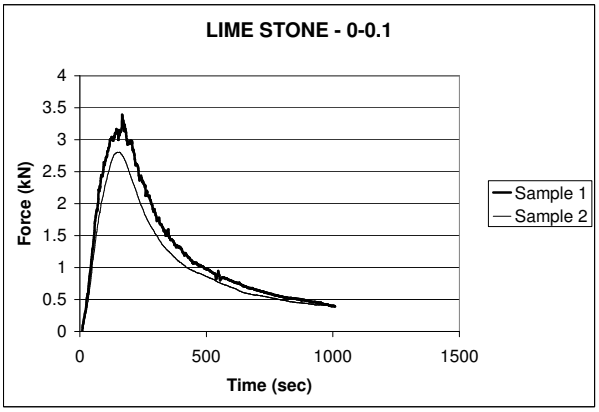

Fig. 26. Limestone, Confinement Pressure = 0 psi, Displacement Rate = 0.1 mm/min

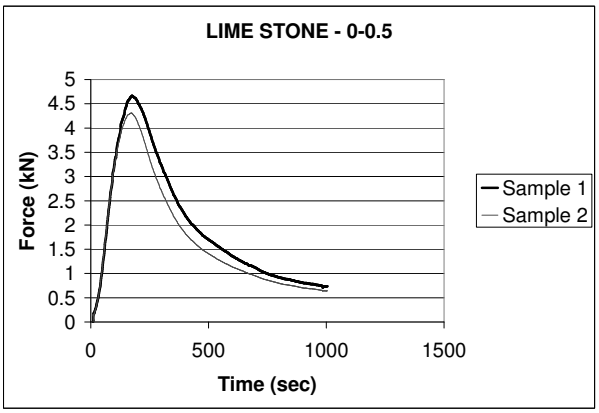

Fig. 27. Limestone, Confinement Pressure = 0 psi, Displacement Rate = 0.5 mm/min

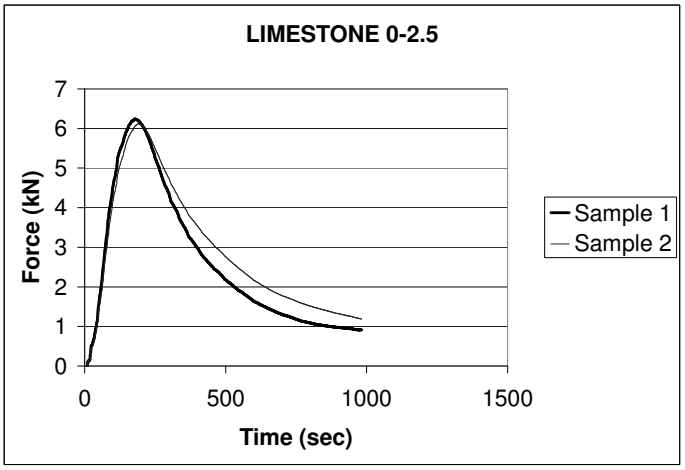

Fig. 28. Limestone, Confinement Pressure = 0 psi, Displacement Rate = 2.5 mm/min

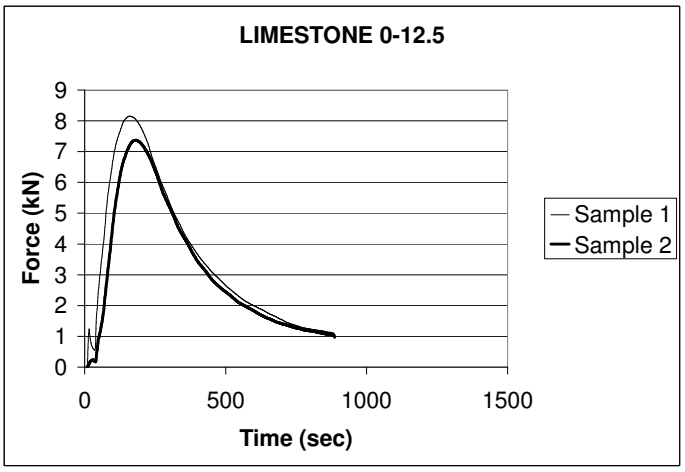

Fig. 29. Limestone, Confinement Pressure = 0 psi, Displacement Rate = 12.5 mm/min

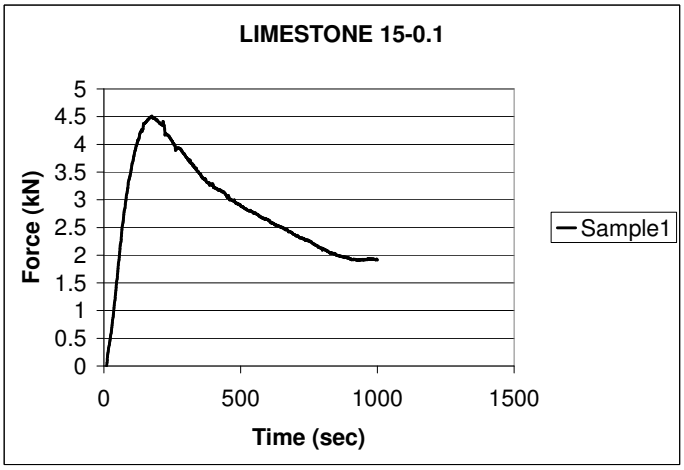

Fig. 30. Limestone, Confinement Pressure = 15 psi, Displacement Rate = 0.1 mm/min

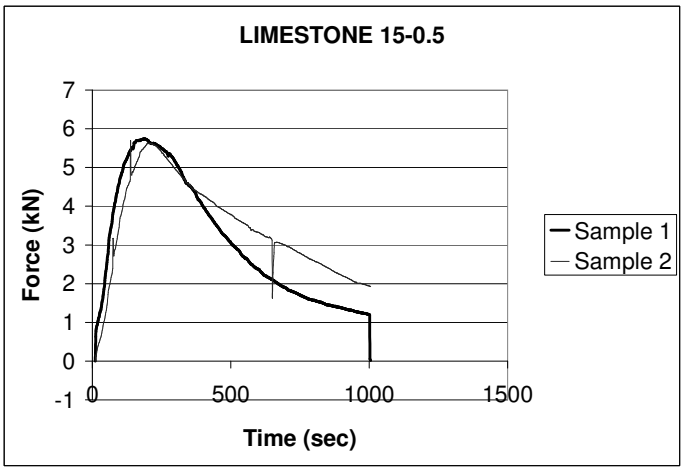

Fig. 31. Limestone, Confinement Pressure = 15 psi, Displacement Rate = 0.5 mm/min

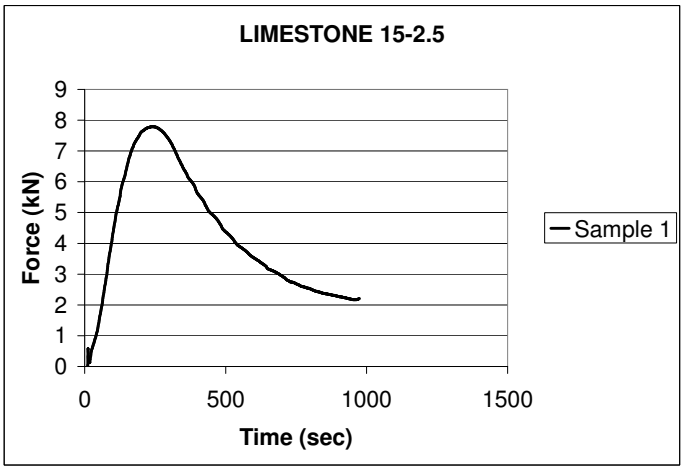

Fig. 32. Limestone, Confinement Pressure = 15 psi, Displacement Rate = 2.5 mm/min

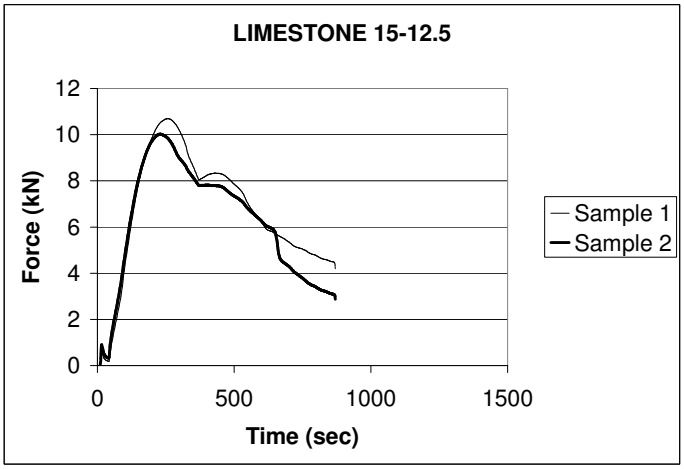

Fig. 33. Limestone, Confinement Pressure = 15 psi, Displacement Rate = 12.5 mm/min

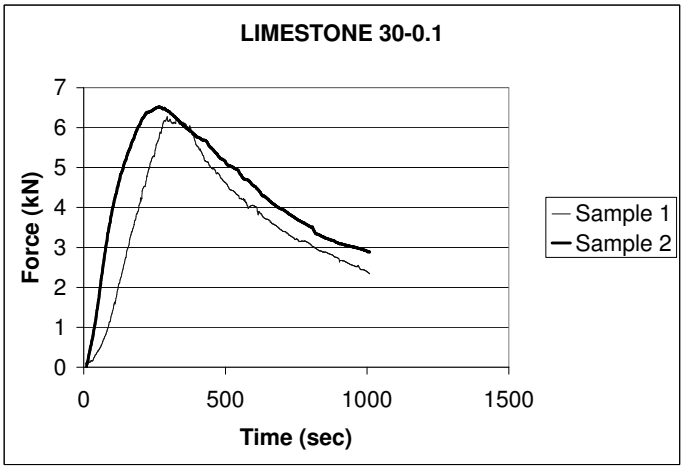

Fig. 34. Limestone, Confinement Pressure = 30 psi, Displacement Rate = 0.1 mm/min

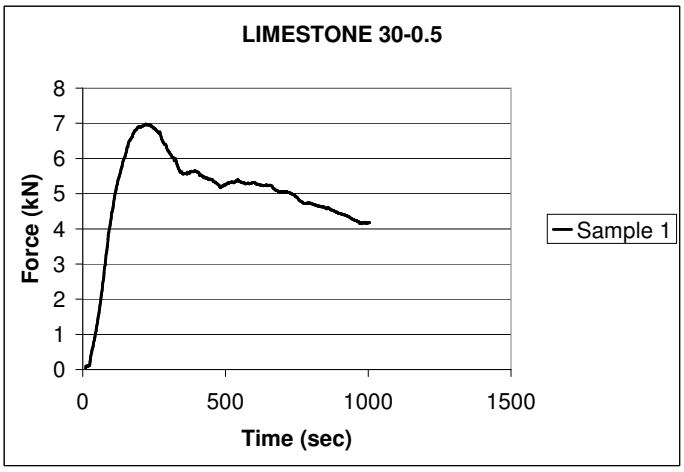

Fig. 35. Limestone, Confinement Pressure = 30 psi, Displacement Rate = 0.5 mm/min

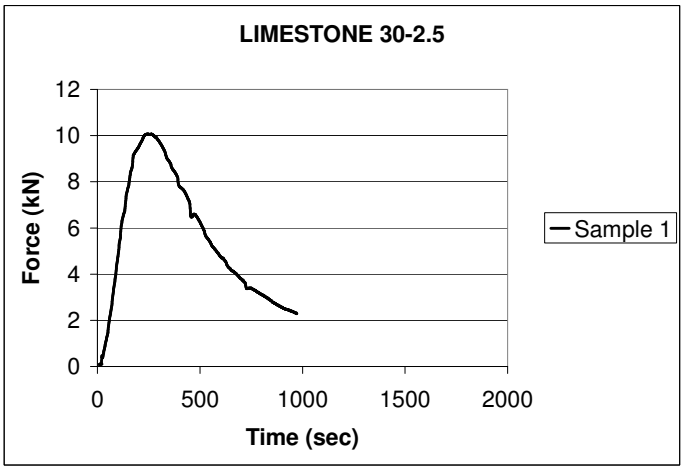

Fig. 36. Limestone, Confinement Pressure = 30 psi, Displacement Rate = 2.5 mm/min

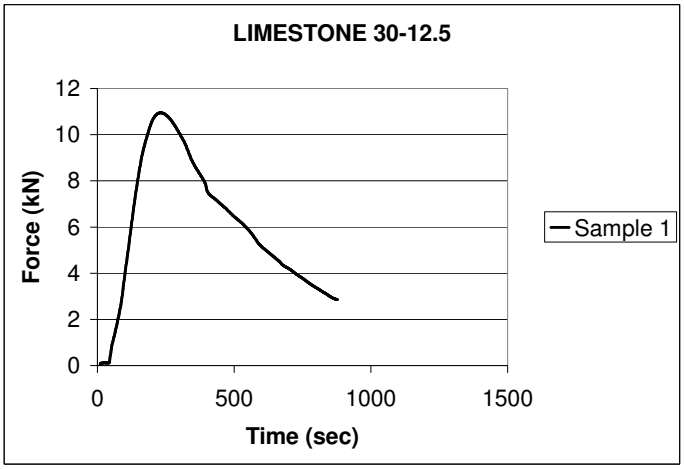

Fig. 37. Limestone, Confinement Pressure = 30 psi, Displacement Rate = 12.5 mm/min

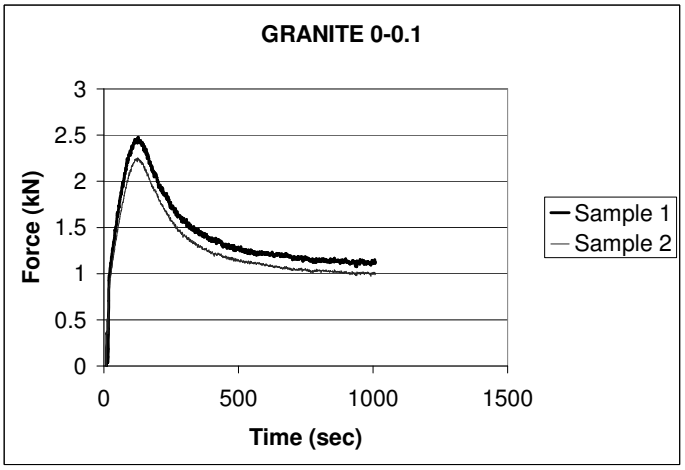

Fig. 38. Granite, Confinement Pressure = 0 psi, Displacement Rate = 0.1 mm/min

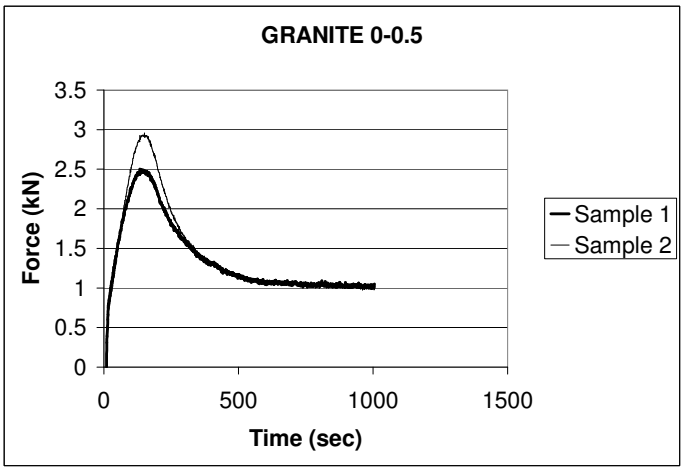

Fig. 39. Granite, Confinement Pressure = 0 psi, Displacement Rate = 0.5 mm/min

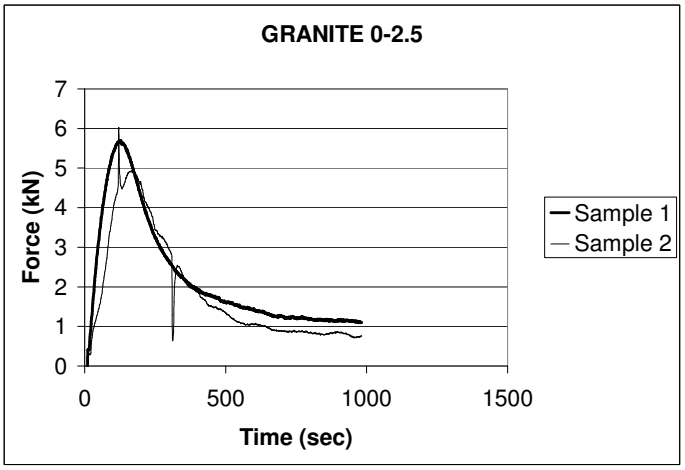

Fig. 40. Granite, Confinement Pressure = 0 psi, Displacement Rate = 2.5 mm/min

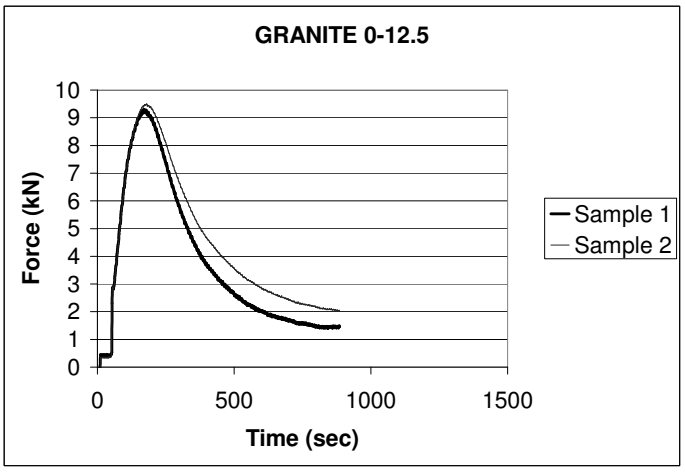

Fig. 41. Granite, Confinement Pressure = 0 psi, Displacement Rate = 12.5 mm/min

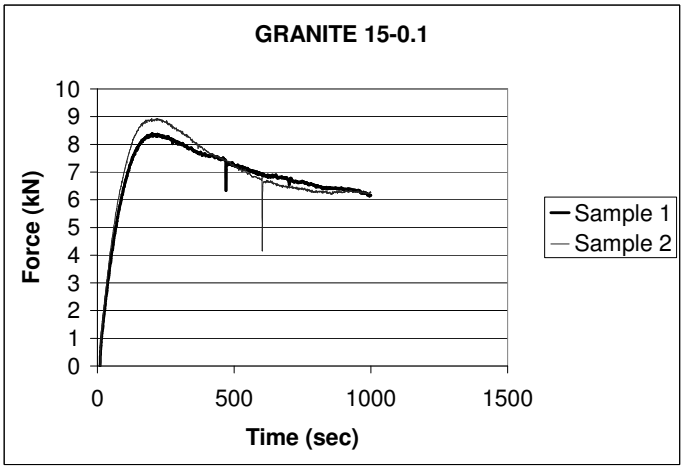

Fig. 42. Granite, Confinement Pressure = 15 psi, Displacement Rate = 0.1 mm/min

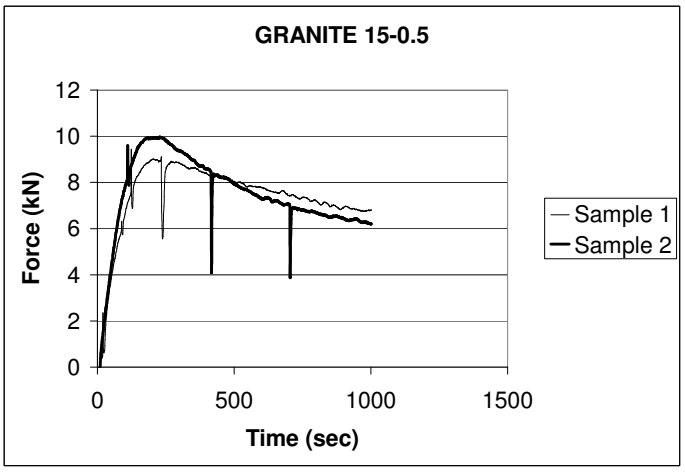

Fig. 43. Granite, Confinement Pressure = 15 psi, Displacement Rate = 0.5 mm/min

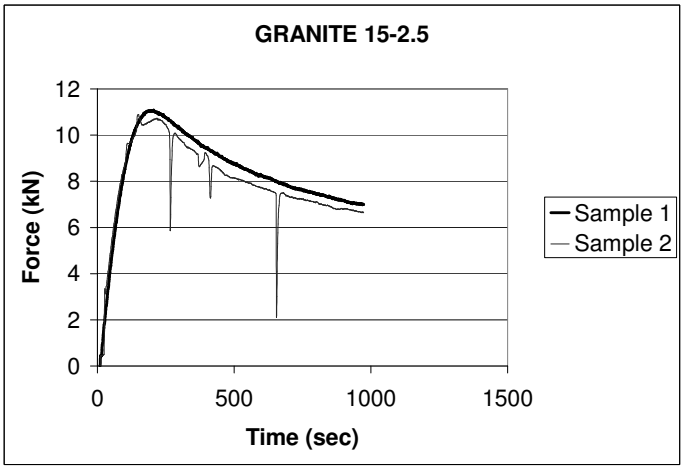

Fig. 44. Granite, Confinement Pressure = 15 psi, Displacement Rate = 2.5 mm/min

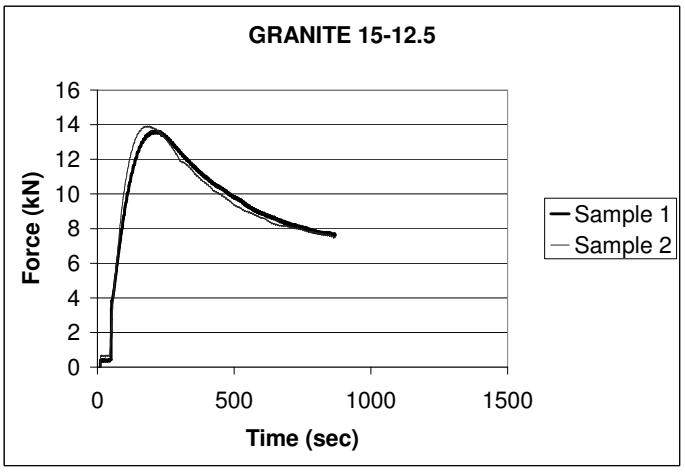

Fig. 45. Granite, Confinement Pressure = 15 psi, Displacement Rate = 12.5 mm/min

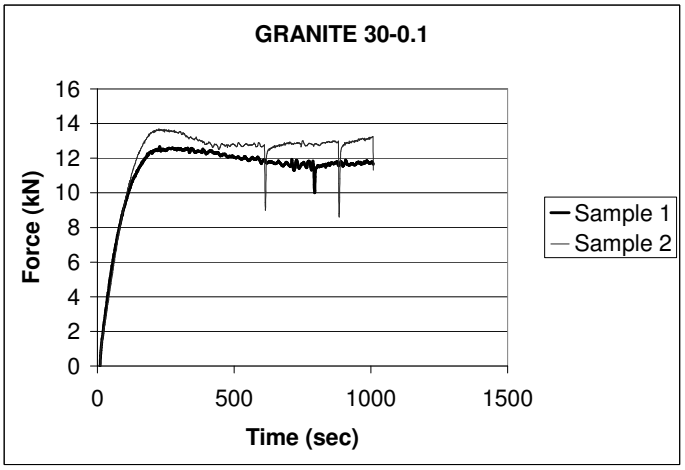

Fig. 46. Granite, Confinement Pressure = 30 psi, Displacement Rate = 0.1 mm/min

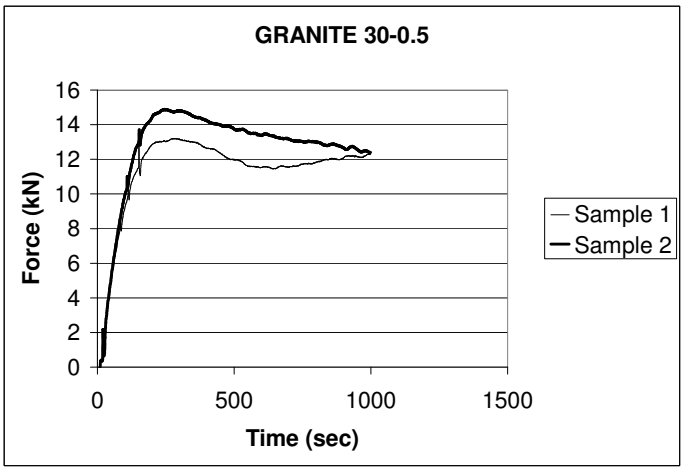

Fig. 47. Granite, Confinement Pressure = 30 psi, Displacement Rate = 0.5 mm/min

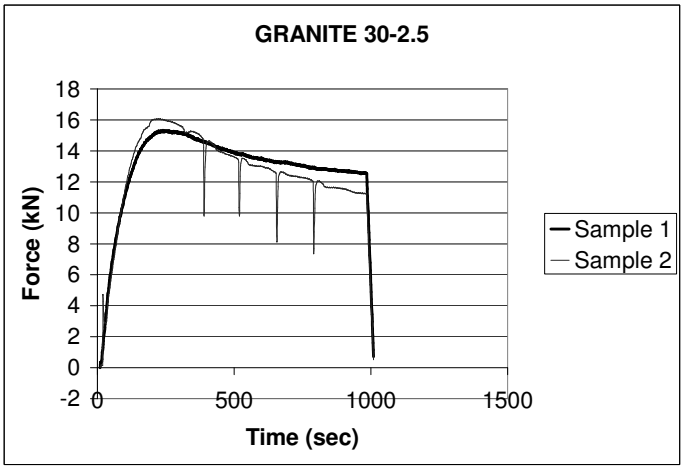

Fig. 48. Granite, Confinement Pressure = 30 psi, Displacement Rate = 2.5 mm/min

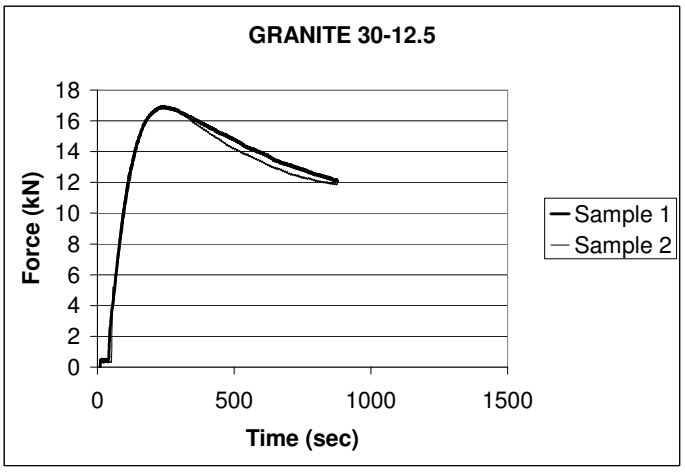

Fig. 49. Granite, Confinement Pressure = 30 psi, Displacement Rate = 12.5 mm/min

VITA

Pradeep Hariharakumar was born in Trivandrum, India on March 18, 1975. He received his Bachelor of Technology degree in civil engineering from the Indian Institute of Technology, Madras, India in May 1998 and his Master of Science in Mechanical Engineering from Texas A&M University in May 2001. The author may be contacted at MGRA 62, MKK Nair Road, Pettah, Trivandrum 695024, Kerala, India or by email at pradeep_h@hotmail.com.

The typist for this thesis was Pradeep Hariharakumar.